2017

Evaluating the source and use of radon for exploring deeply buried uranium deposits

NICKOLAS DUDEK

A thesis submitted to the Faculty of Graduate and Postdoctoral Studies in partial fulfillment of the requirements for a Master of Science degree in Earth Sciences.

Department of Earth Sciences

Faculty of Science

University of Ottawa

Abstract

This project's goal is to evaluate the use of groundwater Rn as a tool for the search of deeply buried U deposits. To do so, the concentrations of major cations, anions, Rn, ^{4}He, and ^{3}H were measured in groundwater. Additionally, the abundance, composition, and distribution of radionuclides (U, Ra, ^{206}Pb, ^{207}Pb, ^{208}Pb), were measured in soil and sandstone above the Denison Mines' Phoenix Deposit (located at a depth of ~450 m).

Rn was extracted from groundwater using mineral oil, and higher groundwater Rn radioactivity (average 0.13 Bq/g of water, n=10) was found in drill holes within ~100 meters of the Phoenix Deposit's surface projection than in distal holes (average 0.072 Bq/g of oil, n=4). High Rn radioactivity is independent of the drill holes' intersection with U ore, indicating that drilling did not transport significant amounts of Rn or parent isotopes to shallow depths. The water table is commonly within the Dunlop Member of the Athabasca sandstones, and groundwater Rn is positively correlated with average U concentrations obtained by modified aqua regia digestion of sandstones (analytical code 2AMS at the Saskatchewan Research Council) and also positively correlated with U in three-acid digestion of sandstones (analytical code 3AMS at the Saskatchewan Research Council). Diffusion models show Rn cannot travel significant distances, and so Rn is likely produced in MFd from the in-situ decay of U and Ra.

^{226}Ra radioactivity was measured for B horizon soil samples (n=39) and sandstone samples (n=20) after a HCl leach followed with $BaSO_4$ precipitation. An extraction efficiency for Ra of 28.2%±3.8%. was determined by comparing the soil $BaSO_4$ precipitation procedure against unprocessed soils. Ra radioactivity in B horizon soil is lower than expected from U contents determined with INAA. Ra radioactivity is comparable to the values expected from INAA U concentrations (n=17) in sandstone, with exception to 4 Dunlop Member samples and 2 samples in the Read Formation and Bird Member. Ra in 4 of 5 samples in the Dunlop Member are 10-50% overabundant, perhaps resulting from Ra percolating downwards from soil. The proposed interpretation is consistent with lower than expected Ra radioactivity of B horizon soil. Ra is 260% and 420% overabundant in the two samples from the Read Formation and the Bird Member (1 each), suggesting upward migration of Ra from the U deposit. Low solute concentration and a neutral-weakly alkaline pH of shallow groundwater in the study area appears to prevent significant travel of Ra ions through groundwater by means of ion absorption competition.

Pb isotopic compositions were determined using an ICP-MS for sandstones and soil via three different leaches; 0.02 N HBr, 2.7 N HCl, and concentrated HBr. Overall, Pb isotopic compositions of MFd (n=5) and B horizon (n=10) are similar, supporting the percolation of acidic surface waters through soil. One sample from RD (among 4 samples) show high ^{206}Pb, suggesting an upward migration of ^{206}Pb from the deposit.

The ratios of $^{4}He/^{3}He$ in ground water ranged between 0.95-1.07; typical of groundwater-atmosphere interaction. The lateral flow of groundwater at deep levels can explain the absence of higher $^{4}He/^{3}He$.

Acknowledgements

This thesis is the culmination of two years of work by the author, but also from great assistance from several notable individuals and organizations. Field work and lab work were funded by the Targeted Geoscience Initiative-4 (TGI-4) grant to Dr. Keiko Hattori. Denison Mines provided logistical support during field work, as well as continued assistance through the two years by providing information to the author when needed. Chad Sorba was the primary contact for assistance at Denison Mines.

In addition to samples collected by the author, samples collected from past students were also used and are features of this study. Dann et al., in 2012 collected sandstone core samples from Denison mines, a subset of 20 were used in this study. Power (2013) collected soil samples from Denison Mines' Wheeler River property, of which 51 were used in this study and an additional 49 were used for the data Power (2013) acquired.

This two-year project has benefitted significantly from expertise in both knowledge and practice from a wide range of people. Mary Devine provided sampling expertise and guidance during field work, lab assistance, and later analytical assistance to the author prior to her completion of her own master's degree. Shishi (Chris) Chen and Ian O'Connell provided field assistance, and Chris later provided statistical know-how when the author needed it. All three of them shared in the duties and responsibilities with the author associated with the shared field season in 2014.

Several professors at the University of Ottawa have helped this study as well. Dr. Jonathon O'Neil provided support to the author during lab procedures taking part in the dedicated clean lab, and taught the author how to use the Milli-Q water dispenser – a device surprisingly complicated given its purpose. Dr. Jack Cornett helped significantly regarding the Ra procedure, processing, and interpretation of the data. He coordinated the transfer of samples to Trent University, was committed to ensuring the author understood the nuanced details of gamma spectrometry, and was a pleasure to work with.

Actual lab procedure was conducted and helped by lab technicians at the University of Ottawa and at Trent University. Monika Wilk-Alemany (University of Ottawa) directed tritium associated lab work, conducted the He analysis, and analysed the author's samples for Rn concentrations with assistance from Mary Devine. Monika ensured that all steps of the procedure were understood by the author, provided help continuously and readily, and she provided needed encouragement to the author at the start of the project. Deuterium, and O isotope samples were analysed in the G.G. Hatch Stable Isotope Laboratory by Paul Middlestead, Wendy Abdi, and Patricia Wickham (University of Ottawa) – all three of which assisted the author in understanding the lab procedure and helped later with the odd request. Pb isotope work as well as major groundwater chemistry was supported and later analyzed by Dr. Nimal DeSilva, Pingqing Zhang, and Smita Ping (University of Ottawa). All three were enormously helpful with continued assistance through the two years, and Nimal specifically helped explain the procedure of ^{204}Hg corrections for Pb isotopes to author on more than one occasion. Wei Wang from Trent University not only received and sent the Ra data, but also ran the gamma spectrometer at Trent for all 59 of the author's samples – at up to three days per sample, it was no small contribution.

Successfully completing a master's project and the associated thesis not only relies on lab and scientific support, but also requires mental well being and emotional encouragement. The author was a teaching assistant for Dr. Simone Dumas and Claude Farley for the introductory Earth Materials course on two occasions, and was also a teaching assistant for Dr. Jack Cornett for the introductory Earth Systems

course also on two occasions. Teaching, lecturing, guiding the students, even the endless marking, and working with the professors was the most enjoyable aspect of being a master's student. It will be missed.

Lastly, Dr. Keiko Hattori provided uncountable hours reviewing drafts for posters, presentations, and this thesis. Keiko also assisted in the field, directly supervised lab work and taught many lab procedures as well as proper lab "etiquette" to the author. She was the supervisor for this project. Most importantly she pushed the author from a coasting undergraduate attitude to one of complex consideration and hard work.

Table of Contents

List of Tables

List of Figures

List of Abbreviations and Short Terms

2AMS	2 acid digestions, modified aqua regia digestion, utilizing concentrated HNO_3 and HCl in a hot water bath at Saskatchewan Research Council (Roscoe, 2012)
3AMS	3 acid digestions, utilizing concentrated HF, $HClO_3$, and HNO_3 in a hot block at Saskatchewan Research Council (Roscoe, 2012)
1F	Ultratrace aqua regia digestion performed by Acme Analytical Labs
DPX	The sample labels applied to sandstone samples collected by Jack Dann (2012)
INAA	Instrumental Neutron Activation Analysis
Medium Leach	15 ml of 2.7 N HCl to leach 0.5 g of sample at room temperature
MF	Manitou Falls Formation
MFb	Manitou-Falls Formation Bird member
MFc	Manitou-Falls Formation Collins member
MFd	Manitou-Falls Formation Dunlop member
PHX	The sample labels applied to soil samples collected by Michael Power (2013)
RD	Read sandstone formation. Formerly known as the MFa sandstone member
SLE	Acetate leach with a pH of 5, performed by Acme Analytical Labs (Power, 2013)
SLM	0.1 M hydroxyalamine leach, performed by Acme Analytical Labs (Power, 2013)
Strong Leach	1 ml of concentrated HBr to leach 0.5 g of sample at 90°C overnight
Weak Leach	15 ml of 0.02 N HBr to leach 0.5 g of sample at room temperature
WR	The drill hole label used by Denison Mines for all drill holes, also used for groundwater samples collected by the author

Introduction

Preamble

In May of 2013, Fission Uranium Corp announced the discovery of 6 Rn anomalies from a survey extension on their Patterson Lake property (Fission Uranium Corp., 2013a). In July, Fission had begun vertical drilling of the anomaly and in August announced multiple zones of mineralization between 122.5 m – 318.5 m. The most U-rich zone was at a depth greater than 200 m (Fission Uranium Corp., 2013c).

Power (2013) found high ^{4}He ($^{4}He/^{22}Ne_{ASW}$ >100) in groundwater from drill holes within 900m of the Millennium Deposit's surface projection. The Millennium Deposit is approximately 750m below surface. Devine (2016) found high Ra (<32.2 pg/g) along vertical fractures within sandstone above the McArthur Deposit. The McArthur Deposit is located approximately 500m below surface.

At 450 below surface, the Phoenix Deposit is less than half the depth of the Millennium Deposit, and a comparable depth to both the McArthur Deposit and the Rn-anomaly identified Patterson Lake mineralization. Given these recent discoveries of how groundwater and sandstone chemistry and composition have been affected by U-ore vertically below, the choice was made to sample primarily above the Phoenix Deposit, within 1 km of the surface projection.

Why is Uranium Important?

In 2015, 8% of global energy supply came from nuclear power (International Energy Agency, 2015) and 4% of energy within Canada is nuclear, with the majority being produced in Ontario (Natural Resources Canada, 2015) where over 50% of generated energy is nuclear. Significant growth of the nuclear industry in both energy production and new technologies is planned to occur throughout Asia, Europe, the Middle East, and the United States.

Growth will fuel continued production and exploration for uranium. Many countries have planned nuclear industries and most will be dependent for supplies of nuclear fuel. In addition, with global climate change becoming an increasing concern, nuclear power represents the most currently viable source of variable output energy. Given current trends, nuclear power is forecasted to provide a 13% emission reduction globally by 2050. (International Energy Agency, 2015)

Objectives

Rn and He are decay products of U and both occur in a gas phase, potentially allowing for easy transportation from a given source. However, these two elements differ in two important ways; ^{222}Rn has a short half life of 3.82 days and is produced only once within the decay series of ^{238}U, whereas ^{4}He is produced twelve times (alpha particle emission) during a single decay sequence and does not decay. The relatively short half life of Rn limits its travel and makes detection of Rn qualitatively more significant than He. Rn's relationship with U has resulted in extensive past use in the search for shallow uranium ore bodies (Dyck, 1980). However, to apply these elements to the future exploration of deeply buried U (hundreds of meters), further understanding of Rn and He's sources and transportation mechanisms is crucial. Thus, the first objective of this study was to determine the location that Rn is produced.

Figure 1: ^{238}U decay chain

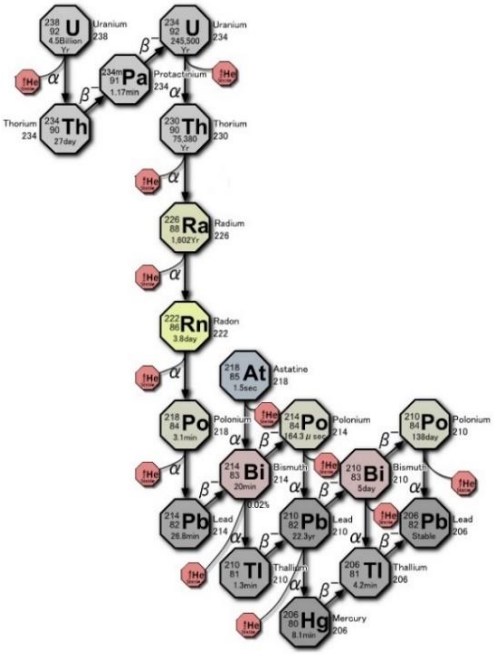

U-238 decay chain modified from © Tosaka/Wikimedia Commons /CC-BY-SA. 3.0. Figure 1:

Two hypotheses were evaluated; Rn at surface could be the result of the direct transport/movement of Rn nuclei, or a complex movement of Rn and its parent isotopes. One such parent is Ra. Thus, the second objective was to measure and describe the relationships between Rn and Ra, as well as Ra and U, and to understand how Ra behaves in the environments above the Phoenix deposit.

Because Rn and Ra are both short lived radionuclides relative to the age of the Phoenix deposit and surrounding geology, Rn and Ra provide a transient view of the environment above the Phoenix deposit. Pb, and its stable isotopes 206, 207, and 208, are the end products of the ^{238}U, ^{235}U, and ^{238}Th decay sequences respectively. ^{206}Pb and ^{207}Pb in sandstones have been spatially correlated to deeply buried U deposits in previous studies (Holk et al., 2003 studied Cigar Lake) (Bonham-Carter and Hall, 2010b). Thus, one of the objectives of this study was to analyze the Pb isotopic compositions of the sandstones and soils above the Phoenix deposit, and investigate any relationship with the deposit and other nuclides.

Thesis Outline

This thesis contains nine sections. The introduction describes the purpose of this research, previous research that has been done concerning Rn and the study area, and briefly outlines contributions of the author.

Research Area is subdivided into Regional Geology, Quaternary Geology, Regional Climate, and lastly the Study Area. The section, Regional Geology, provides an overview of the formational history of the Athabasca Basin, specifically the deposition of the Read and Manitou-Falls Formations. Quaternary Geology briefly describes the last glacial maxima and the results thereof on the environment. The section,

The Regional Climate, describes the ecological and meteorological environment in which samples were taken from, and is relevant to the discussion of groundwater. Lastly details on the Phoenix Deposit and the associated Denison Mines' Wheeler River property itself are reported.

The proceeding Samples section describes the sampling strategy used by the author, as well as by previous students whose samples were also used in this study. The Laboratory Procedures describes how samples were prepared, where necessary digested or leached, and discusses the accuracy, precision, and efficiency of the Pb and Ra experiments. The Laboratory Procedure also describes, where relevant to discussion, the procedures of professional lab services. The Analytical Methods sub-section elaborates on corrective measures applied to data, specifically Ra radioactivity and Pb isotopic compositions.

Results are then presented with interpretations. Outlying points, and possible causes are also described here. The Conclusion is the summary of the findings of the study.

Appendices I through III, and V, can be found in associated files, and Appendix IV at the end of this paper.

Contributions of the Author

In this study, groundwater samples and measurements, soil gas measurements, and groundwater gas samples were collected by the author from above the Phoenix deposit. This study measured Rn, Ra, U, and other element concentrations within groundwater above the Phoenix Deposit, as well as Pb isotopic compositions for both soil and sandstone samples. All sample preparation (groundwater chemistry, soil Pb isotopes, sandstone Pb isotopes, soil INAA, sandstone INAA) and lab procedures were conducted by the author unless otherwise noted. INAA analysis was conducted by Actlabs in Ancaster, Ontario. Analyses of results were also performed by the author.

The results of this research were presented at three conferences (included in Appendix I). Poster presentations were provided at the Saskatchewan Open House in 2014, and the Prospectors & Developers Association of Canada Minerals Colloquium in 2015. The Saskatchewan Open House poster was revised and edited and later published as an open file report (Dudek and Hattori, 2015). Lastly a seminar was given by the author discussing the most recent findings at the Advances in Earth Sciences Research Conference early in 2016.

Previous Research and Exploration

Modern U exploration has relied increasingly on geophysical techniques (Jefferson et al., 2007a). Airborne electromagnetic surveys, gravimetric surveys, resistivity surveys, and additional audiomagnetotellurics methods have provided an unprecedented ability to explore larger scale than is commonly possibly with geochemical approaches. However, geophysical approaches towards U exploration generally target graphitic conductors, but not all U deposits are associated with graphite and not all such conductors are associated with U deposits (Alexandre et al., 2011). Not all graphitic lenses and layers in the basement rocks can be drilled, thus new geochemical approaches would be beneficial for exploration.

The first U exploration into the Athabasca Basin relied heavily on surface radioactivity (from Rn, Ra, and U decay) and resulted in the first discoveries along the rim of the Athabasca Basin (Rabbit Lake and Key Lake deposits) and in the uplift zone around the Carswell structure (Cluff Lake deposit) (Jefferson et al., 2007a). This approach of studying surficial radioactivity later evolved into measuring and contouring

Rn gas emission from soil and groundwater, done with the assumption that it related to underlying U deposits (Dyck, 1980). However, because of Rn's short half life, deeply buried U deposits should not produce surficial anomalies of Rn without a special transportation mechanism (Pereira, 1980). Thus, use of Rn as an exploration tool has yielded mixed results (Jefferson et al., 2007a).

He has also been used with mixed results for U exploration. High He concentrations in groundwater could originate from underlying U deposits, but long residence times and slightly radioactive rocks can also produce high He concentrations and false-positives (Butt & Gole, 1986). The March Formation (a sandy limestone/dolomite), which also produces anomalous Rn, and the Rockcliffe formation (grey-green shales and sandstone) both in the Ottawa area, result in high He (Dyck, 1976). Subsequently, Dyck (1976) noted that high He, without knowledge to the underlying geology, is entirely meaningless. Successful accounts of He's utility as a prospecting tool are lacking in literature. However high groundwater He concentrations have been linked to previously discovered U deposits in many areas including the Elliot Lake area (Dyck, 1976), the uraniferous Witwatersrand conglomerates (Bowie, 1958), and two U mines within the former USSR (Shukolyukov and Tolstikhin, 1965 as cited in Dyck 1967). High abundances of He are linked to underlying deposits include Power (2013) and Devine (2016) for the Millennium U deposit (800 m depth).

With higher demand for U, exploration is required to proceed to deeper depths within the interior of the Athabasca Basin, which promotes research into understanding the chemical exchange between groundwater and deposits (such as Leybourne and Cameron, 2007), and effects on overburden.

Concerning the use of groundwater chemistry in exploration, the results have again been mixed with a few successful cases relating U deposits and groundwater chemistry such as the Oakville Sandstone (Texas), the Wasatch Formation (Wyoming) (Langmuir & Chatham, 1980), but its practicality as an exploration tool is still questioned (e.g., Jefferson et al., 2007a). To attempt to define groundwater chemistry's utility, Earle and Drever (1983) surveyed groundwater across the Athabasca Basin, and found that U, Ra, Rn, and He could be used with an approximate 60% success rate for finding buried deposits within 100 meters of groundwater sample sites – though the threshold distance in which dilution would prevent this style of prospecting was left undefined due to sampling restrictions. Jefferson et al. (2007a) considers the Athabasca group sandstones to be too permeable and groundwater flow is too unconstrained, whereas Leybourne and Cameron (2007) concluded that U was the most useful pathfinder element in groundwater and recommended additional research into U decay-series isotopes (including radiogenic Pb) in groundwater research.

Two additional studies concerning the application of groundwater chemistry to U exploration are also worthwhile mentioning; Giblin and Snelling (1983) found signatures related to U mineralization in groundwater but only in close proximity to the Pine Creek Geosyncline (Australia) deposit whereas Singh et al. (2002) found geochemical spatial gradients indicative of U mineraliation on an area up to 36 km^2 around the Koppunro-Dwarkapuri deposit and a 25 km^2 area around the Julakallu deposit (both in India).

In support of the applicability of groundwater study in U exploration, Bonham-Carter and Hall (2010a) proposed that material in the sandstones could dissolve into groundwater and be transported upwards and concentrate into plant roots, eventually to be incorporated into organic-rich humus soils. Bonham-Carter and Hall (2010a) continued to find anomalies of ore-related elements in soils above the Cigar Lake and McClean Lake deposits, and in addendum (Bonham-Carter and Hall, 2010b), found high $^{206}Pb/^{204}Pb$ and $^{206}Pb/^{207}Pb$ in soil were good predictors for the locations of underlying ore, with the best

predictive abilities within humus (A horizon soil). However, Bonham-Carter and Hall did not examime Pb isotopic compositions for B or C horizon soils. Power (2013) and Krahenbil et al., (2014) explored potential near-surface expressions of the Phoenix and Millenium deposits in the soils (including humus), and had found high ^{4}He in groundwater above the deposit. Devine (2014) found high Ra along vertical fractures in sandstones above the Millenium Deposit, suggesting upward migration of Ra.

Studies such as Earle and Sopuck (1987) supported the investigation of alterations in sandstones; observing that alteration processes, not primary composition, dominate the geochemistry of the Athabasca sandstones. Alteration minerals associated with the mineralization include illite, dravitic tourmaline, alumino-phosphate sulphate minerals (APS), and desilicification (Adlakha and Hattori, 2015). Cocurrent with this study, Chen (2017) applied principle component analysis to the composition of the sandstones above the Phoenix Deposit finding the largest variability in U concentration was associated with REEs, Y, Cu, B, Na, Mg, Ni, and Be. Chen (2017) also found that Pb isotope compositions were similar to expected (as calculated from concentrations of U, Th, and Pb) except for high radiogenic Pb close to the Phoenix Deposit. In other deposits, haloes of anomalous U can be commonly traced vertically through entire sandstone packages, even when thicknesses are in excess of 500 meters regardless of alteration extent (Earle et al., 1989; Jefferson et al., 2007a). Such U haloes are associated with mineralization, as well as later fault reactivations causing redistribution of previous alteration (Wheatley et al., 1996).

In addition to the exploration techniques and findings mentioned, this study has made use of and has been influenced by other studies. Continued study into geochemical expressions of U deposits would be beneficial to reduce the reliance of modern U exploration on geophysical approaches as to distinguish from geophysical false positives and to discover U ore where traditional geophysical anomalies aren't present.

Research Area

Regional Geology; The Athabasca Basin

The Athabasca Basin is one of several uraniferous Paleoproterozoic/Mesoproterozoic sedimentary basins in Canada and the world. It is located in Northern Saskatchewan and Alberta. The Athabasca Basin is believed to have originated as a tectonic escape structure associated with the convergence of the Slave and Superior provinces, Taltson/Thelon magmatic zone (1.9 Ga), and the Trans-Hudson orogeny (1.8 Ga). Since initiation of deposition the basin has been compressed significantly, though an exact compression factor remains uncertain. (Jefferson et al., 2007b)

The Athabasca Basin is filled with the Athabasca Group siliciclastic sequences unconformably overlaying peneplaned Churchill Province-Paleoproterozoic granulite facies metamorphic rocks. Majority of U deposits within the Athabasca Basin are located along this unconformity with many notable mines at the contact of the basement Mudjatik and Wollaston domains. The contact between these two domains has undergone frequent reactivation and remains in a weakened state. (Jefferson et al., 2007b)

The Athabasca Basin has experienced significant structural shape changes resulting from crustal flexures, faulting, and weight of sedimentation during its formation. Because of these changes in shape, four primary deposystems have formed; Moosonees, Ahenakew, Karras, and Bourassa (Figure 2). All four systems are composed of upward fining fluvial arenites with various other minor siliciclastic sediments interbedded. Most variation in primary composition occurs near the base of the sediments; with redbeds, mudstones, and the rare marine sequence being present, though occasional marine sequences are also present at lower depths. (Jefferson et al., 2007b) (Ramaekers et al., 2007)

Figure 2: Deposystems of the Athabasca Basin

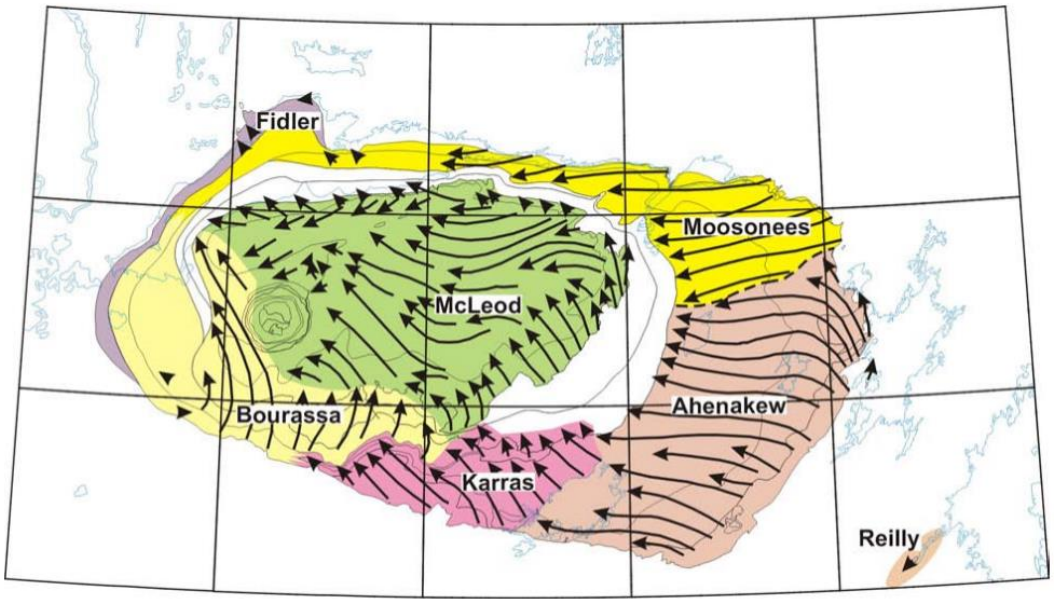

Map of the Deposystems within the Athabasca Basin. (Ramaekers, Yeo, & Jefferson, 2001)

Of interest in this study are sandstone sequences of the Read and Manitou-Falls formation within the Ahenakew deposystem. The exact timing of the deposition is still debated, but is generally considered

to have terminated around 1.5 Ga (Rainbird et al., 2007). In order of deposition are the Read formation (previously known as the Manitou-Falls A member), Bird member (MFb), Collins member (MFc), and Dunlop member (MFd) in the south-eastern Athabasca Basin.

The Read formation (RD) is a 25% quartz arenite sandstone, with significant interbeds of pebbly sandstones, red siltstones, redbeds, and mudstones. Mudstone sections are composed of irregularly compressed sand-filled desiccation cracks and intraclasts. Mudstone and siltstone interbeds are limited to the lower-most levels of the facies. The entire sequence is dominated by low-angle cross-bedding and disseminated pebbles. Red oncoids (similar to stromatolites but form spherical structures instead of columnar forms) are common at the base of the formation. (Ramaekers et al., 2001) Rare marine sequences have been identified above select redbeds (Jefferson et al., 2007b).

The MFb is primarily a quartz arenite with a minor clay matrix (1-3%), though was originally sublithic or subarkosic before diagenesis. Conglomerate (30% of clasts >2 mm with bed thickness >2 cm) interbeds are scattered throughout the sequence in low abundance (>2%). Hematitic and quartz overgrowths on grains are common. (Ramaekers et al., 2001)

The MFc is also primarily a quartz arenite, though one-clast thick pebble beds, scattered pebbles, and clay intraclasts are common. The primary difference between the MFc and MFb beds is the lower abundance of conglomerate (<2 vol.%) in MFc. Purity of the MFc varies subtly between different deposystems, with dirtier sandstones present in the Moosonees, and well sorted pure arenites in the Bourassa. (Ramaekers et al., 2001)

The MFd is predominantly found with the Ahenakew deposystem, and is a medium to fine quartz arenite. It has a greater abundance of clay and mud intraclasts than the MFc member, but a near absence of pebbles. (Ramaekers et al., 2001)

Diagenesis of the Athabasca Group occurred shortly after deposition and is considered to have been hot; temperatures around 200 C. Generally, the basin and its sediments have experienced little alteration or deformation, though evidence of episodic potassic alteration associated with feldspar hydration, thorium alteration, and silicification have been identified. (Ramaekers, Yeo, & Jefferson, 2001)

Basement faults, are deeply traceable within the basement and frequently splay out through the overlying sediments. Although these faults were originally ductile, they have undergone frequent brittle reactivation with offsets of 10s to 100s of meters, for cumulative offsets up to tens of kilometers within the basement. (Jefferson et al., 2007b)

Quaternary Geology

Overlaying the sandstones and basement is a layer of sediments originating from the last glacial maximum (Wisconsinian) as till. After the glaciers retreated, the till has been reworked by rain and river action, as well as biologic activity in the spanning 8200 years (Schreiner, 1983). The combined thickness of the till and soils in surrounding Denison Mines' Wheeler River property varies between 0 m (exposed sandstone or basement which account for 5% of area) up to 120 m (Schreiner, 1983), (Roscoe, 2012). Above the Phoenix Deposit thickness is approximately 10 – 30 m thick. Understanding the last glacial maximum in the region is critical for the discussion of soil and water geochemistry. Such insight has also proven to be economically valuable; boulder trains and lake sediment were used for the initial discovery

of U deposits in the Athabasca Basin, and soil geochemistry has continued to be an important part of many exploration programs (Bonham-Carter and Hall, 2010a).

The path of flowing glacial ice can be determined based on striations in bedrock, drumlins, and other land morphology. In the eastern half of the Athabasca Basin, glacial flow can be generalized as being towards the south south-west.

Figure 3: Wisconsin ice flow direction above the Athabasca Basin

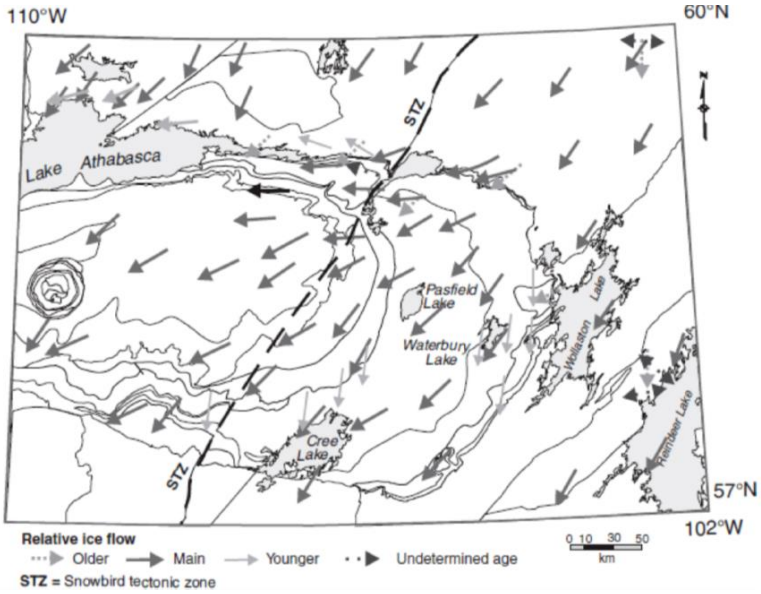

Ice flow directions during the last glacial maximum across the Athabasca Basin from Campbell, 2007.

Regional Climate

The location is composed of boreal forest with interspersed glacially smoothed rocky outcrops. Approximately 5%-10% of the region is composed of wetlands (Natural Resources Canada, 2009) and receives 601-800 mm of rainfall annually (Natural Resources Canada, 2009). During the two week stay at Wheeler River camp there was one significant rainfall. Temperatures vary between 32°C in the summer and -45°C in the winter (Roscoe, 2012), while on site temperature never exceeded the high 20s. No significant wind was noted during the field work, nor permafrost. The region has prominent B soil horizons and all horizons are relatively acidic (pH of 4.5 to 5.5), subsequently classified as dystric-brunisols (Schreiner, 1983).

Study Area; The Phoenix Deposit and Denison Mines' Wheeler River

Phoenix Ore Body

Figure 4: Location of the Phoenix Deposit

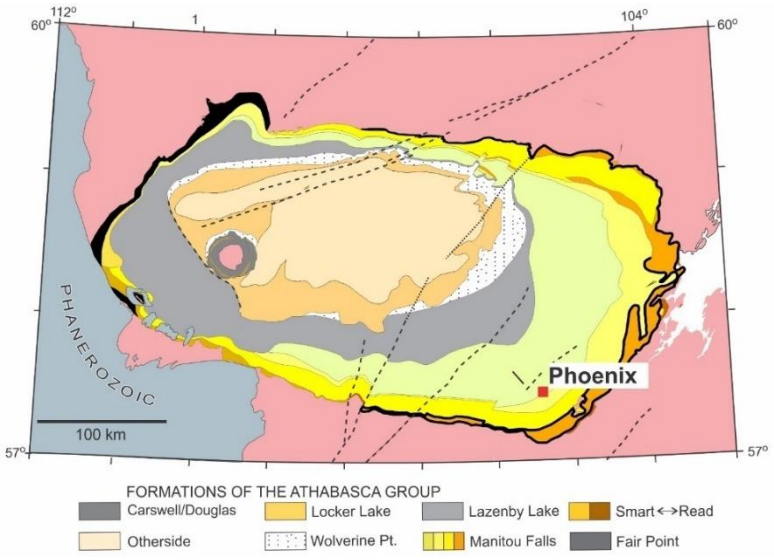

Diagram modified after Jefferson et al. (2007a)

The Phoenix deposit is located near the south-east margin of the Athabasca Basin (Figure 4) within Denison Mines' Wheeler River property. Denison Mines owns 60% of the venture, Cameco Corporation owns 30%, and JCU (Canada) Exploration Company Limited owns the remaining 10% (Roscoe, 2012). The deposit is approximately 450 meters below surface along the unconformity between sandstones and the metamorphic basement and forms a one-kilometer north-east trending series of ore bodies, making it an unconformity type uranium deposit. The Phoenix deposit has a combined resource of 71.3 M lb U_3O_8 with an average concentration of 19.1% (Denison Mines, 2016).

Figure 5: Basement geology surrounding the Phoenix Deposit

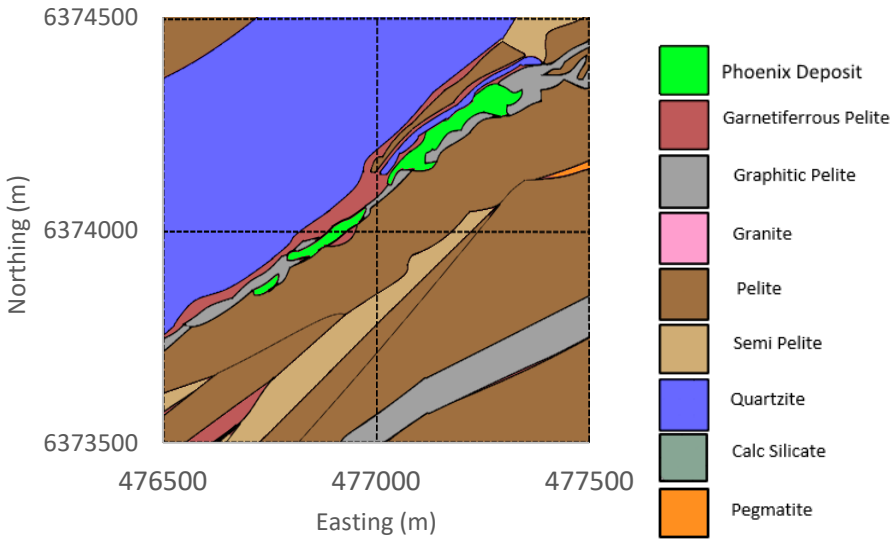

Simplified map of the basement geology surrounding the Phoenix deposit (green), edited from a map provided by Sorba at Denison Mines. UTM Projection WGS 84-13N.

Details on Drilling

Diamond drilling by Denison Mines' within the Wheeler River property has been ongoing since 2005. Core size varies between NQ (47.6 mm in diameter) and HQ (63.5 mm in diameter) dependent on drill hole and depth. Majority of drill holes are sub-vertical. (Roscoe, 2012)

Drill holes have metal casings that extend from the drill collar (or slightly above) to varying depths through the till into the MFd sandstone. Length of casing is partially dependent on till thickness. Drill hole information can be found on page 11.

Local Topography and Hydrology

The surface projection of the Phoenix Deposit is located on a shallow topographic saddle point between three hills; a hill to the west, north, and south-east with deeper valleys between each hill (Figure 6). Changes in relief between the hills and the average height of the surface projection is only 100-150 meters per kilometer. Most lakes in the immediate vicinity have no obvious stream inlet and thus are likely fed by groundwater, with exception to the large lake to the east (Figure 6). The river that passes through the Wheeler River property flows from west to east, eventually to flow south out of the map-frame (Figure 6).

Figure 6: Subsection of the topographic Wheeler River property map

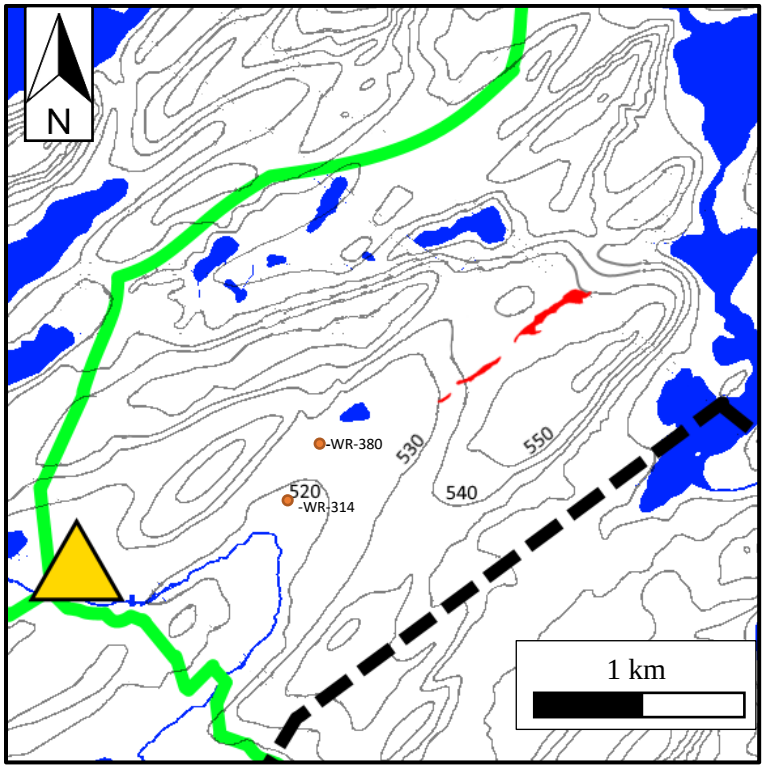

Surface topography of the area surrounding the Phoenix Deposit surface projection, edited from Roscoe, 2012. Contours are every 10 meters above sea level, with four height markers for reference. Phoenix deposit's surface projection is red, roads are green, the yellow triangle is Denison Mines' Wheeler River Camp, dashed line is the edge of the Wheeler River property, lakes and rivers are blue, contours are grey. Contour labels are provided near the surface projection. Approximate locations of WR-314 and WR-380 are included for future reference.

Sample Overview

In June 2014, the author collected approximately 3 liters of groundwater from sixteen diamond drill holes. Rn abundances in groundwater was measured with three different procedures; direct water sample, oil extraction, and oil-based gas diffusers. Among the sixteen holes, seven holes were sampled for He via gas diffusion samplers. Gas diffusion samplers were lowered until the samplers audibly hit the static water level or a change in buoyancy was felt on the line, and then samplers were lowered for an additional meter or two to make sure that the samplers were in water. Only the diffusion sampler from WR-314 didn't pass its drill hole's casing. Additionally, all sixteen holes were sampled for the concentrations of tritium, cations (Ca, K, Mg, Na, Pb, Th, and U), anions (F, Cl, and Br), D/H, 18O/16O, and the concentration and isotopic compositions of dissolved inorganic and organic carbon (DIC, DOC respectively). Of the three liters taken per hole, one liter of ground water was taken for future use. Unless otherwise noted, all samples were taken within 2 m below the water table. While on site, the pH, redox potential, and conductivity of groundwater was measured along with the height of the water table.

The depth to the water table varies significantly above the Phoenix Deposit, from water present at surface (WR-314) to depths of 41 meters (WR-439). Drill casing lengths, for the holes sampled from, vary between 13 meters to 34 meters. Below is a table listing the groundwater samples that were taken from within the casings, and the distance to the end of the respective casings.

Table : Depths to water table, end of casings, and to MFd

Sample	Water Table Depth (m)	Casing Depth (m)	Depth to MFd (m)
WR-396	22.4	25.5	21
WR-312	20.3	25.5	33.8
WR-314	0.5	30.4	10
WR-380	3.4	25.5	8.6
WR-403	21	24	15

All water samples were taken within the upper 2 meters of groundwater. Casing lengths were provided by Denison Mines.

Because of the surface topography, the location of the static water level relative to the underlying geology varies significantly in the study area. For holes above the Phoenix deposit, the water table was within the MFd sandstones. Holes WR-314 and WR-380, which are to the south-west of the deposit (Figure 6), the water table was within the soil or the till respectively, but the casings extended downwards into the MFd sandstone member. Hole WR-312, just to the north-east of the surface projection of the deposit, had a water table within the till, and the casing did not go deeper than the till (refer to Table 1).

Unfortunately, several samples lost labels during shipping back to the University of Ottawa. Of the sixteen samples collected for dissolved inorganic carbon (DIC) and dissolved organic carbon (DOC) analysis, only 7 had legible labels. The water based Rn samples shipped to Université du Québec à Montréal suffered the most with partial or full loss of most labels. Consequently, values of Rn based on the oil-extraction method are used dominantly in this study. Only three water based Rn values are presented in this study, and are used for the depth profile of WR-314.

Locations of Samples

Figure 7: Sample sites by project above the Phoenix Deposit

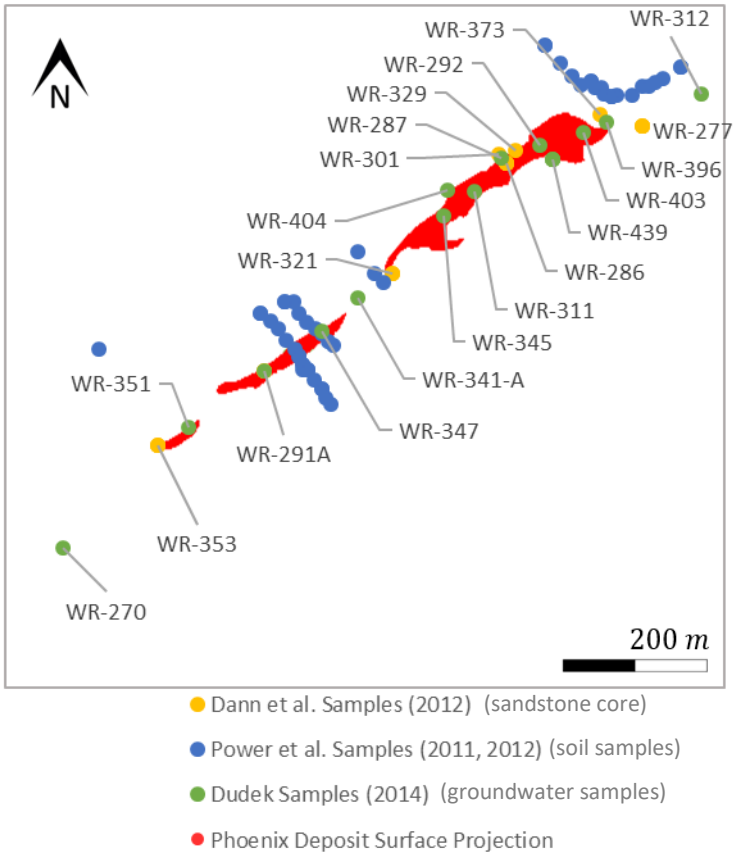

Only samples used in this study are featured above. Dann et al., (2012) sampled drill core, and so the drill collars are labeled above. Dudek et al., (2014) samples are groundwater from drill holes, and so drill collar labels are provided. Power (2013) sampled soil, and soil sampling sites are provided.

Samples taken by previous students were also used in this study. Power (2013) performed several soil-sampling transects perpendicular to the main trend of the Phoenix Deposit. Of samples taken, four A-horizon and C-horizon soil samples were used, as well as forty-three B-horizon soil samples. In 2012, Dann et al, (2012) took drill core samples, and from these samples a total of 20 were used for this project (five per sandstone bed). Figure 7 shows the location of drill hole collars from which Dann et al., (2012) samples were taken. Soil and sandstone samples used in this study were chosen based on their proximity to the Phoenix Deposit's surface projection, and their previously measured Pb concentrations.

Soil Sampling

Initial sampling was conducted by Power (2013). Samples were taken along three principle transects roughly perpendicular to the last main ice flow and cross cutting the Phoenix Deposit's main north-east trend (Figure 7). Samples were taken exclusively from relatively undisturbed and dry locations. No samples were taken from marsh-lands, as wet locations do not contain humus and B-horizon soil. Furthermore, there is no marsh lands in the sampling transects (Power, 2013). Samples had been oven-dried at 60 °C overnight and sieved to -60 mesh by Power (2013). For this project, 40 samples were selected based on their proximity to the main Phoenix ore bodies for Ra extraction and Pb isotopic compositions.

Sandstone Samples

Sandstone samples used in this study were collected by Dann et al. in 2012. Samples are all drill core. The original goal of sampling was to assess the roles of faults for alteration, however systematic sampling also took place. The effects of any potential sample bias are not considered in this report.

For this study, five sandstone samples were selected per sandstone bed. Drill core were taken from the same drill holes sampled for Rn for comparative purposes, or due to relative proximity. One exception exists; sample DPX 147, an MFc sandstone from drill hole WR-284, which was chosen with intent to get a measurement of sandstone values distal to the deposit. All sandstone samples were thoroughly described by the author, and this information is available in the Appendix V (page 90).

Field Procedure

Sampling and Groundwater Chemistry

In June 2014, the author collected approximately 3 liters of groundwater from the 16 drill holes. Most drill holes had a cap and required removal before sampling. In one such case, the removal of the cap resulted in WR-314 momentarily becoming an artesian well (<1 second at height of approximately a foot and a half above land surface). Groundwater was collected using a 200-meter reel and a small capped copper pipe as a bucket. Later a small plastic laminated steel-can was used after the copper bailer was lost in a drill hole. Groundwater was stored in new 500 ml Nalgene bottles.

Water was immediately passed through 0.45 µm Millipore Sterivex^{TM} HV filter units and groundwater intended for inorganic and organic carbon isotopes was stored separately in 40 ml amber borosilicate vials with silicone-Teflon septa. No headspace was present within the vials. Groundwater intended for anion concentrations were also filtered using the Millipore Sterivex^{TM} HV filters.

Groundwater, stored in the 500 ml Nalgene bottles, to be analysed for major, minor, and trace element concentrations was not filtered. Therefore, the values are total metal concentrations in groundwater.

Conductivity, oxidation reduction potential, temperature, and pH of the groundwater were measured immediately upon sampling. Oxidation-reduction potential was measured using an ExStick (model RE300) produced by ExTech. The ExStick was initially calibrated with YSI 3682 Zobell Solution before field work by Mary Devine, and then was rinsed with distilled water between each measurement while in field. ORP values are converted to standard hydrogen electrode (SHE) values using the electrode-specific compensation value of 204.6 mV. Temperature, pH, and conductivity were all measured using a Combo pH and EC waterproof meter (model HI 98129) produced by Hanna Instruments. The combo meter was calibrated with a 1413 µS/cm solution and a pH 7 solution prior to the field season by Mary Devine and was later rinsed with distilled water between each measurement. Since the instrument was not calibrated in the field between measurements, accuracy of pH values may be in question.

Rn

Rn Oil Extraction Procedure

The method is described by Leaney and Herczeg (2006); approximately 250 ml of groundwater was taken from each drill hole and temporarily stored in Nalgene bottles. Within 24 hours, 30 ml of the groundwater was removed and replaced with 30 ml of “High Efficiency Mineral Oil Scintillator for the detection of Rn in water and soil samples” (Perkin Elmer product number: 6NE9571). The mixture of oil and water was shaken continuously for approximately 5 minutes. Using a syringe, 22ml of oil was removed from the sample and stored directly into 20 ml plastic scintillation vials. The loss of 2 ml of oil represents an approximate 27% loss in Rn content. Additionally, the fraction of Rn extracted by oil from groundwater of this sampling method was measured by Leaney and Herczeg (2006) to be approximately 43% after 4 minutes of shaking time before oil extraction. Combined with this efficiency, Rn in 22 ml of oil is approximately 55% of the total Rn in water. Reported Rn contents in groundwater have been corrected for the 45% loss as a correction factor.

Rn Water Extraction Procedure

The method is described by Lefebvre et al. (2013), where approximately 250 ml of water was stored in glass bottles and sent to Université du Québec à Montréal for analysis. Only the depth profile for hole WR-314 is featured in this study.

Rn Soil Gas

Soil gas Rn measurements were taken around two drill holes (WR-314 and WR-380, Figure 6). The two holes were chosen due to their proximity to one another (360 m apart) and similarity in elevation (515 m and 516 m above sea level) in hopes of getting comparable environments. Their distance from the Phoenix deposit was also considered; drilling pads above the Phoenix deposit extend considerably and interconnect, making nearby undisturbed forests and soil difficult to find. At both sites, two measurements were taken within 2 meters from the drill hole and on the drill pad and an additional two measurements taken in nearby non-disturbed forest and at least 10 meters away. Measurements were taken within 15 minutes of one another. Sampling used the Soil Radon Monitoring System RM-2, made by Dr. Fronka Nuclear Technology in the Czech Republic. 250 ml cylindrical ionization canisters are evacuated using a vacuum pump. A steel pipe 1.1 meters long and initially with a removable metal point is pounded into the ground with a rubber mallet to a depth of 30-80 cm. Using a tightly fitting rubber tube, a 250 ml syringe was attached to the steel pipe and the atmosphere residing within the pipe was pumped out. The rubber tube was then clamped shut. The steel pipe was lifted gently 1-2 cm to drop the metal point into the hole and open the tube to the soil gas. The syringe is then reattached to the rubber tube and 250 cc of soil gas is sucked up. The rubber tube is then clamped shut again, and removed from the steel tube and connected to an ionization canister. The valve on the canister is opened, and the clamp released. Soil gases are sucked into the canister. The canister was not disturbed for 15 minutes to allow for secular equilibrium to be reached between Rn and its daughter products. Following, the canister was connected to the electrometer using alligator clips and the results of the detection are displayed on the built-in screen. Canisters were thoroughly cleaned, their seals tested, and evacuated after each measurement, however were not reused while in field.

He

Groundwater from seven holes was also sampled for He via gas diffusion samplers. Gas diffusion samplers are made from two copper pipes 0.64 cm in diameter and up to 15 cm in length, both lengths crimped at one end. The open ends are connected by an over-fitting silicon tube which is zip-tied to the two copper pipes and then wrapped in black electrical tape. The silicon tube is filled with 3 mm and 5 mm glass beads which are trapped within the silicon tube and prevented from entering the copper pipes by two steel paper clips. The apparatus is gas permeable, but water impermeable. The method is described by Sanford et al., 1996; Sheldon et al., 2003; and Hamilton et al., 2005.

Diffusion samplers were submerged in 1-2 meters below the static water and left for more than 48 hours to allow for equilibration with groundwater. Following the 48-hour period, diffusion samplers were retrieved and the copper pipes were crimped on the silicone end to trap the diffused gases. Crimping results in a cold-weld and seals the copper piping. Sample depth was acquired by measuring the length of fishing line used to suspend them. Water level was recorded at the time of lowering.

Laboratory Analytical Procedure

Rn

Rn Oil Extraction Procedure

Oil extracted Rn was analyzed at the University of Ottawa on a Perkin Elmer 1220 Quantulus Ultra Low Level Liquid Scintillation Spectrometer by Monika Wilk-Alemany with assistance from Mary Devine. Rn decays via alpha emission to ^{218}Po and then to ^{214}Po by gamma emission, and the released energy from the decay of ^{218}Po is absorbed by the scintillant and reemitted as light detected by the spectrometer.

Rn Water Extraction Procedure

Water collected for the Rn water extraction procedure was analyzed at the Université du Québec à Montréal on a Hidex 300 SL automatic TDCR Liquid Scintillation Counter using Maxilight scintillant (Lefebvre et al., 2013).

Groundwater Chemistry Preparation

Cations

HNO_3 was added to the unfiltered groundwater samples and placed in an ultrasonic bath for up to 4 hours to free cations and particulates from the walls of the Nalgene containers. Then samples were diluted 10x with Milli-Q water. Samples were analysed for Ca, K, Mg, Na, Pb, Th, and U using an Agilent 7700 inductively coupled plasma mass spectrometry at the University of Ottawa. Masses measured were 204, 206, 207, 208 for Pb, 232 for Th, and 235 and 238 for U.

Anions

Unfiltered water samples were analysed for F^-, Cl^-, and Br^- using the ion chromatography on a DIONEX Liquid Chromatographer at the University of Ottawa.

Sandstone Sample Preparation

Samples were rinsed with Milli-Q to remove drilling mud and other detritus. Sample DPX 256 lacked structural integrity and pieces of the sample disintegrated when washed, and so this step was skipped. Samples were split lengthwise using a rock saw or manually divided. Samples were then put through a rock crusher. Sandstone was then sieved to -60 (0.25 mm) mesh for further analysis.

Procedure for Helium Isotope Compositions

Copper capsules were weighed to ensure no water had leaked in. Capsules were then loaded into a vacuum system. The cold weld is mechanically opened within the first depressurised chamber, releasing the sampled gases. The subsequent chambers contained activated charcoal or were in a liquid nitrogen bath to remove most impurities. Light noble gasses were introduced to the Helix SFT mass spectrometer in the University of Ottawa's Radiohalide and Tritium Laboratories to measure ^{3}He, ^{4}He, ^{20}Ne, and ^{22}Ne.

At the Université du Québec à Montréal, He isotopic ratios were analyzed for three diffusion samplers on a Pfeiffer HiQuad 410 quadrupole mass spectrometer in the Noble Gas Laboratory. In addition, ^{36}Ar, ^{40}Ar, ^{84}Kr, and ^{132}Xe were also measured.

Tritium Procedure

The procedure was described by Plastino et al., (2007). Samples with greater than 200 µmho/cm conductivity had 0.1 gram per 300 µmho/cm of mixed bed ion exchange resin added and were swirled for

up to four hours. Only groundwater from WR-345 had a conductivity greater than 200 µmho/cm. Samples were then decanted.

Large metal reaction cells were used for the enrichment. The metal cells are composed of an outer container which serves as the anode, and an inner cylinder which acts as the cathode and lid. 250 grams of each sample were weighed and placed in a beaker, and half of the sample was immediately poured into the metal cell. 1 g of Na_2O_2 was added into the metal cell. The cathode central column was then inserted slowly, sealed, and the outlet tub was clamped shut. The entire cell is then suspended in a freezer air-bath and wired in series and electrolyzed for several days. Samples were then drained into bulbous glass containers with stoppers.

Distillation occurs in an inverted U tube apparatus. Glass container, A, containing sample is sealed to one end of the tube and a second glass container, B, is sealed to the other end. Glass A is chilled with liquid nitrogen until frozen and the U tube is drained with a vacuum pump. Valves along the U tube are closed, and glass B is now also chilled with liquid nitrogen as glass A is heated with a heating cushion. The valves are opened, and sample is evaporated from glass A to freeze into glass B over approximately 5 hours. The salts from the enrichment procedure precipitate into glass A and are disposed. Glass B is allowed to warm to room temperature and the now-thawed sample is poured into a glass scintillation tube with 13 ml of Ultima Gold LLT (fluorescing cocktail).

All tubes are passed to the Perkin Elmer 1220 Quantulus Ultra Low Level Liquid Scintillation Spectrometer and analysis was performed by Monika Wilk-Alemany (University of Ottawa) and involved counting photon emissions from the scintillant after it had absorbed beta emissions during the decay of ^{3}H to ^{3}He with energies between 15-160 kEv. Samples were typically counted for six rounds of 1 hour each.

B Horizon Soil and Sandstone Ra Procedure

To measure Ra radioactivities, Ra was co-precipitated with Ba following the method described by Doerner & Hoskins, 1925. 20 grams of sample (soil or sandstone) were transferred to a glass beaker. Samples were reacted with 20 ml of single-distilled 6 N HCl acid at 90°C. Initial reaction lasted between 2 and 8 hours. To avoid desiccating the samples, screw-top Teflon vials were later used instead of open glass beakers. For the initially desiccated samples an additional 5 ml of single-distilled 6N HCl and 10-20 ml of Milli-Q water was added. Samples were submerged in a sonic bath for 30 minutes to loosen material from the glass beakers or the Teflon walls.

Samples were centrifuged for 10 minutes, then the resultant liquid was decanted into a new glass beaker. Distilled water was added to the centrifuge tubes and centrifuged two more times, after both rounds the fluid was decanted into respective glass beakers. 3 ml of 10% BaCl were added to each sample solution. 5 ml of 13% H_2SO_4 (prepared from Fisher Chemical Concentrate) was added to each sample, and then samples were brought to a gentle boil within a fume-hood. The resultant Ba and Ra sulfate crystals were filtered out of solution using Pall Life Sciences Metricel Membrane Filters (0.45 µm). Additional 13% sulfuric acid was added to the filtrate to check for additional residue. Precipitate and filter membranes were transferred to a single gamma-spectrometer polystyrene vial (plastic vial 1.5 cm in diameter and 8.5 cm long) produced by Sarstedt Inc. Corks were cut from a Frank's dish sponge and inserted into the vial above the filter paper and precipitate. The purpose of the sponge is to compress the filter paper to the base of the vial for greater counting efficiency and to give the samples uniform geometry. The height of the sponge and sample within the tube was noted, and total height aimed to be

consistent. A layer of epoxy-resin greater than 1 cm thick was poured over each of the sponge corks to seal the samples (Figure 8). Samples sat for three weeks to equilibrate before passing into the Ortec Hyperpure gamma spectrometer (with well-geometry, HPGe). Three photonic peaks were measured; 294 KEV and 351 KEV for Pb-214 and 609 KEV for Bi-214, all associated with the decay of Ra daughter products, and the results averaged.

Figure 8: Sample geometry for gamma spectrometry

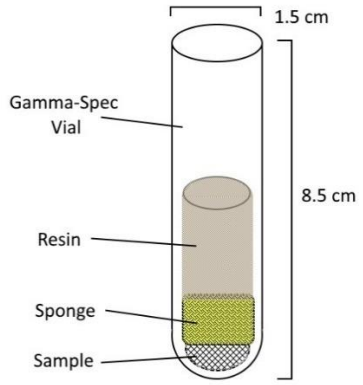

Note: Image is not to scale. No images of the vials were taken before being shipped to Trent University, ON.

Like the procedure applied to soil samples, approximately 10 g from 20 different sandstone samples were leached with 6 Normal HCl and heated to 90°C overnight within the Teflon containers. Samples were centrifuged and decanted, then rinsed twice with distilled water. Following, 6 ml of $BaCl_2$ and 13% H_2SO_4 were added to each sample, and boiled again for at least five minutes. Samples were filtered through Pall Life Sciences Metricel Membrane Filters (0.45 µm), and resultant $BaSO_4$ (containing Ra) were placed in gamma spectrometer vials and sealed with a sponge cork and epoxy and allowed to equilibrate for at least three weeks. Samples equilibrated for three weeks to ensure that the only significant Ra will be ^{226}Ra.

All vials were shipped to Trent University (ON) for counting in the Ortec Hyperpure gamma spectrometer. Due to the low radioactivity of all samples, counting time was long, ranging from 2 to 3 days. Three photonic peaks were measured; 294 KEV and 351 KEV for the decay of ^{214}Pb and 609 KEV for the decay of ^{214}Bi; all daughter products of Ra, and the results averaged.

The position that samples occupy in the vials are important because the vials are placed in a narrow tube within a cylindrical germanium crystal. Decay releases gamma rays in uniformly random directions, when one such gamma rays strikes an electron or atom within the Ge crystal, a variation in voltage and current is measured, and this is recorded. The opening from which the vial is placed represents a field of directions that gamma rays would not be detected. When the sample is compressed to the base of the vial the apparent size of the crystal opening decreases, and fewer gamma emissions are lost. When the sample sits high in the vial the angles from which gamma emissions can escape increases. Thus, maximal detection would occur for a sample infinitesimally thin.

Pb Isotope Compositions of Soil and Sandstone

Majority of procedure was carried out in a clean lab (dust-controlled laboratory). Approximately 0.5 g of sample were added to centrifuge tubes; group A. 15 ml of Milli-Q water were added to each tube,

and the solution was shaken for a minute. Tubes were centrifuged for 10 minutes, and liquid was decanted to new centrifuge tubes. 15 ml of 0.02 N HBr was added to tubes of group A, and again were shaken for a minute. Samples were left to sit overnight, and then were centrifuged again and decanted to a new group of vials, referred to as weakly leached in this report. For medium leach samples; approximately 15 ml of 2.7 N HCl were added to each tube in group A. Samples were left to sit overnight, and then were once more centrifuged and decanted to a new set of tubes. For strong leach samples; approximately 1 ml of concentrated HBr were added to group A tubes, and then heated overnight in a graphite heater to just below 90C°. No sandstone samples were analysed for strong leach. Samples were then allowed to cool, and 10 ml of Milli-Q water was added to each solution. Samples were centrifuged and decanted to a new set of tubes.

Table 2: Leach procedures terminology applied to the Pb isotope analysis

Weak Leach	Medium Leach	Strong Leach
0.5g sample in 15 ml of 0.02 N HBr, 24 hours	0.5 g sample in 15 ml of 2.7 N HCl, 24 hours	0.5 g sample 1 ml conc. HBr at 90°C, overnight

To reduce any potential interference from cations during the ICP-MS analysis, samples underwent cation separation procedure using anion resin like as described in Tatsumoto et al., 1972. For every column, 0.2 ml of a 1:1 mix of AGIx8 anion resin was added. 10 ml of 0.2 N HNO_3 was passed through each column as a rinse. Columns were conditioned with first 0.3 ml of Milli-Q water and then 0.3 ml of 0.5 N HBr. 7 ml of leachate was added to the resin. 1.5 ml of 6 N HCl was used to elute Pb. This solution was gently heated (below 90°C) until a droplet remained. Columns were rinsed with Milli-Q water, and 20 µl of the 1:1 AGIx8 anion resin was added to each column. Resin was cleaned with 1 ml of 0.2 N HNO3, and 0.1 ml of Milli-Q water and then conditioned with 0.1 ml of 0.5 N HBr. The single droplet of sample was loaded into the resin. An additional 0.2 ml of 0.5 N HBr was added and then rinsed twice with 0.1 ml of 0.5 N HBr. 1.4 ml of 6 N HCl were used to elute Pb. Following, the collected 1.4 ml was gently heated (below 90°C) and then diluted to 1% HNO_3 with a volume of 10 ml.

Samples with less than 1000 counts per second of 204 mass were removed from the data set. The method used to correct for mass interference is explained on page 21.

2 and 3 Acid Digestions for Sandstones

Sandstone samples were submitted to the Saskatchewan Research Council Geoanalytical Laboratories (SRC) by Denison Mines' from 2008-2011. For 2AMS, the sample is digested in a mixture of ultra pure concentrated HNO_3 and HCl in a screw top Teflon vial within a hot water bath, and then diluted with 15 ml of de-ionized water for the analysis with a Perkin-Elmer ICP-MS. (Roscoe, 2012)

For 3AMS, the sample is digested in a mixture of ultra pure concentrated HF, HNO_3, and HCl. Residue is then dissolved in 15 ml of 5% HNO_3 diluted with de-ionized water for the analysis with a Perkin-Elmer ICP-MS. (Roscoe, 2012)

Leach and Digestion Procedures for Soils from Power, 2013

In 2011 and 2012 soil samples (A, B, and C horizons) were submitted by Michael Power to Acme Analytical Laboratories in Vancouver, BC for trace element shortly after the samples were collected. All samples were dried at 60°C and sieved to -80# mesh before leach or digestion. This report will reference these three different procedures using the Acme Laboratories' analytical codes; SLE, SLM, and 1F.

Table 3: Outline of leach procedure codes of ACME Analytical Laboratories, Vancouver

SLE	SLM	1F
Ammonia Acetate leach @ pH 5	0.1 M hydroxyalamine leach	Ultratrace Aqua Regia

INAA Procedure for Soils and Sandstones

Soil and sandstone samples were submitted by the author to Actlabs for Instrumental Neutron Activation Analysis (INAA) to determine total U contents.

Analytical Methods

Ra

Accuracy, Precision, and Efficiency of the Ra analytical procedure

Efficiency of $BaSO_4$ precipitation for the detection of Ra

To measure the BaSO4 precipitation procedure's efficiency, 1 gram each of three soil samples (PHX-031B, PHX-213B, PHX-231B) were sealed within vials to measure Ra.

The comparison of processed and non-processed samples shows an average efficiency of 28.2% and with minimal deviation (3.8%). The relatively low efficiency accounts for the Ra within crystal phases that are not dissolved in HCl.

Table 4: Efficiency of $BaSO_4$ precipitate procedure for the recovery of Ra

Sample Name	**Unprocessed Ra Bq/g**	**Processed Ra Bq/g**	**Efficiency**
PHX-031B	$3.18 * 10^{-2}$	$7.69 * 10^{-3}$	24.1%
PHX-213B	$3.30 * 10^{-2}$	$9.47 * 10^{-3}$	28.7%
PHX-231B	$2.88 * 10^{-2}$	$9.14 * 10^{-3}$	31.8%
		Average	$28.2\% \pm 3.8\%$

Calibrating the Trent University Gamma Spectrometer

Samples were analysed on the Trent University detector, a set of three (triplicates) of BL-5 were run in addition. BL-5 has a Ra-226 radioactivity of 857 Bq/g +/- 38 Bq/g (95% confidence) (Smith & Steger, 1983). Using calibration values from the University of Ottawa's gamma spectrometer, the measured Ra radioactivity (of BL-5) averaged 1164 Bq/g (1.35x). Subsequently, all Ra counts were corrected accordingly.

Table 5: Measured values of BL-5 compared with recommended value of 857 Bq/g Ra

Sample	Ra-Radioactivity Bq/g	Uncertainty Bq/g
BL-5-1	1314	17
BL-5-2	1116	8.6
BL-5-3	1062	8.5
Average Measured	**1164**	**12**
Consensus Value*	**857**	**38**
	Correction Factor	**1.35x**

**Consensus value of BL-5 from Smith and Steger (1983) and endorsed by Natural Resources Canada.*

Precision

The precision based on the BL-5 triplicates is shown in Table 5. The three values only deviate by 12 Bq/g or within 11% of the average value, shown in Table 4 and provides a measure of reproducibility associated with the $BaSO_4$ precipitation procedure. For comparison, the entire Ra radioactivity data set has an interquartile range of 85%, significantly more variation than the measured reference materials and the efficiency values.

Table 6: Ra radioactivity of soil and sandstone population distribution

Quartiles (n=59)	Ra-Radioactivity Bq/g	% Difference from Q2*
Lower Quartile	0.014	30.1
Median	0.020	n/a
Upper Quartile	0.031	54.7
Interquartile range	**0.017**	**85%**

**Q2 is the median*

Pb Isotope compositions

Accuracy and precision of the Pb isotope analysis procedure

Pb isotopic compositions were acquired at two separate times in 2015 and 2016, and a third time for reference materials in 2016, though with identical procedure. Initial samples, referenced below as series 1, contain five B-horizon soil samples and were prepared in a Hepa-filtered fume hood in the Advanced Research Complex (ARC). Series 2, composed of soil and sandstone samples, as well as the reference materials were entirely prepared in the class 1000 ARC clean lab.

Correcting for Mercury 204 Mass Interference

To correct for mass interference, three Hg-bearing solutions with set incremental mercury concentrations were analyzed for masses 201 and 202 (Hg), and 204 (Hg and Pb) on the Agilent 8800 Triple Quadrupole ICP-MS (8800 ICP-MS) prior to samples and blanks.

The correction, aims to isolate $^{204}Pb_{total}$ on both sides of the equation, and thus involves the cancelation of all Hg related terms on the right:

$$^{204}Pb_{total} = {}^{204}(Pb + Hg)_{measured} - (^{201}Hg + {}^{202}Hg) * \frac{(^{201}Hg + {}^{202}Hg)}{^{204}(Pb + Hg)_{measured}}$$

Equation 1: Mass interference (204) full correction formula. Everything to the right of $^{204}Pb_{sample}$ will cancel out.

Simplifying the above formula by subbing in the value of the denominator obtained from the standards, and expanding on what the 204 mass measurements include (total ^{204}Pb + total ^{204}Hg) results in:

$$^{204}Pb_{total} = {}^{204}Pb_{total} + {}^{204}Hg_{measured} - (^{201}\mathrm{Hg} + {}^{202}\mathrm{Hg}) * 0.1578$$

Equation 2: Mass interference (204) correction formula with subbed in 204 factor obtained from standard reference materials.

The calculated ^{204}Hg contribution to mass 204, were low (Table 7) for samples that underwent the cation separation procedure. For the first set of samples, that underwent cation separation, the mean

^{204}Hg contribution was 0.2%. For the second set of analysis, the mean ^{204}Hg contribution was 0.1%. For the Pb isotope reference materials (JF1, JF2, and BCR2), the mean ^{204}Hg contribution was 0.1%.

Table 7: Average ^{204}Hg contribution to 204 mass peak and corrected average ^{204}Pb counts

Analysis Series	# of Analysis	^{204}Hg contribution	^{204}Pb after Hg correction	Correction
Series 1	40	9.2 cts/s	2100 cts/s	0.2%
Series 2	38	48.8 cts/s	44 000 cts/s	0.1%
Reference Materials	9	36.2 cts/s	29 000 cts/s	0.1%

Pb Isotope Analysis Applied to Reference Materials

Pb isotope compositions of three international references (JF1, JF2, BCR2) were measured on the Agilent 8800-ICP-MS. JF1 and JF2 are two feldspar samples from the Geologic Survey of Japan. BCR2 is from the Columbian River Basalt from the United States Geologic Survey. Digestion of samples and separation of Pb followed the method described on page 18.

The greatest difference is observed between the measured ^{206}Pb/^{204}Pb values and the referenced ^{206}Pb/^{204}Pb values ranging from 1.2% to 1.4% of the observed value. The difference in ^{207}Pb/^{204}Pb ratios varied between 0.45% and 0.87%. ^{208}Pb/^{204}Pb ratios differed between 0.68% and 1.1%. These differences are very small compared to the overall variation of the Pb isotope data set measured in this study. More importantly, the differences are small compared to expected difference between samples and U ore. Therefore, the data can be used to assess the contribution of Pb from the ore to sandstones and soil samples.

Table 8: Measured Pb isotopic compositions of reference JF1

Sample	^{206}Pb/^{204}Pb	^{207}Pb/^{204}Pb	^{208}Pb/^{204}Pb	^{206}Pb/^{208}Pb	^{207}Pb/^{208}Pb	%^{204}Hg/^{204}Pb
JF1-1	18.61	15.47	38.87	0.48	0.40	0.30
JF1-2*	18.70	15.49	39.43	0.47	0.39	0.10
JF1-3*	18.62	15.62	38.94	0.48	0.40	0.19
Average JF1	**18.64**	**15.52**	**39.08**	**0.48**	**0.40**	**0.20**
Tanimizu & Ishikawa, 2005	**18.42**	**15.64**	**38.81**	**0.48**	**0.40**	**n/a**
% Difference	**1.2%**	**0.72%**	**0.68%**	**0.53%**	**1.4%**	**n/a**

**Duplicate analysis of one solution*

Table 9: Measured Pb isotopic compositions of reference JF2

Sample	^{206}Pb/^{204}Pb	^{207}Pb/^{204}Pb	^{208}Pb/^{204}Pb	^{206}Pb/^{208}Pb	^{207}Pb/^{208}Pb	%^{204}Hg/^{204}Pb
JF2-1	18.79	15.40	39.41	0.48	0.39	0.03
JF2-2*	18.76	15.25	38.49	0.49	0.40	0.07
JF2-3*	18.80	15.84	39.32	0.48	0.40	0.18
Average JF2	**18.78**	**15.50**	**39.08**	**0.48**	**0.40**	**0.09**
Tanimizu & Ishikawa, 2005	**18.52**	**15.63**	**38.66**	**0.48**	**0.40**	**n/a**
% Difference	**1.4%**	**0.87%**	**1.1%**	**0.36%**	**1.9%**	**n/a**

**Duplicate analysis of one solution*

Table 10: Measured Pb isotopic compositions of reference BCR2

Sample	$^{206}Pb/^{204}Pb$	$^{207}Pb/^{204}Pb$	$^{208}Pb/^{204}Pb$	$^{206}Pb/^{208}Pb$	$^{207}Pb/^{208}Pb$	$\%^{204}Hg/^{204}Pb$
BCR2-1	18.92	15.61	39.02	0.48	0.40	0.30
BCR2-2*	19.09	15.66	39.15	0.49	0.40	0.14
BCR2-3*	18.95	15.78	39.16	0.48	0.40	0.42
Average BCR2	**18.78**	**15.50**	**39.08**	**0.48**	**0.40**	**0.29**
Woodhead & Hergt, 2000	**18.75**	**15.62**	**38.69**	**0.48**	**0.40**	**n/a**
% Difference	**1.3%**	**0.45%**	**1.1%**	**0.18%**	**0.62%**	**n/a**

**Duplicate analysis of one solution*

By comparing both the measured values to those recommended from literature (additional comparisons in Figure 9, Figure 10, and Figure 11), the greatest source of inaccuracy is associated with ^{206}Pb. The greatest loss of precision, however, is associated with ^{207}Pb. It is unknown what specifically controls these two sources of uncertainty. Measured values of $^{207}Pb/^{204}Pb$ and $^{208}Pb/^{204}Pb$are higher than the recommended values for most cases, which suggests that 204 is not properly measured. Alternatively, the interference correction was overestimated.

Figure 9: Measured vs recommended $^{206}Pb/^{204}Pb$ for JF1 reference material

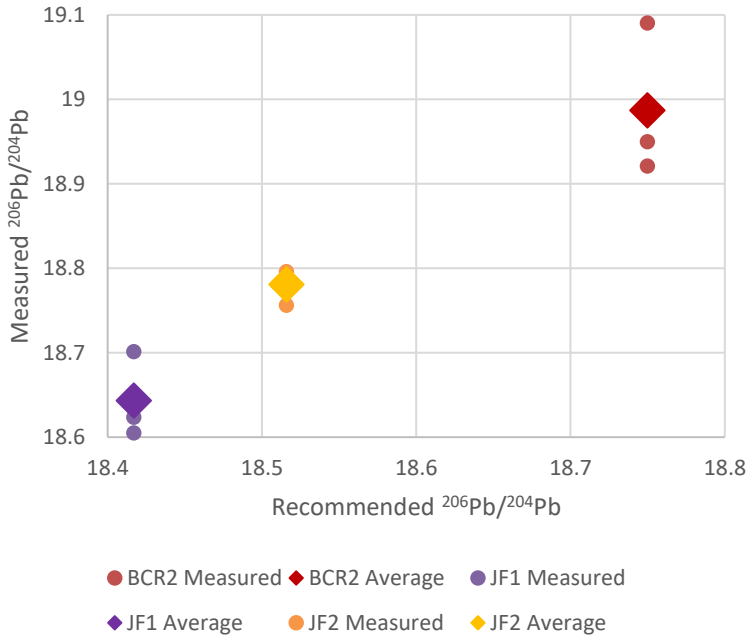

Average values (diamonds) are averages of measured values.

Figure 10: Measured vs recommended $^{207}Pb/^{204}Pb$ for JF1 reference material

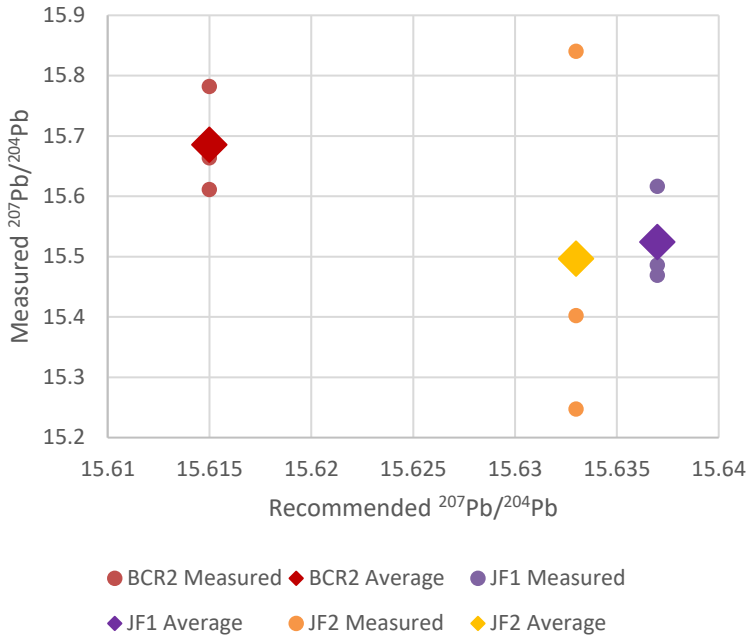

Average values (diamonds) are averages of measured values.

Figure 11: Measured vs recommended $^{208}Pb/^{204}Pb$ for JF1 reference material

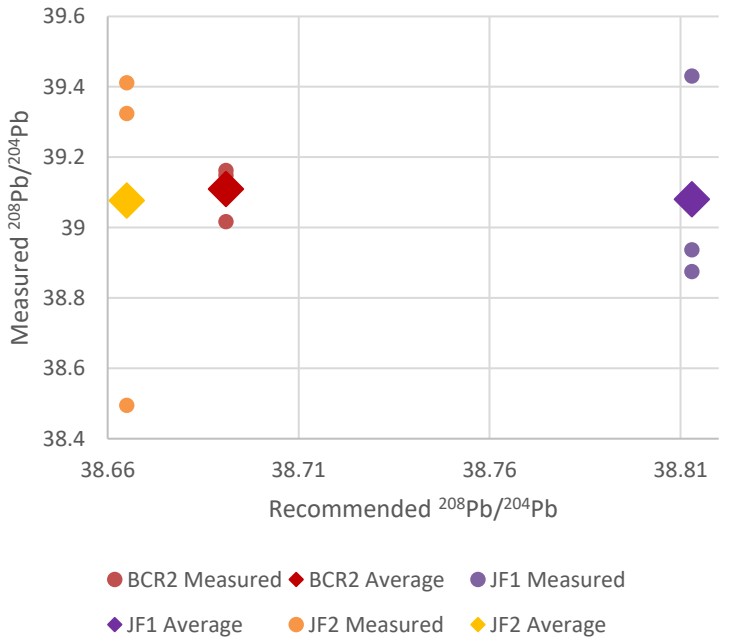

Average values (diamonds) are averages of measured values.

The difference between the measured Pb isotopic compositions of these reference materials and the recommended values from literature are smaller than the variation within the sample set used in this study. Causes for the deviations from recommended values are not certain.

Procedural Blanks

A procedural blank of Milli-Q water was run (Blank A). During the second round of lab work, two additional procedural blanks were prepared (Blank B-1 and Blank B-2). Shown below are the results from the three blanks to three significant figures, measured in percent standard deviations.

Table 11: Procedural blank of Pb

	$^{206}Pb/^{204}Pb$	$^{207}Pb/^{204}Pb$	$^{208}Pb/^{204}Pb$	Pb ng*
Blank A	14.5	11.1	28.9	0.7
Blank B-1	18.4	15.2	37.2	0.8
Blank B-2	14.6	12.2	29.3	0.6
% Deviation	14.1%	16.5%	17.3%	13.7%
Average Deviation	**16.0%**	**Standard Deviation**		**1.79%**

*Blank A was run during the 1st analysis of Pb isotopic compositions (10 B horizon soil samples). Blank B-1 and B-2 were run with the 2nd analysis of Pb isotopic compositions (19 sandstone samples, 4 A horizon soil samples, 5 B horizon soil samples, and 4 C horizon soil samples). *Pb detection limit is 0.003 ppb in a solution.*

To measure potential blank contribution, the median Pb concentration of the blanks and their associated sample sets are shown below to two or one figure, depending on proximity to the detection limit, for both weak and medium leached samples, as well as for non-separated and separated samples.

Table 12: Concentration of Pb in median weak acid leachate compared to procedural blanks

	Blank Pb	Resin Separated Samples	Non-Separated Samples	% Contribution
1st Analyses (1)	0.7 ng	6.57 ng	3410 ng	10% - 0.02%
2nd Analyses (2)	0.7 ng (average n=2)	28.4 ng	6700 ng	2% - 0.01%

% Contributions are rounded to the nearest significant figure. Note (1); 1st analyses were of 10 B horizon soil samples. Note (2); 2nd analyses were of 19 sandstone samples, 4 A horizon soil samples, 5 B horizon soil samples, and 4 C horizon soil samples.

Table 13: Concentration of Pb in median medium/strong leachate compared to procedural blanks

	Blank Pb	Resin Separated Samples	Non-Separated Samples	% Contribution
1st Analyses (1)	0.7 ng	40.7 ng	11600 ng	2% - 0.006%
2nd Analyses (2)	0.7 ng (average n=2)	51.4 ng	26200 ng	1% - 0.003%

% Contributions are rounded to the nearest significant figure. Note (1); 1st analyses were of 10 B horizon soil samples. Note (2); 2nd analyses were of 19 sandstone samples, 4 A horizon soil samples, 5 B horizon soil samples, and 4 C horizon soil samples.

Sample Duplicates

Sample DPX 289 (an MFb sandstone) had its rock powder split to assess the reproducibility of the cation separation procedure. Results from the duplicates will be compared similarly to those of the blank samples. Shown below are the results of the duplicates, to three significant figures, measured in relative difference of the Pb isotopic compositions.

Table 14: Pb isotope compositions of duplicates of weak leachates

	$^{206}Pb/^{204}Pb$	$^{207}Pb/^{204}Pb$	$^{208}Pb/^{204}Pb$	
DPX 289-1	33.4	16.6	54.7	
DPX 289-2	36.7	17.1	59.2	
% Difference	9.42%	2.54%	7.65%	
Average Dif.	**6.55%**	**Standard Deviation**		**3.57%**

Table 15: Pb isotope compositions of duplicates of medium leachates

	$^{206}Pb/^{204}Pb$	$^{207}Pb/^{204}Pb$	$^{208}Pb/^{204}Pb$
DPX 289-1	39.4	17.4	65.4
DPX 289-2	40.3	17.5	66.0
% Difference	**2.34%**	**0.485%**	**0.958%**
Average Dif.	**1.26%**	**Standard Deviation**	**0.964%**

Table 16: Pb isotope compositions of weak acid leachate standard deviation

	$^{206}Pb/^{204}Pb$	$^{207}Pb/^{204}Pb$	$^{208}Pb/^{204}Pb$
Variation between Samples	4.81	0.83	6.49
Variation between Duplicates	2.45	0.31	3.20
Difference Factor	**1.96x**	**2.69x**	**2.03x**

Table 17: Pb isotope compositions of medium acid leachate standard deviation

	$^{206}Pb/^{204}Pb$	$^{207}Pb/^{204}Pb$	$^{208}Pb/^{204}Pb$
Variation between Samples	5.71	0.58	12.6
Variation between Duplicates	0.64	0.07	0.42

The variation between duplicates is smaller than the variation between samples within the larger sample populations (weak and medium leach respectively). Inter-population deviation ranges from ~2x

larger, up to 30x larger. Why the difference in precision exists between the weakly leached duplicates and medium leached duplicates is unknown.

Results

Infield Results

The lowest pH was measured in hole WR-312, and the highest from hole WR-439. The lowest Eh value was measured in hole WR-380, and highest in hole WR-351. Lowest and highest conductivity were measured from holes WR-439 and WR-314 respectively. Eh and pH values may not be accurate as the instrument was only calibrated prior to field work.

Table 18: Field measurements of groundwater properties in June

Drill Hole	Date of Measurement	pH	Eh (mV)	Conductivity (µS/cm)	Temperature (°C)	Water Table (m)
WR-270	6/21/2014	6.5	389	16	8.9	24.6
WR-287	6/23/2014	7.8	452	35	16	39
WR-291	6/22/2014	6.4	442	28	14.2	40.4
WR-311	6/23/2014	7.2	434	69	10.2	32
WR-312	6/21/2014	5.9	240	60	14	20.3
WR-314	6/20/2014	6.1	391	101	NAN	0.5
WR-341	6/22/2014	6.0	409	31	14	39.4
WR-345	NAN	7.2	450	92	11.5	38
WR-347	6/23/2014	8.0	447	25	10	41.2
WR-351	NAN	7.4	477	28	18.9	34
WR-380	6/21/2014	6.5	206	80	10	4.5
WR-396	6/21/2014	6.4	262	66	14.6	22.4
WR-403	6/24/2014	8.8	440	38	NAN	21
WR-404	6/22/2014	7.1	345	28	10.5	39.8
WR-409	NAN	7.2	434	69	10.2	32
WR-439-0 m	6/24/2014	7.8	402	34	13.8	25
WR-439-20 m	6/24/2014	8.0	375	39	NAN	n/a
WR-439-40 m	6/24/2014	8.2	446	13	NAN	n/a
Average	**n/a**	**7.0**	**391**	**50**	**12.6**	n/a
Median	**n/a**	**7.1**	**421**	**36**	**12.6**	n/a

Mean and median values do not include the two additional points from WR-439. NAN values represent not measured. N/a represents non-applicability. The locations of drill hole collars are shown in and listed in Appendix II.

Figure 12: Box and whisker plots of groundwater properties

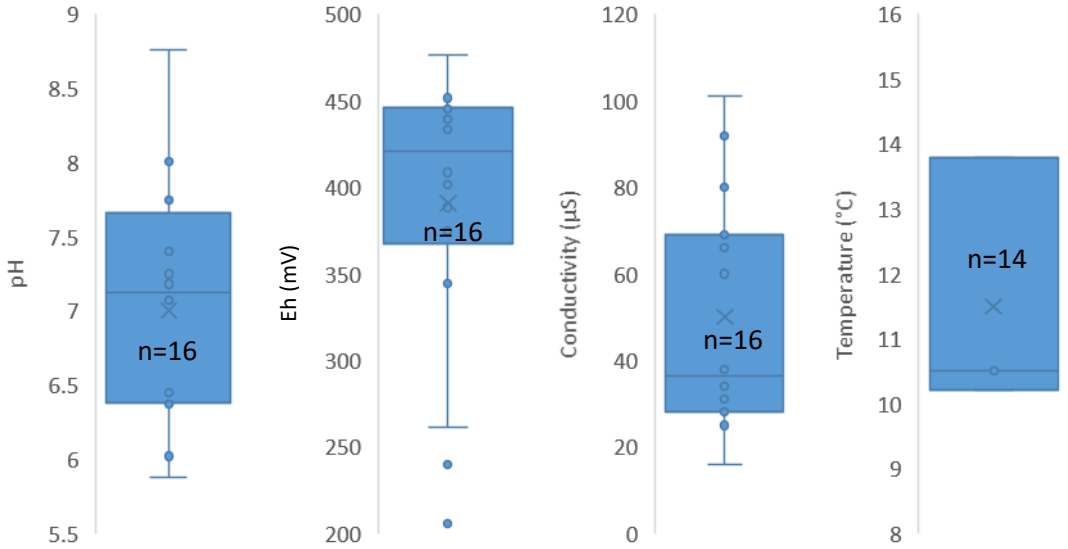

Basic groundwater chemistry was only measured at depth for one hole, WR-439. pH and possibly Eh increase with depth, whereas conductivity decreases by a factor of 2 from the uppermost 20 meters of groundwater.

Figure 13: Groundwater chemistry depth profiles of WR-439

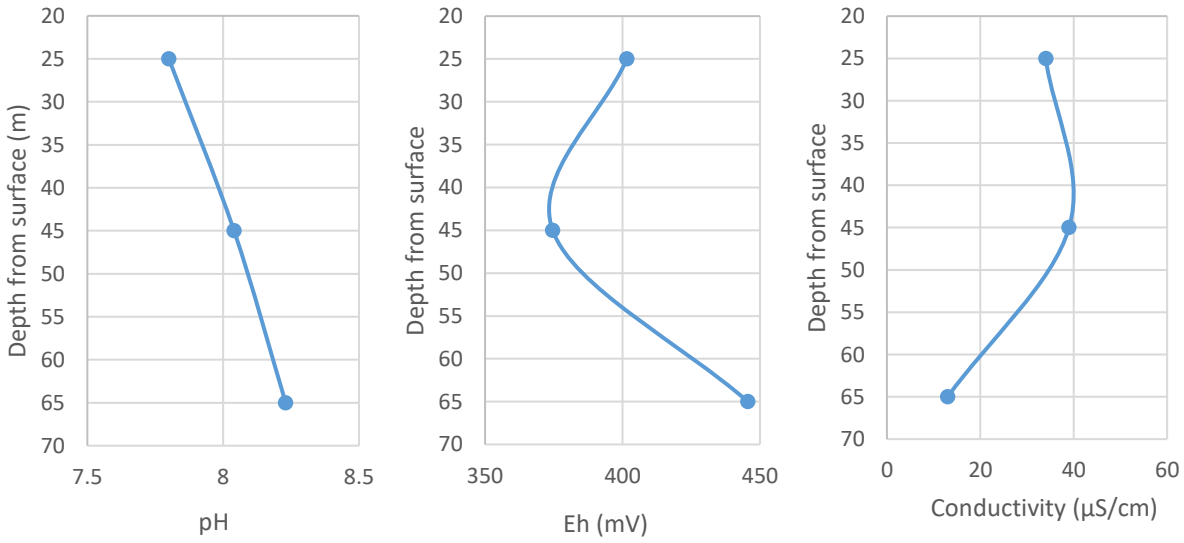

WR-439 is directly above the north-eastern end of the Phoenix deposit.

Rn

Rn content in groundwater was acquired from 14 drill holes in the Wheeler River property. Four additional samples were taken from two drill holes (two extra samples per hole) at 20m depth increments. Rn content of soil gas was measured around two drill holes.

Oil Extracted Rn

Oil Extracted Rn is the primary method Rn was measured in this study. Values are presented below in Table 19 and Figure 14, in units of Bq/g of water using the efficiency correction of the method.

Table 19: Groundwater Rn sampling coordinates and values by oil extraction

Sample/Drill Hole	Sample Date	Rn (Bq/g)
WR-314	6/20/2014	0.017
WR-380	6/21/2014	0.020
WR-270	6/21/2014	0.20
WR-291A	6/22/2014	0.17
WR-347	6/23/2014	0.089
WR-341-A	6/22/2014	0.26
WR-404	6/22/2014	0.15
WR-311	6/23/2014	0.14
WR-287	6/23/2014	0.14
WR-439	6/24/2014	0.062
WR-439-20m	6/24/2014	0.086
WR-439-40m	6/24/2014	0.082
WR-292	6/25/2014	0.12
WR-403	6/24/2014	0.14
WR-396	6/21/2014	0.039
WR-312	6/21/2014	0.056

Drill holes are ordered from south-west to north-east along the trend of the Phoenix Deposit.

Figure 14: Groundwater Rn radioactivities by oil extraction

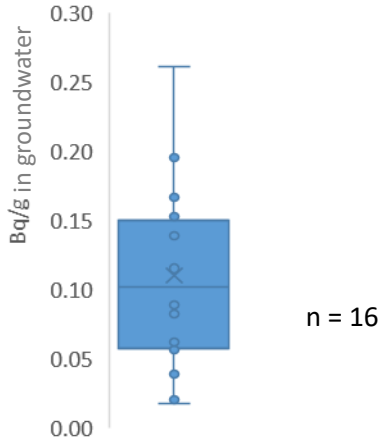

The x represents the average value.

Groundwater Rn concentrations are generally larger (average of 0.13 Bq/g of water n=10) near (within 100m) to the Phoenix Deposit's surface projection (Figure 15) than distal holes (average 0.072 Bq/g of water, n =4). Drill holes sampled within the surface projection are more closely spaced than those sampled outside the surface projection. Distance between sampled holes within the surface projection range 20 m - 100 m, whereas spacing between sampled holes outside the surface projection are all >100 m. Significant variation still exists within both subsets.

Figure 15: Groundwater Rn concentrations by sample site by oil extraction

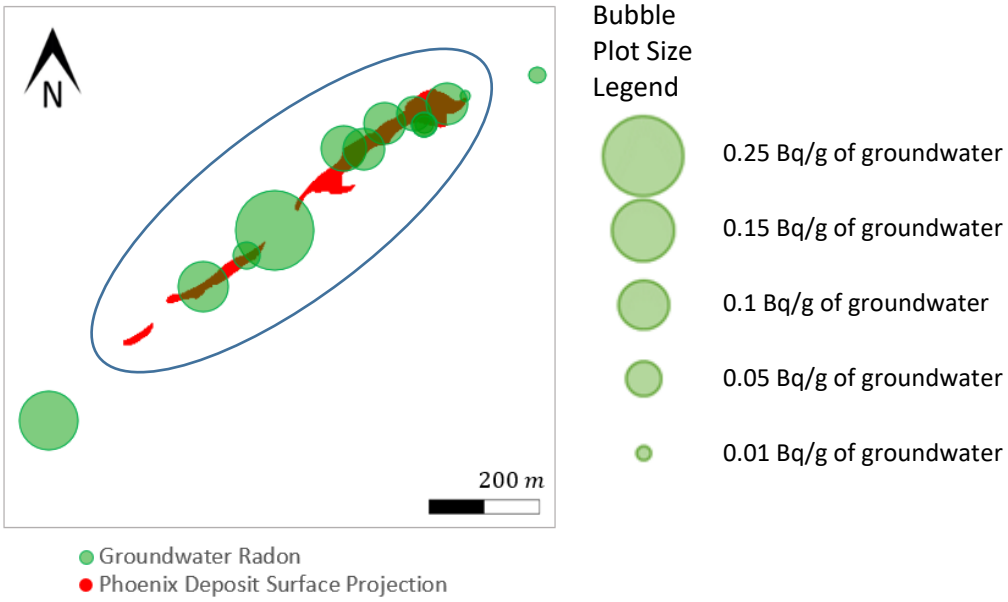

Surface projection of the Phoenix Deposit (red) overlain by a bubble plot (green) showing radioactivity of Rn/g of groundwater by sample location. Holes considered proximal to the Phoenix Deposit's surface projection are found within the (approximately) circled area. Two additional samples exist to the south-west; see Figure 6.

Soil Gas Rn

Radon contents in soil gas were measured around drill holes WR-314 and WR-380 (refer to Figure 6). Duplicate measurements were taken within 2 meters of the respective drill hole, and two sets of duplicate measurements were taken in surrounding undisturbed forest (typically more than 10 meters away). The lower detection limit for the RM-2 Soil Radon Monitoring System is 3 kBq/m^3 (equivalent to 3Bq/L, or 0.003 Bq/cm^3) and majority of measurements were below this value. The data suggests that aqueous fluids or pore gas in soil contain much lower concentrations of Rn than groundwater.

Table 20: Soil gas Rn radioactivity measurements

	WR-314			WR-380		
Sample	Measurements (kBq/m^3)		Location	Measurements (kBq/m^3)		Location
Near	1.4	1.1	<2 m	1.7	1.4	<2 m
Far 1	0.6	0.3	>13 m @350°	16.8	4.3	>15 m @190°
Far 2	1.9	1.5	>23 m @ 220°	2.7	4.8	<23 m @ 33°

Direction is measured from UTM Zone 13's North, in the WGS 84 system. Near samples were taken within 2 meters of the drill hole, and far samples were taken more than 10 meters away. Far 1 and Far 2 correspond to the first and second measurements.

Depth Profiles of Rn

Two deeper samples were taken from drill holes WR-314 and WR-439 at approximate 20 meter intervals to construct Rn depth profiles. The sample highest in elevation was taken from within 1-2 meters of the water table. For hole WR-314, Rn radioactivity decreases consistently over the subsequent 40 to 45-meter depth. However, Rn radioactivity within WR-439 increases in the first 20 meters and then decreases for the last 20 meters making it difficult to conclude how Rn behaves with greater depth.

Importantly, the two different depth profiles were constructed from different sampling methods. WR-314 used direct water sampling and WR-439 used the in-field oil extraction method. Not enough water extracted samples exist to correct for the differences in method, as such the two profiles should only be compared relatively.

Figure 16: Rn depth profiles measured in Bq/g of groundwater

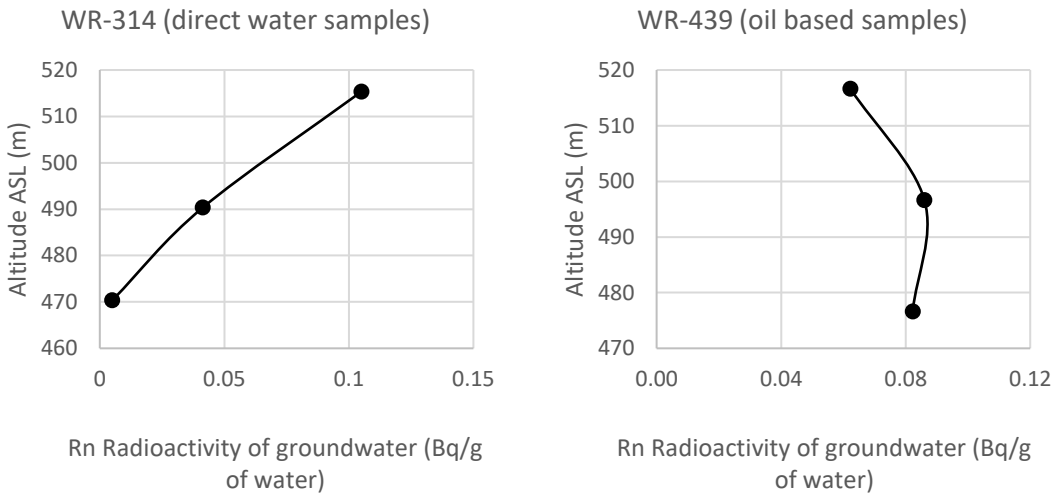

Rn Depth profiles were taken using two different sampling methods; direct water sampling that were analysed at the Université du Québec à Montréal and oil extracted samples analysed at the University of Ottawa.

He

Figure 17: Diffusion sampler deployment sites

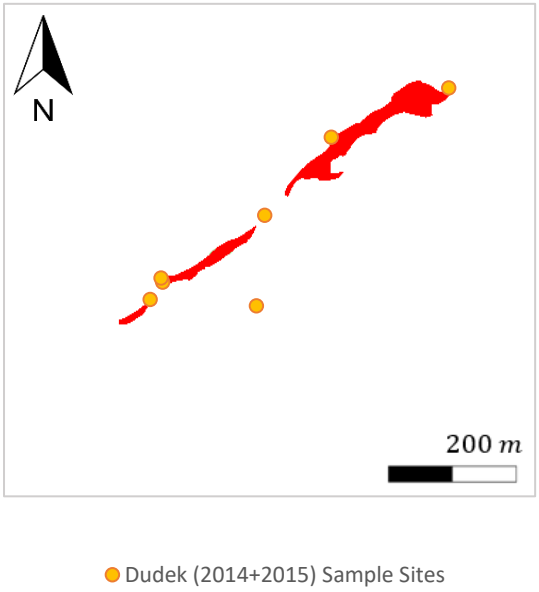

Figure 18: Distribution of He measurements

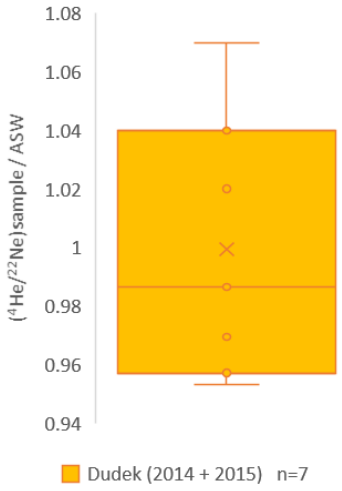

All values are close to air saturated water, indicating equilibration between atmosphere and groundwater.

2 and 3 acid digestions and INAA analysis for Th and U in Sandstones

2-acid and 3-acid digestions (2AMS and 3AMS) analyses were performed on most core samples by Saskatchewan Research Council for Denison Mines. The results of these values will not be discussed, however the respective sample values for 2AMS and 3AMS will be compared to those acquired by INAA here.

All sandstone samples featured in this study underwent 2AMS and 3AMS digestions, and the subset that underwent Ra and Pb isotope analyses were also analysed using the INAA method. The comparison of the three assays is shown in Figure 19 and Table 21. INAA resulted in nearly twice the detected U than 3AMS digestion. Median U and Th concentrations for 17 samples by 2AMS digestion are 0.45 and 1.52 ppm respectively. Median U and Th concentrations for 17 samples by 3AMS digestion are 1.89 ppm and 6.67 ppm respectively. Median U and Th concentrations for 17 samples by INAA are 2.8 and 14.8 ppm respectively.

Figure 19: Comparison of assay methods for U and Th from MF and RD sandstones

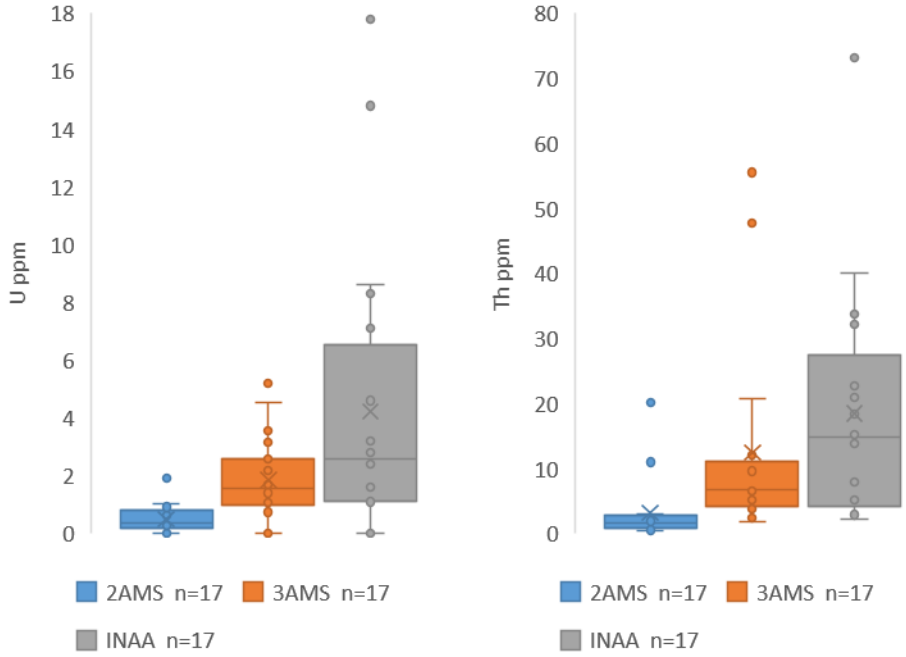

The x in each subplot represents the average value.

Seven of the seventeen samples returned INAA values lower than their respective values after 3AMS analysis for either U or Th concentrations (four for U, and five for Th). In the seventeen cases the concentrations of U and Th measured by 3AMS were over 5x the detection limits of the concentrations measured by INAA, thus no reason is readily available to explain this discrepancy. Notably, the occurrences of INAA U < 3AMS U is not associated with cases where 3AMS U concentrations were low.

Table 21: Comparison of U and Th concentrations from 3AMS and INAA in sandstones

RD samples	3AMS U (ppm)	INAA U (ppm)	3AMS Th (ppm)	INAA Th (ppm)
D. Limit	0.02	0.5	0.02	0.5
DPX 077	3.57	14.8	9.98	15.2
DPX 256	5.21	17.8	6.5	22.7
DPX 240	**3.16**	**1.2**	6.94	5.3
DPX 131	1.4	2.8	**47.8**	**33.8**
MFb samples				
DPX 199	**1.69**	**<0.5**	**55.5**	**32.2**
DPX 148	1.06	8.6	10	73.1
DPX 289	1.89	8.3	12.1	20.9
MFc samples				
DPX 269	1.28	4.6	5.58	14.8
DPX 162	1.94	2.8	**20.8**	**13.9**
DPX 143	1.31	2.4	6.67	18.4
DPX 147	1	4.8	9.6	40
DPX 186	0.74	1.3	5.13	5.2
MFd samples				
DPX 282	0.99	1.6	2.37	3.1
DPX 257	**2.17**	**1.1**	1.79	2.2
DPX 182	2.6	3.2	**3.83**	**2.9**
DPX 167	2.59	7.1	3.28	7.9
DPX 177	**4.54**	**1.7**	**4.5**	**2.9**

Samples mentioned in the text, and associated values are bold.

Outlier DPX 069

DPX 069, a RD sandstone sample from drill hole WR-239, contained the highest concentrations of U and Pb for both 2AMS and 3AMS leach types. The sample was taken from approximately 420 meters below surface. No sample was left for INAA analysis. U concentrations were 580 ppm and 584 ppm for 2AMS and 3AMS respectively. Median U concentrations for the sandstones was 0.45 and 1.89 (2AMS and 3AMS respectively). Pb concentrations of the sample were 239 ppm and 312 ppm for 2AMS and 3AMS respectively. Median Pb concentrations were 0.63 ppm and 2.71 ppm (2AMS and 3AMS respectively).

Because of the large difference between the Pb and U concentrations of DPX 069 and those of the rest of the sandstones, the concentration values are considered unrepresentative of the RD sandstones.

SLM, SLE, 1F leaches and INAA analysis for Th and U in soils

Soil samples underwent three different leach forms (SLE, SLM, and 1F, refer to Table 3) by Power (2013). The results will be compared to those acquired by INAA here.

Soil samples can be divided into two groups based on the leach performed upon them; samples that underwent SLM and SLE leaches, and samples that underwent 1F digestions by Power (2013). No overlap exists between these two groups. Subsequently, Figure 20 compares all U and Th concentrations for the B horizon samples analyzed. Median U and Th concentrations for SLM and SLE leaches are considerably lower than 1F and INAA results. Median U and Th concentration for 1F are approximately

450 ppb and 3500 ppb respectively. Median U and Th concentrations for INAA are approximately 1600 ppb and 6700 ppb respectively.

Figure 20: Comparison of assay methods for U and Th from B horizon soils

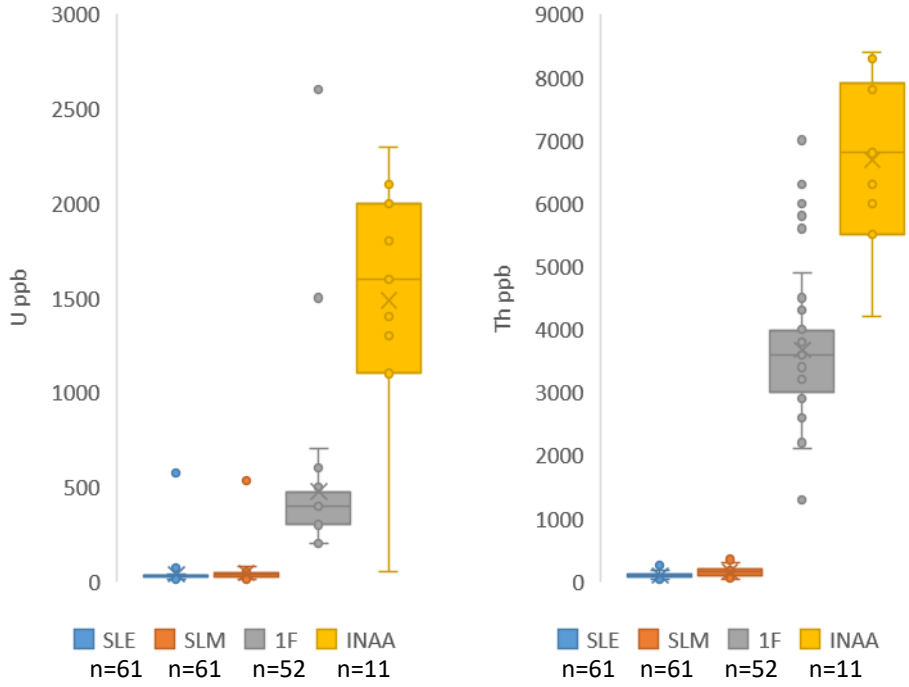

The x in each subplot represents the average value.

Only four samples were submitted for INAA from A and C horizons (two each), and neither horizon underwent SLE or SLM leaches by Power (2013). Table 22 compares the U and Th concentrations acquired from both methods for the four samples. Median concentrations for the entire horizons are also provided. Oddly, both C horizon samples and PHX 045A had less U detected by INAA than was measured with 1F leach but this could be due to the 1F U contents (and presumably the total concentration as well), of these three samples being close to the respective detection limits on INAA. INAA also detected less Th than 1F for sample PHX 027C, and there is no clear reason for this – though possibly a nugget effect of the analysis.

Table 22: Comparison of U and Th concentrations from 1F and INAA in A and C horizons

A horizon sample	1F U (ppb)	INAA U (ppb)	1F Th (ppb)	INAA Th (ppb)
Detection Limits	100	100	100	500
PHX 009A	400	800	50	3000
PHX 045A	300	<100	<100	2100
Median A Horizon	**300**		**200**	

C horizon sample	1F U (ppb)	INAA U (ppb)	1F Th (ppb)	INAA Th (ppb)
Detection Limits	100	500	100	500
PHX 021C	500	<500	4800	5400
PHX 027C	500	<500	4600	2900
Median A horizon	**500**		**4500**	

Comparisons between U, Ra, Rn, and Pb

U and Rn

Given the possibility that Rn is present near surface due to transport of parent isotopes like Ra or U, Rn concentrations were compared with both 2AMS and 3AMS U concentrations of the sandstones from Denison Mines' assay data. However, Rn radioactivity was measured from within 2 meters of the static water level per drill hole and not measured from individual sandstone samples, so comparing with individual sandstone samples would not be meaningful. Furthermore, without knowing how the groundwater moves over short distances, measured Rn could have been sourced from more than one sandstone sample. So, U concentrations were averaged across each sandstone unit for each respective drill hole to get an average U content of the sandstone bed in that location. Meaning for a hypothetical drill hole that crosses all four sandstone units with 20 samples from each unit, the concentrations of the 20 samples are averaged to produce one average value for each of the sandstone units.

By this reasoning, INAA data is not used in the following comparisons because any single sandstone sample is not representative of the entire drill hole from which Rn radioactivity was measured from. Furthermore, overlap between the two data sets is limited. Rn radioactivity and U content in soils will not be compared either as overlapping coverage of the two sets is also limited.

MFd

Rn radioactivity in upper groundwater positively correlates with average MFd U content (both 2AMS and 3AMS) for respective drill holes. If U in MFd is decaying to produce the Rn sampled from groundwater, such a positive correlation is expected. However, positive correlations are observed between groundwater Rn and averaged U content for all MF members. For reference, above the Phoenix Deposit MFd averages ~45 m thick, and can be found at depths as shallow as 4 m, and as deep as 75 m (variation depending primarily on till). This thickness variation of MFd may partly explain the lack of positive correlation between Rn radioactivity in groundwater and U in MFd sandstones.

Figure 21: Comparison between groundwater Rn and MFd U

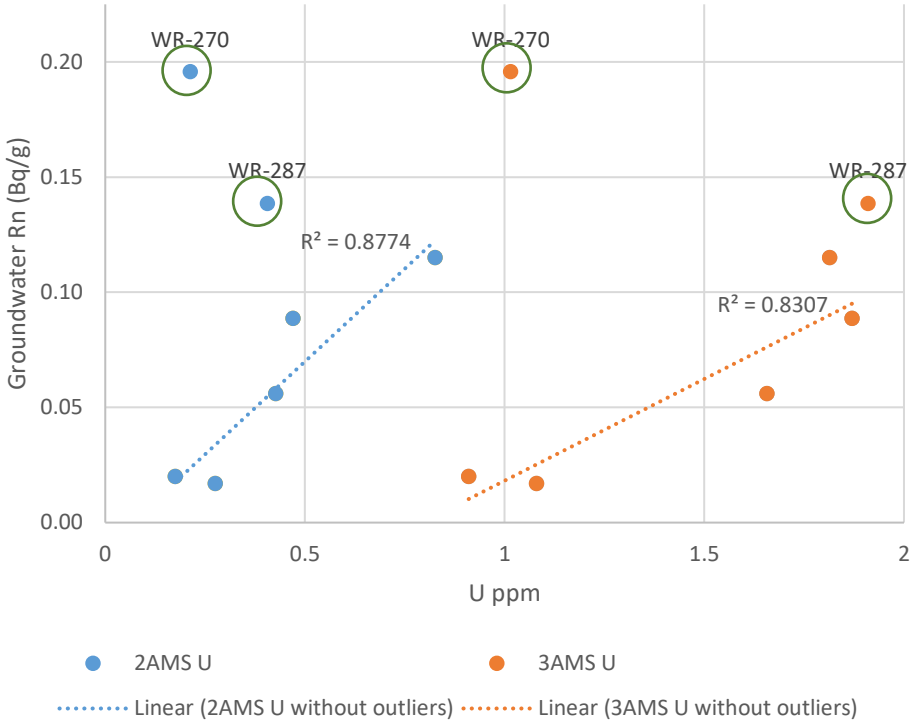

Four outlying points are identified based on their distance from the main data trend and are circled. WR-270 and WR-287 are identified as outlying points when compared to MFc U concentration as well. Linear regressions shown do not include the outliers. WR-287 was not removed from the 3AMS U regression.

MFc

Rn radioactivity in upper groundwater is positively correlated with average MFc U content (both 2AMS and 3AMS) for respective drill holes. If U in MFc is decaying to produce the Rn sampled from groundwater, such a positive correlation is expected. For reference, above the Phoenix Deposit MFc averages ~150 m thick, and can be found at depths between 30 m and 260 m below surface (depending on the thickness of till).

Figure 22: Comparison between groundwater Rn and MFc U

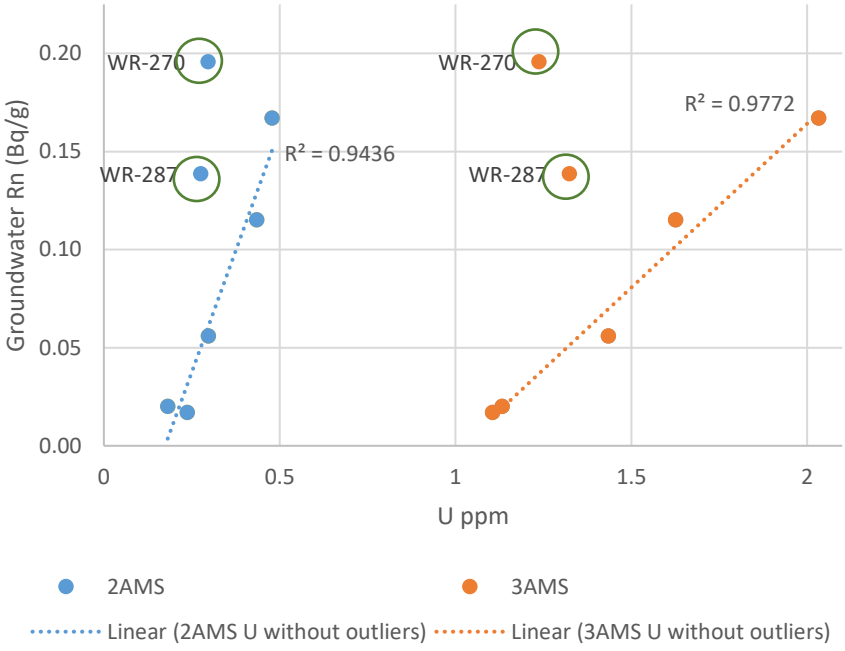

Four outlying points are identified based on their distance from the main data trends and are circled. WR-270 and WR-287 are identified as outlying points when compared to MFd U concentration as well. Linear regressions are shown for the respective leach types, and do not include the outliers.

MFb

Rn radioactivity in upper groundwater is positively correlated with average MFb U content (both 2AMS and 3AMS) for respective drill holes. If U in MFb is decaying to produce the Rn sampled from groundwater, such a positive correlation is expected. For reference, above the Phoenix Deposit MFb averages ~135 m thick, and can be found at depths between 120 m and 340 m below surface (depending on till).

Figure 23: Comparison between groundwater Rn and MFb U

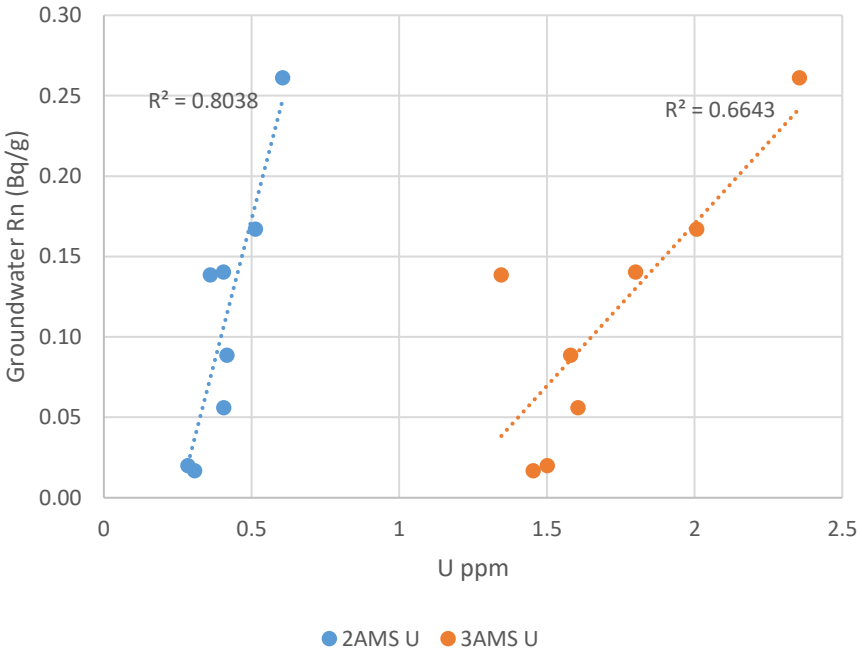

RD

No correlations are observed between Rn radioactivity from upper groundwater and U content of the RD sandstones (both 2AMS and 3AMS U). A lack of correlation suggests that the presence of U in RD has no association with Rn in upper groundwater. For reference, above the Phoenix Deposit RD averages ~115 m thick, and can be found at depths between 240 m and 420 m below surface (depending on till).

Figure 24: Comparison between groundwater Rn and RD U

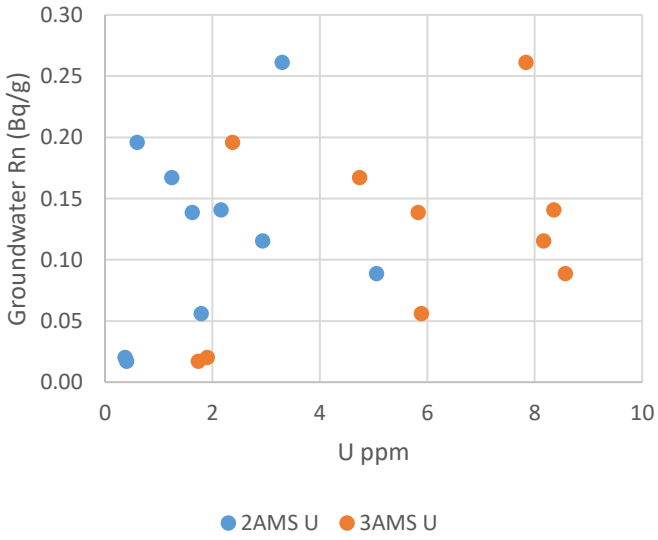

Outlying Points

When comparing Rn concentrations of groundwater to average U concentrations for individual sandstone beds, holes WR-270 and WR-287 regularly have Rn concentrations larger than expected for MFd and MFc U-Rn trends. In attempt to justify labelling these points as outlying, the characteristics and data of both holes will be examined in closer detail.

Figure 25: Groundwater Rn concentrations and sites of WR-270 and WR-287

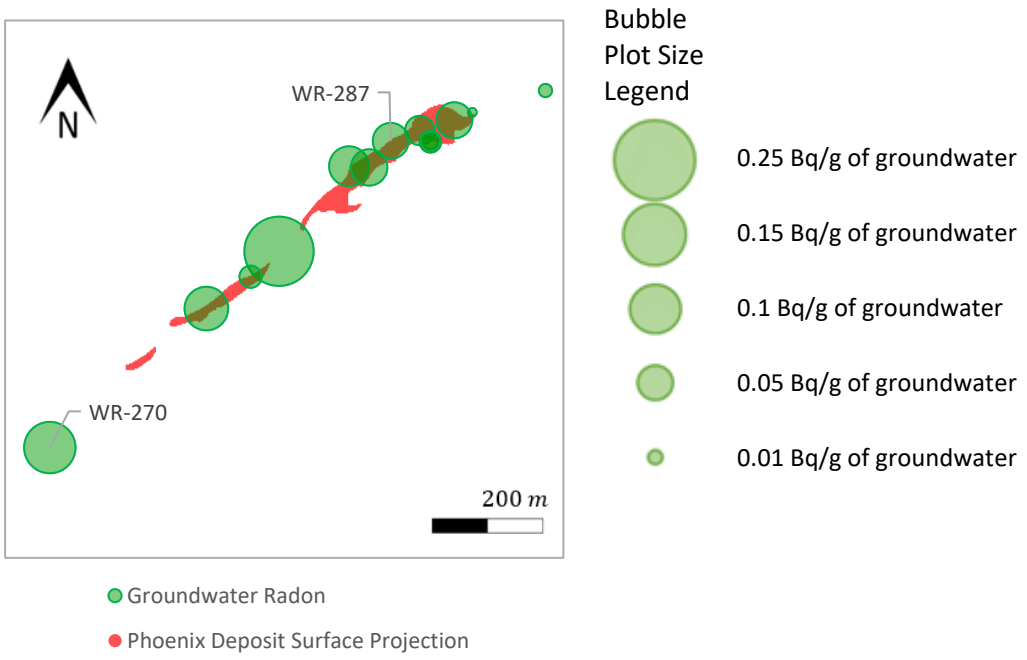

WR-270

Approximately 1 km south-west and downhill of the Phoenix deposit surface projection is a small (unnamed) marsh land present on the side of topological saddle point with no clear inlets or outlets visible from satellite imagery or on the Wheeler River Property Map (Figure 6 on page 10) (Roscoe, 2012). Continuing south-west and downhill a small meandering river (unnamed) is present flowing also towards the south-west. Given the non-arid climate of Wheeler River (Natural Resources Canada, 2009), it is assumed that groundwater flow feeds the surface water environment. Thus, the high amount of Rn (relative to the U-Rn trend) may result from Rn (or parent isotopes) being carried by lateral groundwater flow. In regards to groundwater chemistry, WR-270 is unremarkable.

It should be noted that holes WR-314 and WR-380 are downhill from the surface projection and have very little Rn, though these holes are 1.1 and 0.8 km further south-west (respectively) than WR-270. Given that groundwater flow rates are much slower than surface water flow, its possible that most Rn has decayed before reaching WR-380.

WR-287

WR-287 is directly above the largest ore body of the Phoenix Deposit, and so a hydrologic explanation isn't possible. However, groundwater taken from WR-287 had the highest concentrations of Pb, Th, and U of all holes sampled. With nearly 0.5 ppm as total U in water, combined particulates and

dissolved. No definitive answer to the high U content is available. For reference, the hole with the second greatest amount of total U was WR-345 with 0.08 ppm and just over 100 meters away (no Rn data is available for WR-345).

U and Ra

The Ra measured in any given substrate has two possible sources; outside the substrate or within the substrate by the decay of U.

If a sample has a higher Ra radioactivity than the value expected from the concentration of U, then Ra has been added or U has been lost. If a given sample has a lower measured radioactivity than the expectant value, again calculated from the sample's concentration of U, then it can be concluded that Ra has been lost from the sample or U has been recently added.

By combining the equations for secular equilibrium and radioactivity (in Bq/g) the following equation is derived:

Equation 3:

$$A_{\frac{bq}{g}} = \frac{\frac{\lambda_U}{\lambda_{Ra}} U_{\frac{g}{g}}}{m_{Ra}} * A_N * \frac{ln(2)}{t_{\frac{1}{2}Ra}}$$

B Horizon Soil

A comparison between measured Ra, the three U leaches (SLE, SLM, 1F) and total U measured with INAA reveal no correlations (Figure 26). Range of measured Ra values are slightly below expected Ra values from INAA U (Figure 27). This could be explained by the loss of Ra from the B soil or the gain of U. Another possible explanation is the site of U. INAA measures the total U contents including U in refractory mineral grains. Such mineral grains likely retain all decay products, such as Ra, which are not available with acid digestion.

Figure 26: B horizon soil comparison between U concentration and Ra radioactivity

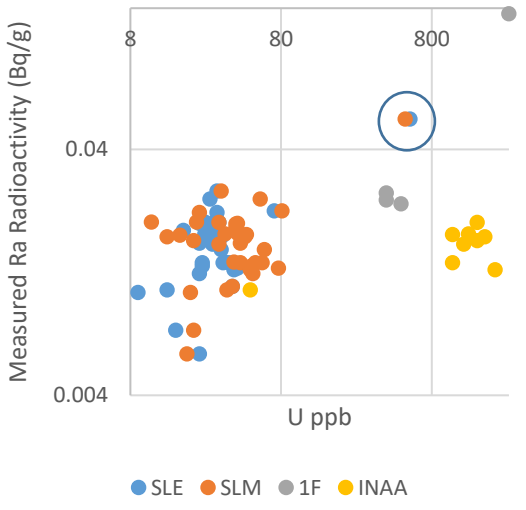

Potential outliers are circled.

Figure 27: Measured vs expected Ra radioactivity in B horizon soil

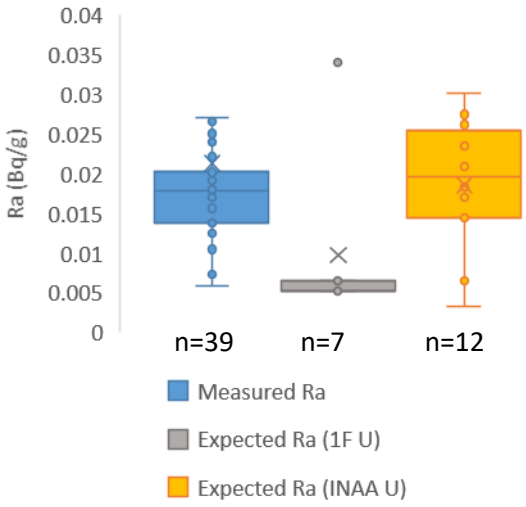

X marks the average value

MFd

A comparison between measured Ra, the two U digestions (2AMS and 3AMS) and INAA reveal two separate results. No correlations are present between Ra and either digestion (Figure 28) and when compared to 3AMS there is a significant overabundance of Ra (Figure 29). Ra and INAA U are positively correlated and INAA U would produce a similar magnitude of Ra, though measured Ra is still higher.

Figure 28: MFd comparison between U concentration and Ra radioactivity

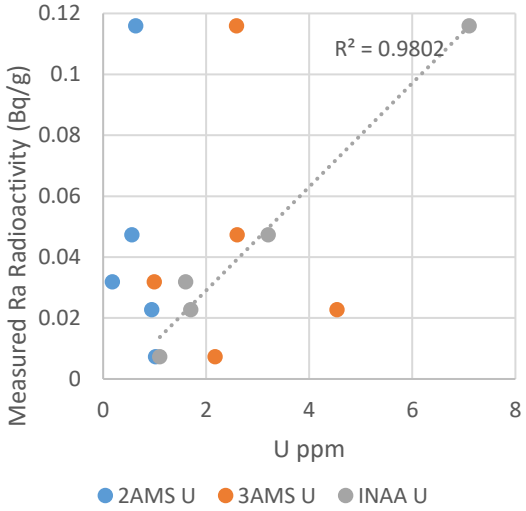

Figure 29: Measured vs expected Ra radioactivity in MFd

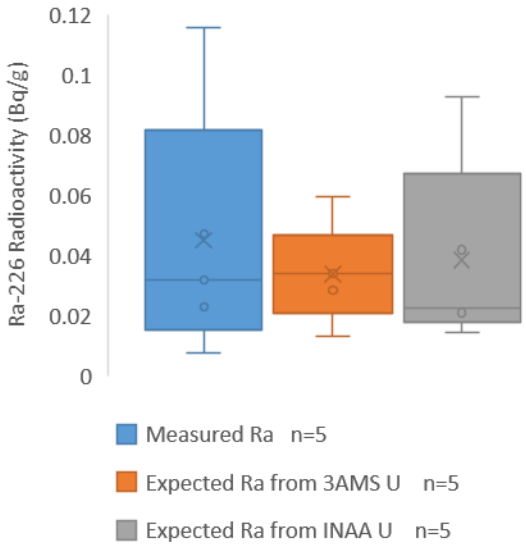

X marks the average concentration.

Given the similar range in values for measured Ra radioactivity and expected Ra radioactivity and the positive correlation between INAA U and measured Ra, individual samples are compared in Table 23. Three of the five samples contained more Ra than to be expected from INAA U, suggesting Ra of foreign origin or the loss of U. Contrary, one sample had half the Ra that was expected, suggesting that Ra was lost from this sample or that U was added. Only one sample had nearly the same amount of Ra expected.

Table 23: Comparison between measured Ra and expected Ra (from INAA U) in MFd

Sample	Measured Ra (Bq/g)	Expected Ra (INAA U) (Bq/g)	Difference Factor*	Comment
DPX 282	0.032	0.021	1.5	Unsupported Ra
DPX 257	0.007	0.014	0.5	Missing Ra or added U
DPX 182	0.047	0.042	1.1	Unsupported Ra
DPX 167	0.116	0.093	1.2	Unsupported Ra
DPX 177	0.023	0.022	1.0	Match

*Table 23: *Factor difference is "Measured Ra" divided by the "Expected Ra".*

MFc

A comparison between measured Ra and all types of U assay reveal correlation between Ra radioactivity and U concentrations depending on the inclusion of DPX 147 to the regressions (Figure 30). Including DPX 147, there is no regressive fit for 3AMS and 2AMS comparisons, but a better fit for INAA U. Refer to page 45 for details on this outlier. Similar to other sandstone beds, Ra appears to be

overabundant when compared with 3AMS, but comparison with INAA U suggests Ra has been lost from the samples (Figure 31).

Figure 30: MFc comparison between U concentration and Ra radioactivity

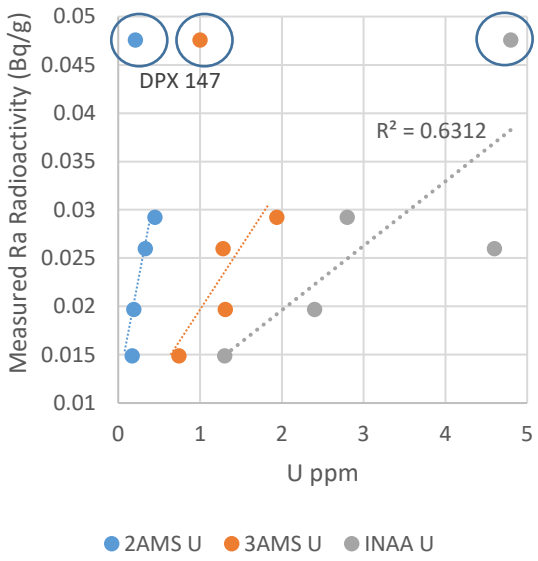

Possible outlier (DPX 147) is circled.

Figure 31: Measured vs expected Ra radioactivity in MFc

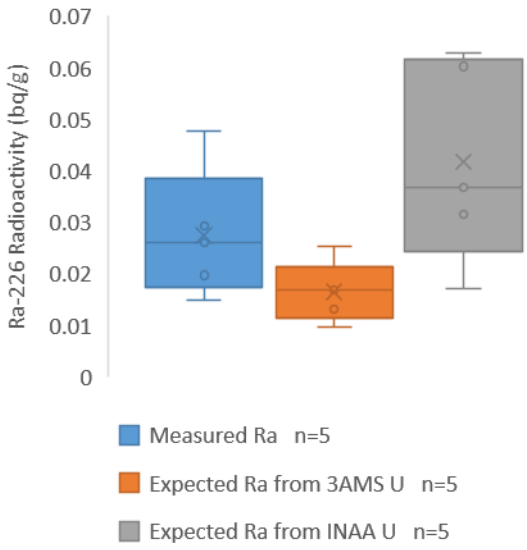

X marks the average concentration.

Similarly, to the presentation of MFd results, a sample by sample comparison of measured Ra an expected Ra (calculated from INAA U) is in Table 24 due to the above correlation and similarity in range. All samples had less Ra than was expected from INAA U; suggesting that either Ra has been lost or U added. MFc is known to contain detrital heavy minerals (Ramaekers et al., 2007). U in such refractory heavy minerals are measured with INAA, but Ra is not released during the analysis with HCl. This may explain higher expected Ra contents than measured values.

Table 24: Comparison between measured Ra and expected Ra (from INAA U) in MFc

Sample	Measured Ra (Bq/g)	Expected Ra (INAA U) (Bq/g)	Difference Factor*	Comment
DPX269	0.026	0.060	0.4	Missing Ra
DPX162	0.029	0.037	0.8	Missing Ra
DPX143	0.020	0.031	0.6	Missing Ra
DPX147	0.048	0.063	0.8	Missing Ra
DPX186	0.015	0.017	0.9	Missing Ra

**Difference factor is the "Measured Ra" divided by the "Expected Ra".*

MFb

A comparison between measured Ra radioactivity and both leaches of U reveal no correlation between either pairing (Figure 32). However, INAA U and Ra are positively correlated with one caveat; Ra in MFb might be divided into two groups (high and low radio-activities) but not enough data exists to cement this possibility. Like other sandstone beds, there is a significant overabundance of Ra compared with the expected value from 3AMS U (Figure 33); either Ra has been gained or U has been lost. However,

when compared with INAA, the measured Ra values appear as expected, though with higher median values.

Figure 32: MFb comparison between U concentration and Ra radioactivity

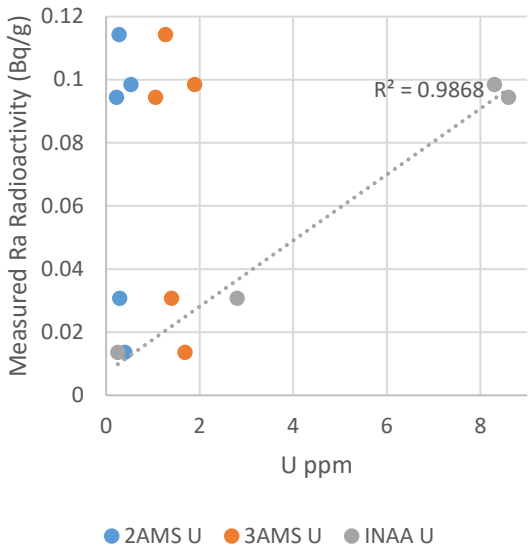

Figure 33: Measured vs expected Ra radioactivity in MFb

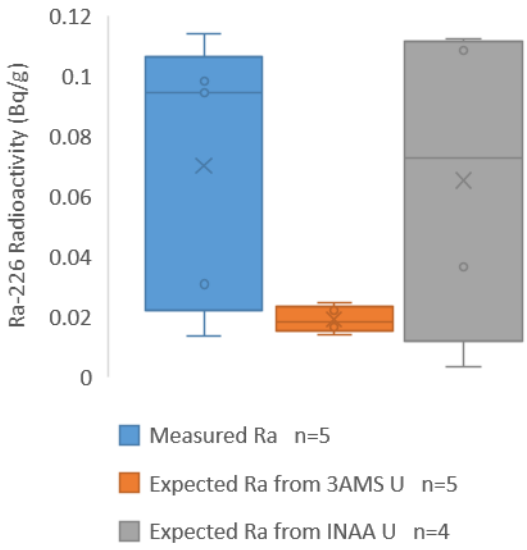

X marks the average concentration.

Expected Ra (as calculated from INAA U) and measured Ra are similar in value and range, and are also well correlated and so individual samples are compared in Table 25. Three of the four samples had more INAA U than was expected given the measured Ra, suggesting that Ra has been lost or U added. One sample, DPX 199, contained 4.2 times more Ra than was to be expected, suggesting the addition of foreign Ra or the loss of U.

Table 25: Comparison between measured Ra and expected Ra (from INAA U) in MFb

Sample	Measured Ra (Bq/g)	Expected Ra (INAA U) (Bq/g)	Difference Factor*	Comment
DPX 131	0.031	0.037	0.8	Missing Ra
DPX 199	0.014	0.003	4.2	Unsupported Ra
DPX 148	0.094	0.113	0.8	Missing Ra
DPX 289	0.099	0.109	0.9	Missing Ra

Difference factor is the "Measured Ra" divided by the "Expected Ra".

RD

A comparison between measured Ra radioactivity and both leaches of U reveal no correlation between either pairing (Figure 34). Like other sandstones, measured Ra and INAA U are well correlated, however notably, only three INAA U data points are available for the RD sandstone. When measured, Ra is compared with expected Ra calculated from 3AMS, Ra is overabundant (Figure 35). Oppositely, when compared with the three values calculated from INAA U, measured Ra has similar magnitude, though a lower range.

Figure 34: RD comparison between U and Ra

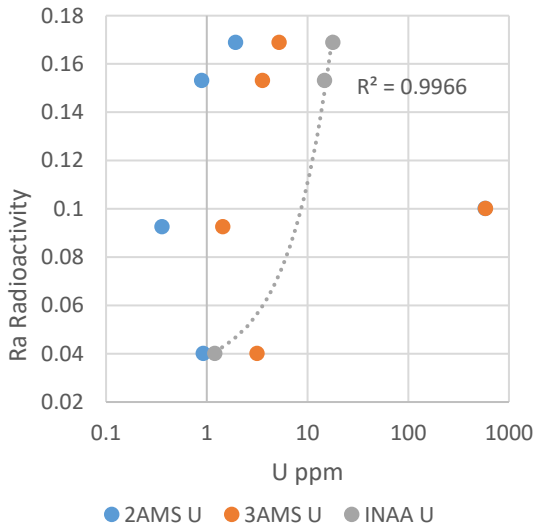

Note that the x axis increases logarithmically in the figure, and that the regression line is linear.

Figure 35: Measured vs expected Ra in RD

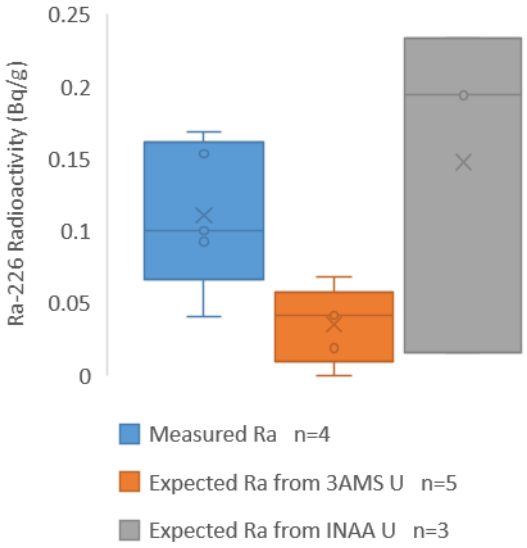

DPX 069 contains 500 ppm U (from 3AMS) and was removed from the figure.

Similar to other sandstones, the three samples' measured Ra and expected Ra contents (calculated from INAA U) are compared individually in Table 26. Two samples contained less measured Ra than was expected from INAA U, indicating that Ra has been lost from the samples or U was added. The third sample contained 2.6x more Ra than was expected, indicating that Ra has been added to the sample.

Table 26: Comparison between measured Ra and expected Ra (from INAA U) in RD

Sample	Measured Ra (Bq/g)	Expected Ra (INAA U) (Bq/g)	Difference Factor*	Comment
DPX 077	0.153	0.194	0.8	Missing Ra
DPX 256	0.169	0.233	0.7	Missing Ra
DPX 240	0.040	0.016	2.6	Unsupported Ra

**Difference Factor is the "Measured Ra" divided by the "Expected Ra".*

Outlier DPX 147

DPX 147, a sample from MFc, was identified in Figure 30 as having more Ra than the rest of MFc samples measured. This sample was first mentioned because it was taken from WR-284, a drill hole approximately 1 km to the north of the Phoenix Deposit surface projection. No specific reason for its high Ra content is known. The sample is at the intersection of two distinct alteration fronts; an iron oxide/ hematization front and a dark purple/black front (potentially also iron oxide). Otherwise the sample is largely unremarkable.

U and Pb

An isotopically closed system, the Pb isotopic composition from U can be calculated per the following formula:

$$\frac{^{206}Pb}{^{204}Pb_t} = \frac{U_{ppm} * 99.284\%}{Pb_{ppm} * 1.4\%} * \left(e^{\lambda t} - 1\right) + \frac{^{206}Pb}{^{204}Pb_{1500Ma}}$$

Equation 4: Formula used to calculate the expected $^{206}Pb/^{204}Pb$ for the given sandstone beds. The formula used for $^{207}Pb/^{204}Pb$ is identical in form, however the factor that U is multiplied by is now 0.72% to reflect the relative abundance of U-235. 1500 Ma, and associated Pb isotopic compositions, were chosen as approximation to the age of formation of the Phoenix Deposit

The modern concentration of U is assumed to have been similar to the concentration at the approximate time of formation for the sandstone beds (1500 Ma). The Pb isotopic composition for the sandstones at the time of formation is assumed to be the average crustal value at 1.5 Ga of Stacey and Kramer (1975). By extrapolating back in time using modern concentration of Th, the $^{208}Pb/^{204}Pb$ composition of average crust at 1.5 Ga was also calculated. U and Pb concentrations used are 2AMS and 3AMS.

This comparison will not be performed for soil samples. The soil and till have not existed for a significant amount of time (~8.5 ka compared to decay of U) (Dyke, 2004).

MFd

Expected Pb isotopic compositions ($^{206}Pb/^{204}Pb$ and $^{207}Pb/^{204}Pb$) calculated from U contents are significantly higher than the measured compositions, regardless of leach and digestion pairing. $^{208}Pb/^{204}Pb$ isotopic compositions are similar, though below, expected from 2AMS and 3AMS digestions. Refer to Table 27 for expected $^{208}Pb/^{204}Pb$ and Stacey-Kramer curve modified from Stacey & Kramer (1975). Figure 36 for expected $^{206}Pb/^{204}Pb$ and $^{207}Pb/^{204}Pb$.

Table 27: Comparison between measured and expected $^{208}Pb/^{204}Pb$ values in MFd

	Measured $^{208}Pb/^{204}Pb$		Expected $^{208}Pb/^{204}Pb$	
Sample	Weak Leach	Medium Leach	2AMS	3AMS
DPX 167	39.1	38.9	46.8	46.6
DPX 177	38.1	44.4	50.2	50.3
DPX 182	37.5	39.2	48.1	49.9
DPX 257	38.5	39.0	47.0	46.5
DPX 282	38.4	38.8	46.5	46.5
Average	**38.3**	**40.1**	**47.7**	**48.0**

Figure 36: MFd Pb isotopic compositions compared to expected values from U concentrations

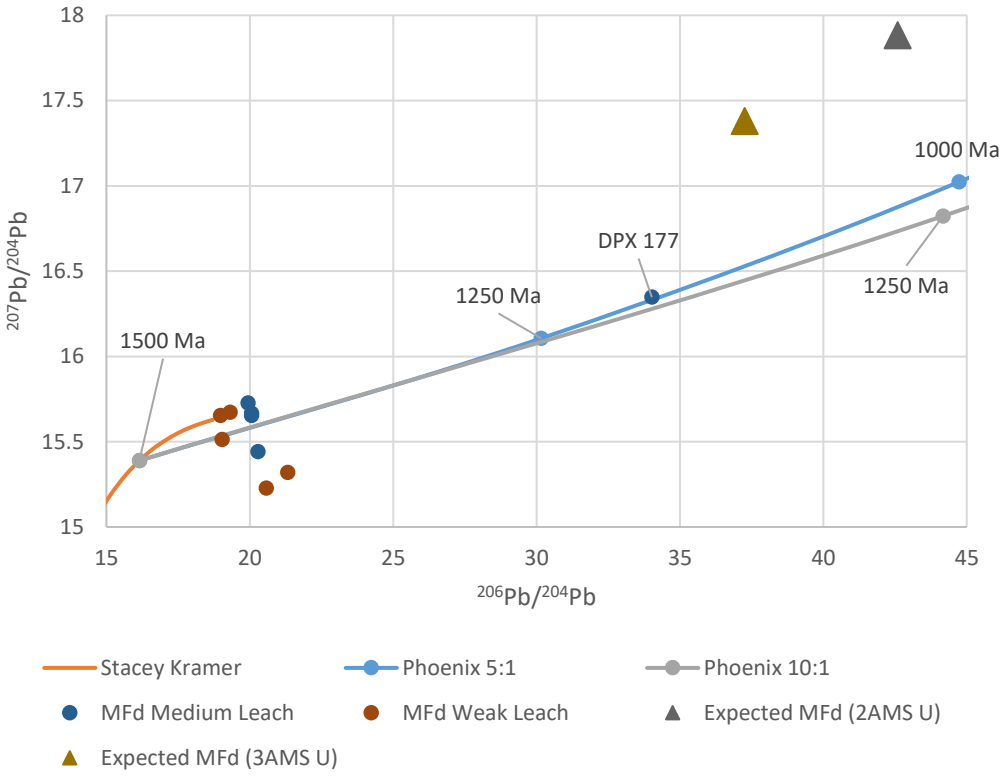

High value, and potential outlier, DPX 177 is labelled. Expected values are averaged from 5 samples each. Phoenix Deposit evolution curves are generated using a 10:1 and a 5:1 U:Pb initial concentration at 1.5 Ga. Stacey-Kramer curve modified from Stacey & Kramer (1975).

Correlation exists between $^{207}Pb/^{204}Pb$ and the 2AMS and 3AMS leaches in MFd. None exist for $^{206}Pb/^{204}Pb$.

Figure 37: MFd Pb isotope compositions compared to U concentrations

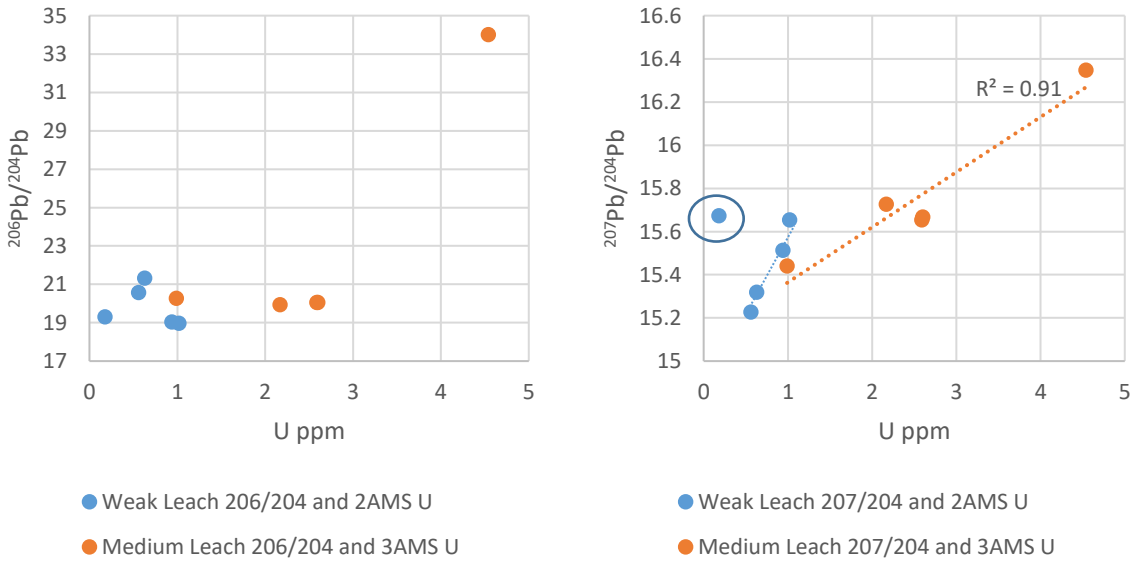

MFc

Measured Pb isotopic compositions ($^{206}Pb/^{204}Pb$ and $^{207}Pb/^{204}Pb$, and $^{208}Pb/^{204}Pb$) associated with the weak leach procedure are lower than the expected values from both digestion types (2AMS and 3AMS) given modern concentrations of U and Th. This is opposite to the medium leach radiogenic Pb which are generally higher than expected. Refer to Table 28 and Stacey-Kramer curve modified from Stacey & Kramer (1975). Figure 38 for the values.

Table 28: Comparison between measured and expected $^{208}Pb/^{204}Pb$ values in MFc

	Measured $^{208}Pb/^{204}Pb$		Expected $^{208}Pb/^{204}Pb$	
Sample	Weak Leach	Medium Leach	2AMS	3AMS
DPX 143	39.1	64.4	51.6	50.2
DPX 147	43.5	65.3	60.5	61.0
DPX 162	37.4	46.4	65.9	78.8
DPX 186	38.2	54.6	51.0	52.2
DPX 269	38.6	39.2	49.0	51.1
Average	**39.4**	**54.0**	**47.7**	**48.0**

Figure 38: MFc Pb isotopic compositions compared to expected values from U concentrations

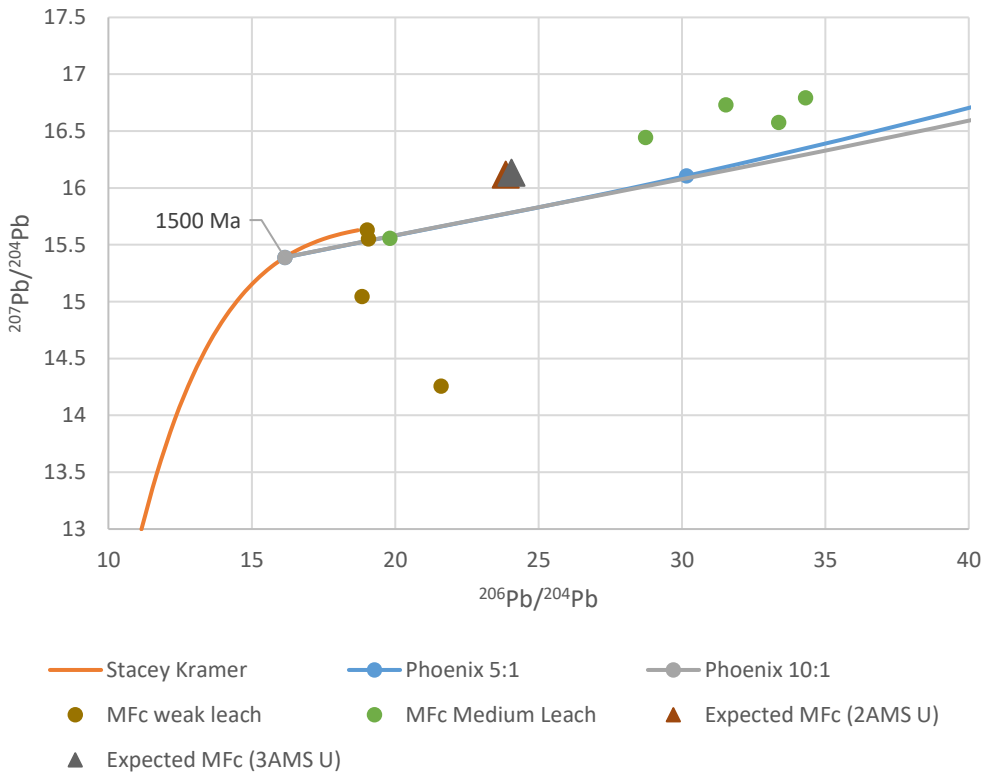

Expected values are averaged from 5 samples each. DPX 269, is highlighted as it resembles weakly leached Pb isotopic compositions. Phoenix Deposit evolution curves are generated using a 10:1 and a 5:1 U:Pb initial concentration at 1.5 Ga. Stacey-Kramer curve modified from Stacey & Kramer (1975).

Correlation exists between medium leach $^{206}Pb/^{204}Pb$ and 3AMS U in MFc. No other correlations are observed.

Figure 39: MFc Pb isotopic compositions compared to U concentration

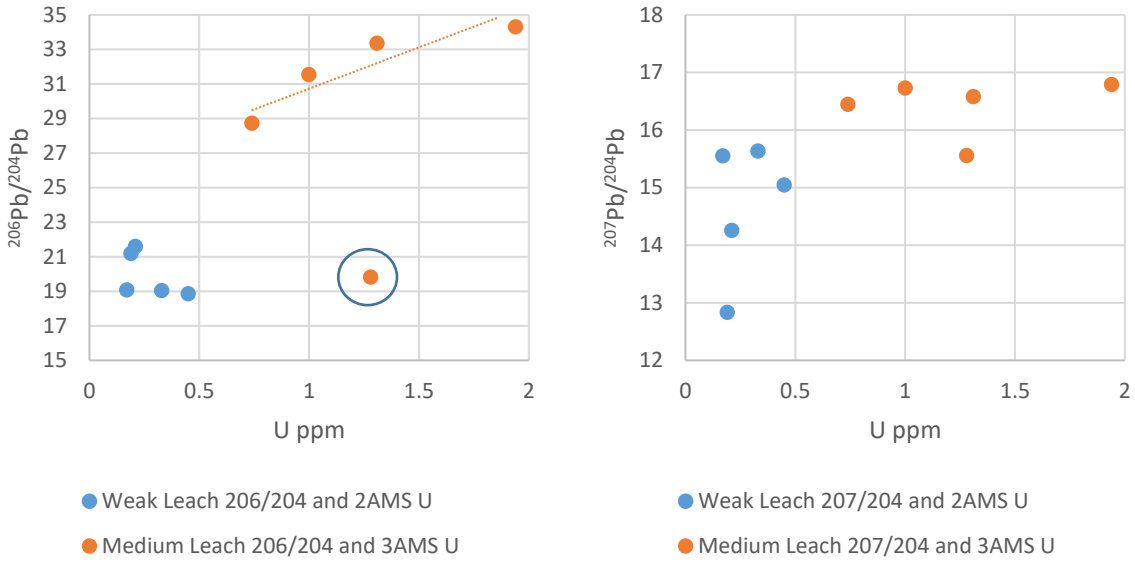

MFb

Uranogenic Pb to common Pb ratios, $^{206}Pb/^{204}Pb$ and $^{207}Pb/^{204}Pb$, are similar to expected values regardless of leach or digestion form. However, thorogenic Pb to common Pb ratios, $^{208}Pb/^{204}Pb$, are lower than expected given modern concentrations of Pb and Th. Refer to Table 29 and Figure 40 for the values.

Table 29: Comparison between measured and expected $^{208}Pb/^{204}Pb$ values in MFb

	Measured $^{208}Pb/^{204}Pb$		Expected $^{208}Pb/^{204}Pb$	
Sample	Weak Leach	Medium Leach	2AMS	3AMS
DPX 131	61.0	83.9	102.8	94.6
DPX 148	38.9	42.1	63.4	64.2
DPX 199	41.2	39.4	130.3	117.9
DPX 289	54.7	65.4	54.8	64.9
DPX 289-2	59.2	66.0	54.8	64.9
Average	**49.5**	**57.9**	**87.8**	**85.4**

Figure 40: MFb Pb isotopic compositions compared to expected values from U concentrations

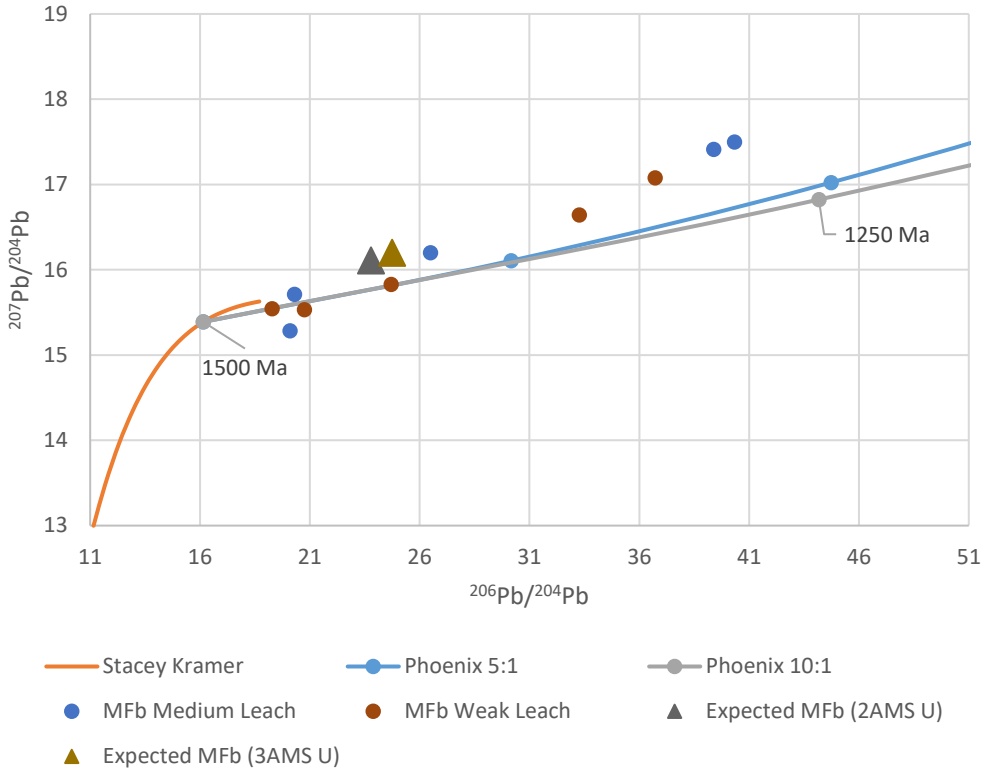

Expected values are averaged from 5 points each. Phoenix Deposit evolution curves are generated using a 10:1 and a 5:1 U:Pb initial concentration at 1.5 Ga. Stacey-Kramer curve modified from Stacey & Kramer (1975).

Positive correlations exist for both $^{206}Pb/^{204}Pb$ and $^{207}Pb/^{204}Pb$ (regardless of leach type) and both digestion types (2AMS and 3AMS) in MFb. Combined with the uranogenic Pb being similar to expected suggests that the MFb sandstone member is in isotopic equilibrium between U and Pb. How Th and Pb are not in equilibrium is an open question. This may be related to different extraction methods for Th concentrations and Pb isotope compositions. Th is most likely within refractory heavy minerals in sandstones, whereas Pb extraction for isotope analysis used relatively weak acid.

Figure 41: MFb Pb isotopic compositions compared to U concentrations

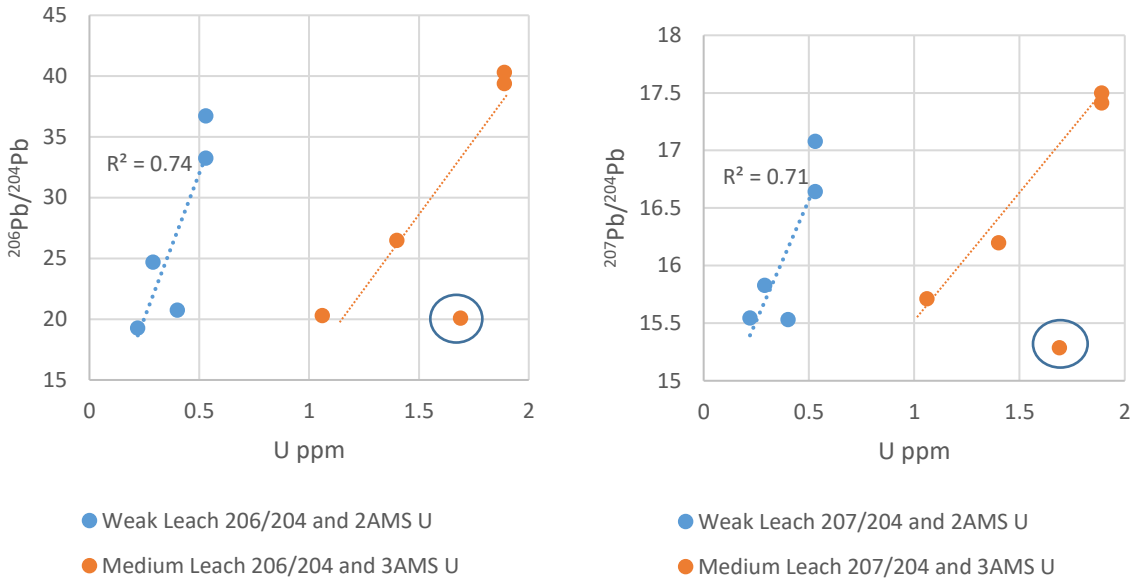

RD

All radiogenic Pb ($^{206}Pb/^{204}Pb$, $^{207}Pb/^{204}Pb$, and $^{208}Pb/^{204}Pb$) are lower than expected values, regardless of leach type or digestion type, and given modern concentrations of Th, U, and Pb. Refer to Table 30 and Figure 42. Sample DPX 145 (circled in Figure 43), shows significantly higher $^{206}Pb/^{204}Pb$ and $^{207}Pb/^{204}Pb$ values. Since it is located near the bottom of the sandstone sequence, high ^{206}Pb and ^{207}Pb may be related to the Phoenix Deposit.

Table 30: Comparison between measured and expected $^{208}Pb/^{204}Pb$ values in RD

	Measured $^{208}Pb/^{204}Pb$		Expected $^{208}Pb/^{204}Pb$	
Sample	Weak Leach	Medium Leach	2AMS	3AMS
DPX 069*	53.26	54.00	40.46	40.65
DPX 145	46.86	61.84	59.46	61.60
DPX 240	38.26	38.79	57.40	58.26
DPX 256	38.06	39.44	59.59	53.98
Average	**44.11**	**48.52**	**54.23**	**53.62**

Sample DPX 069, has a high Pb content (>200 ppm) resulting in lower expected values; refer to Equation 4. .

Figure 42: RD Pb isotopic compositions compared to expected values from U concentrations

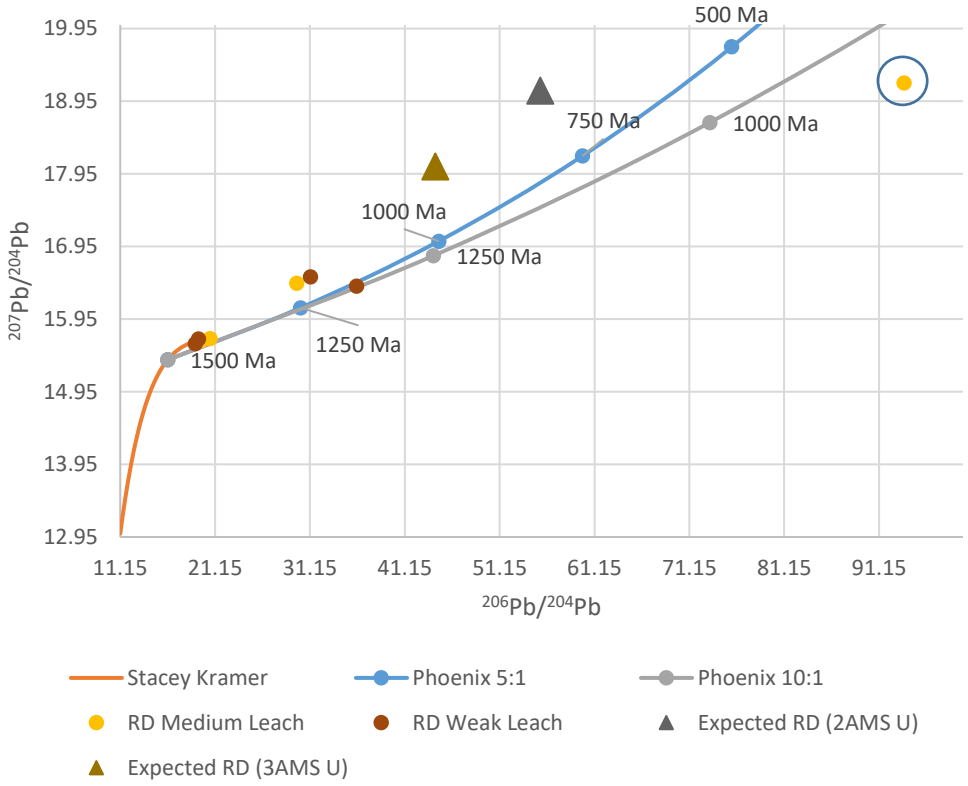

Expected values are averaged from 5 points each. The circled value is sample DPX 145. Phoenix Deposit evolution curves are generated using a 10:1 and a 5:1 U:Pb initial concentration at 1.5 Ga.

No correlations are present between uranogenic Pb ($^{206}Pb/^{204}Pb$ and $^{207}Pb/^{204}Pb$) and U concentrations regardless of leach and digestion type in the RD. Combined with the measured vs the expected values, Pb and its parent nuclei are not in isotopic equilibrium within the RD sandstone formation.

Figure 43: RD Pb isotopic compositions compared to U concentrations

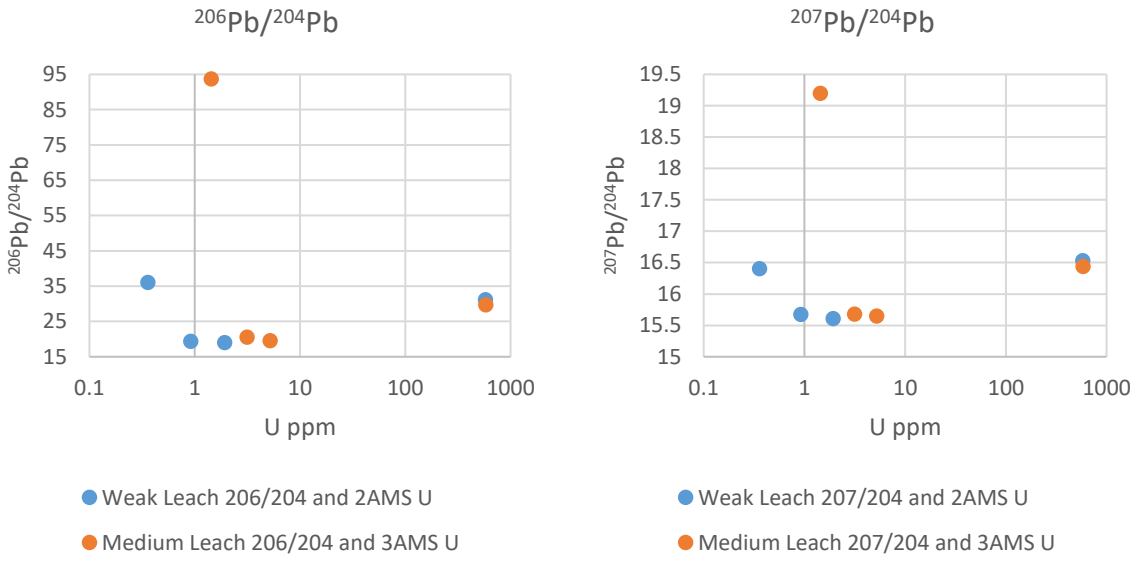

Outlier DPX 177

DPX 177 was highlighted in Stacey-Kramer curve modified from Stacey & Kramer (1975). Figure 36 for having greater $^{206}Pb/^{204}Pb$ and $^{207}Pb/^{204}Pb$ than the rest of samples analyzed from the MFd sandstone. However, Pb isotope composition of the sample is similar to that of the MFc sandstone samples, and the closest to the expected Pb isotopic composition of the MFD formation (as calculated from 3AMS U). It was also the only sample from MFd noted for having similar measured Ra and expected Ra (calculated from INAA U) as shown in Table 23. The similarity to MFc samples, and the parity between measured and expected Ra suggests that the local environment of DPX 177 is unlike those from other MFd samples.

Ra and Pb

B Horizon Soil

Positive correlations are observed between ^{206}Pb ($^{206}Pb/^{204}Pb$ and $^{206}Pb/^{208}Pb$) and Ra radioactivity (Bq/g) obtained from the medium leach procedure for Pb in B horizon soils.

Figure 44: B horizon soil comparison between Ra and ^{206}Pb

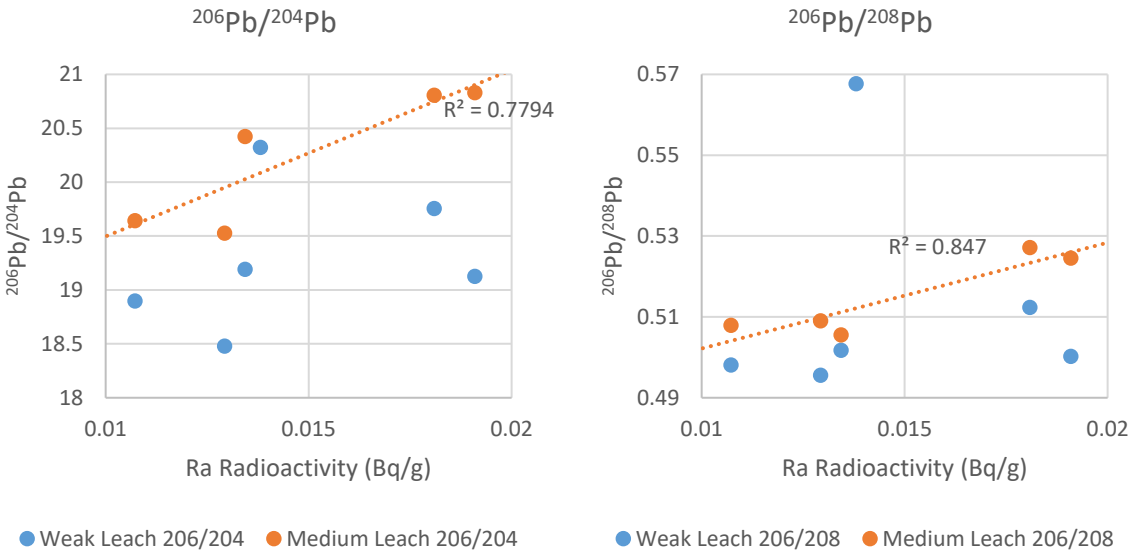

Not enough overlap exists between strongly leached Pb isotope compositions and Ra radioactivity data sets for comparison and is not presented.

MFd

Positive correlations are observed between ^{206}Pb ($^{206}Pb/^{204}Pb$ and $^{206}Pb/^{208}Pb$) and Ra radioactivity (Bq/g) obtained from the weak leach procedure in the MFd sandstone member. However, the correlation is tentative, as the sample points can also be grouped into high and low $^{206}Pb/^{208}Pb$ and $^{206}Pb/^{204}Pb$ compositions – those above a $^{206}Pb/^{204}Pb$ ratio of 20 or a $^{206}Pb/^{208}Pb$ of 0.51.

Figure 45: MFd comparison between Ra and ^{206}Pb

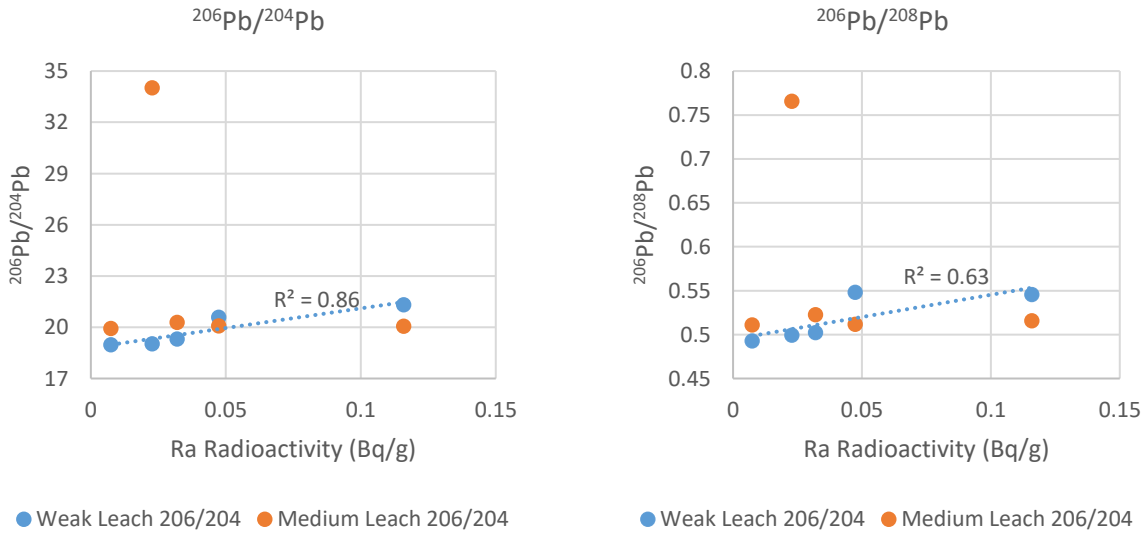

MFc

No correlation exists between ^{206}Pb and Ra radioactivity (regardless of leach type or chosen denominator in the ratio). Thus, ^{206}Pb and Ra appear to be in isotopic disequilibrium within the MFc sandstone member.

Figure 46: MFc comparison between Ra and ^{206}Pb

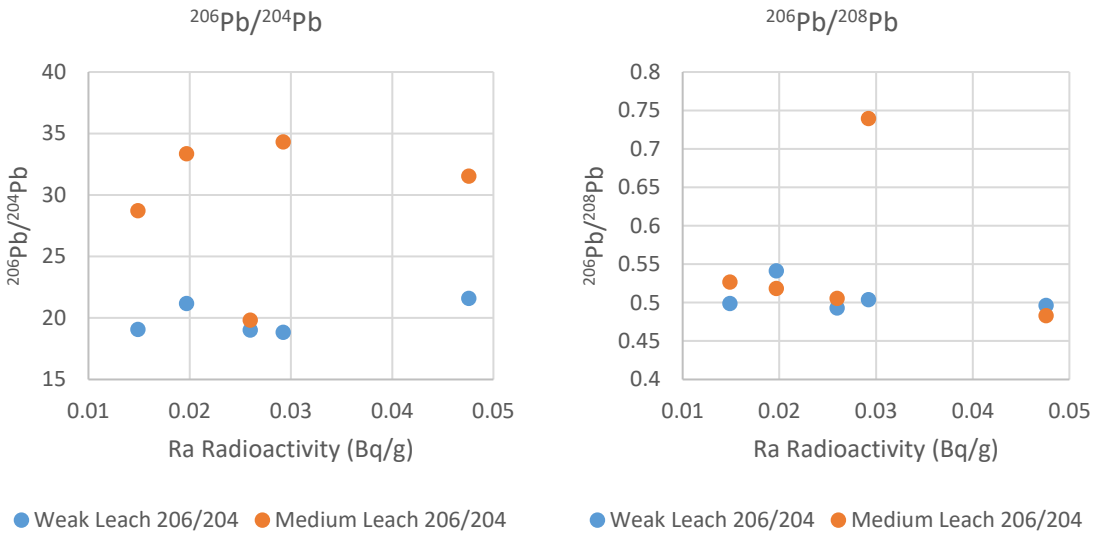

MFb

No correlation exists between ^{206}Pb and Ra radioactivity (regardless of leach type or chosen denominator in the ratio). Thus, ^{206}Pb and Ra appear to be in disequilibrium within the MFc sandstone member.

Figure 47: MFb comparison between Ra and ^{206}Pb

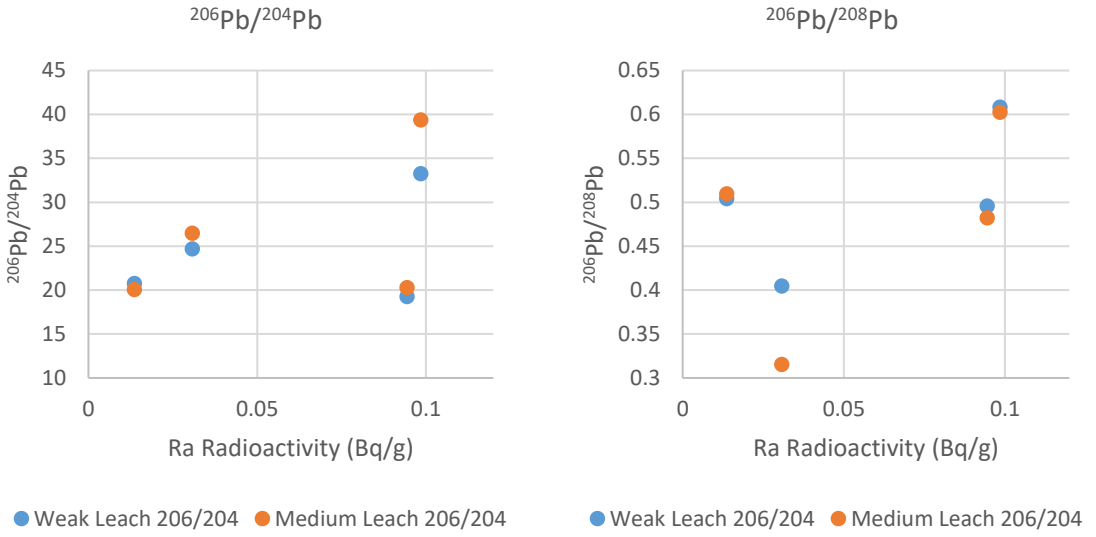

RD

No correlation exists between ^{206}Pb and Ra radioactivity (regardless of leach type or chosen denominator in the ratio). Thus, ^{206}Pb and Ra appear to be in disequilibrium within the RD sandstone formation.

Figure 48: RD comparison between Ra and ^{206}Pb

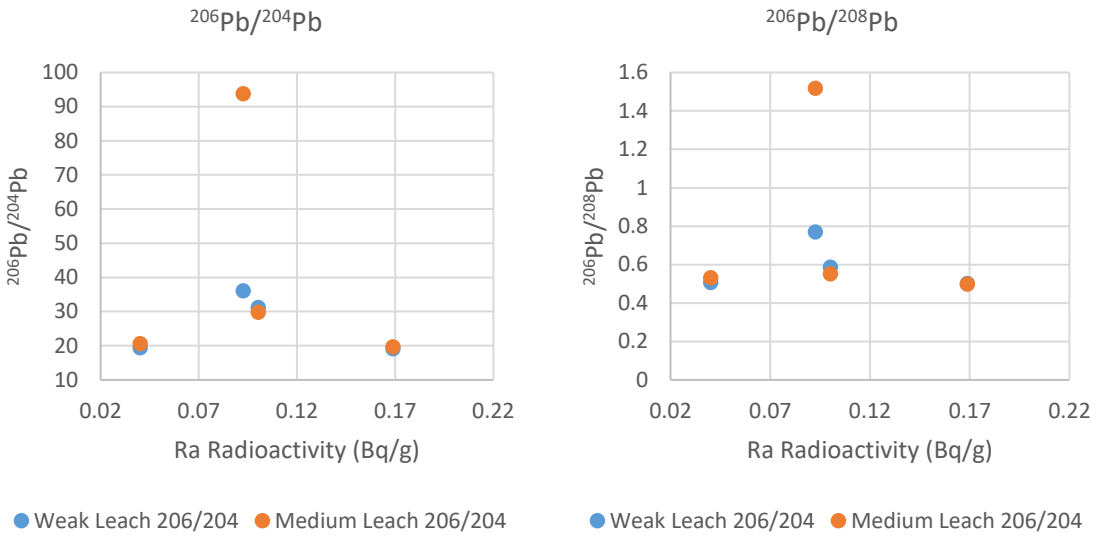

Deuterium and 18O of Groundwater

Samples were analysed for $^{2}H/^{1}H$ and $^{18}O/^{16}O$ contents. Samples appear to be offset from the global meteoric water line; sitting generally below the line (Figure 49). No specific O or H isotope data could be found in the literature for the south-east Athabasca Basin, so data from four proximal Global Network of Isotopes in Precipitation (GNIP) measuring stations and one sample from Wolfe et al. (2007) from Lake Athabasca were used instead.

The GNIP data sets used are:

- Churchill (MB);
  - Approximately 700 km to the east and taken
  - Measurements between 1989-1993 (inclusive)
- Fort Smith (NWT/AB);
  - Approximately 500 km to the west north-west
  - Measurements between 1960-1969 (inclusive)
- Edmonton (AB);
  - Approximately 700 km to the south-west
  - Measurements between 1960-1969 (inclusive)
- The Pas (MB);
  - Approximately 500 km to the south south-east
  - Measurements between 1975-1982 (inclusive)

Wolfe et al. (2007) took his sample from near Fort Chipewyan (AB); approximately 400 km to the west north-west.

Despite the distance between measuring stations, the data taken from GNIP and Wolfe et al. (2007) are similar in both average, variance, and deviation from the meteoric water line; enabling comparison with the Wheeler River data.

Figure 49: Wheeler River samples, meteoric water line, and GNIP (2004) data

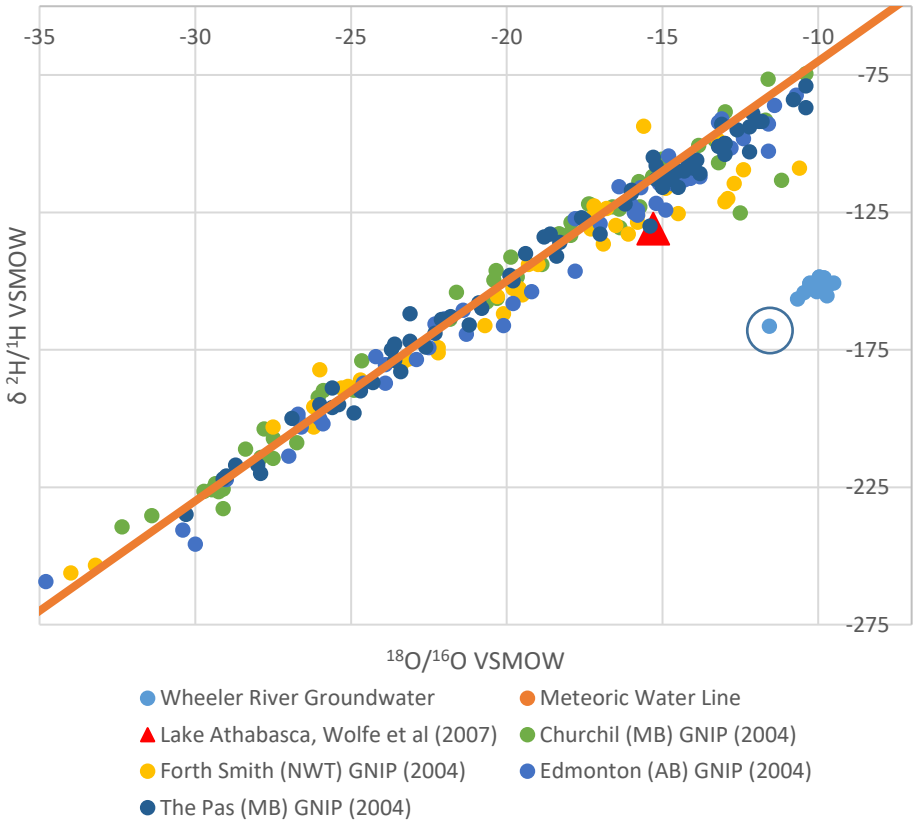

GNIP data sets are taken from the nearest sampling sites around the Wheeler River property. WR-312 is circled for being outlying from the rest of the Wheeler River data set.

Outlier WR-312

All values cluster together in $^{18}O/^{16}O$-$^{2}H/^{1}H$ diagram (Figure 49) except for one measured from groundwater in WR-312. Groundwater from WR-312 is notable for having the lowest pH (Table 18) but is otherwise unremarkable. No reason is known to explain its position, relative to other samples, in the 18O-Deuterium diagram.

Tritium of Groundwater

Tritium was measured from groundwater. The longest lasting record of tritium concentrations from within Canada have been measured monthly from Ottawa. Other long term records also exist closer to the Athabasca Basin at Fort Smith, The Pas, and Churchill (GNIP, 2004), however are limited to specific time intervals. Tritium values measured at Wheeler River are slightly below modern ratios taken in Ottawa

but well within variation, however the Wheeler River values are also intersected by both The Pas' and Churchill's isolated groundwater forecasts (Figure 50). The triple intersection makes it difficult to judge the age of groundwater.

Figure 50: Tritium records since 1960 and evolution compared with Wheeler River

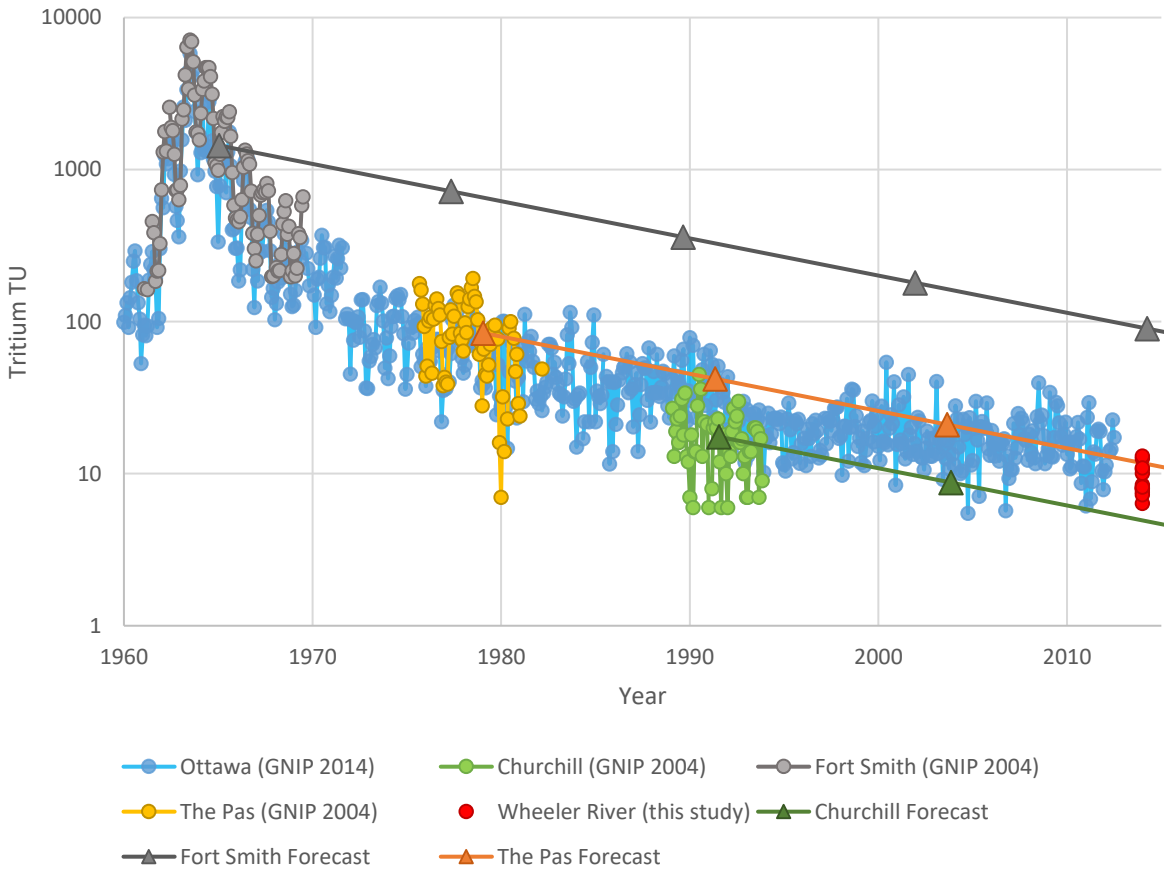

Forecasted tritium paths are calculated by taking the average tritium concentration and the median sample year. Forecast and data set are color coordinated.

Dissolved Inorganic Carbon and Dissolved Organic Carbon Content and Isotopes

Due to Rn's known affinity for organics, dissolved C concentrations and isotopic compositions were analysed. Interpretations offered will be dependent on Table 31.

Table 31: List of possible sources of carbon and typical carbon isotope compositions

Source	$\delta^{13}C$ ‰
C3 plants	-23 to -34
C4 plants	-6 to -23
Methane	-25 to -50
Soil-derived CO_2	-23 to -28
Carbonates	0 to -5

δ ‰ (compared to Pee Dee belemnites) from Faure (1988) and Palmer (2001).

Organic Carbon

Dissolved organic carbon (DOC) concentration and isotopic compositions were measured in 8 samples between 5 drill holes, four measurements from at the water table and two below it (at 20 meter intervals). Average and median concentration were ~2.5 ppm, and median $\delta^{13}C$ was -26‰. Organic ^{13}C compositions ranged from -22.9‰ to 28.2‰ typical range for C3 plants.

Table 32: DOC concentrations and compositions by drill hole

Sample	ppm C DOC	$\delta^{13}C$ ‰ DOC
WR-292	3.12	-27.5
WR-314-25*	0.60	-22.9
WR-314-45*	0.68	-22.9
WR-403	2.12	-26.4
WR-439	4.23	-27.3
WR-439-20*	3.34	-27.2
WR-439-40*	5.62	-28.2
WR-287	2.56	-26.8
Average	**2.53**	**-26.2**
Median	**2.56**	**-26.8**

** Samples were taken from within 1-2 meters of the water table.*

Figure 51: DOC concentrations and isotopic compositions

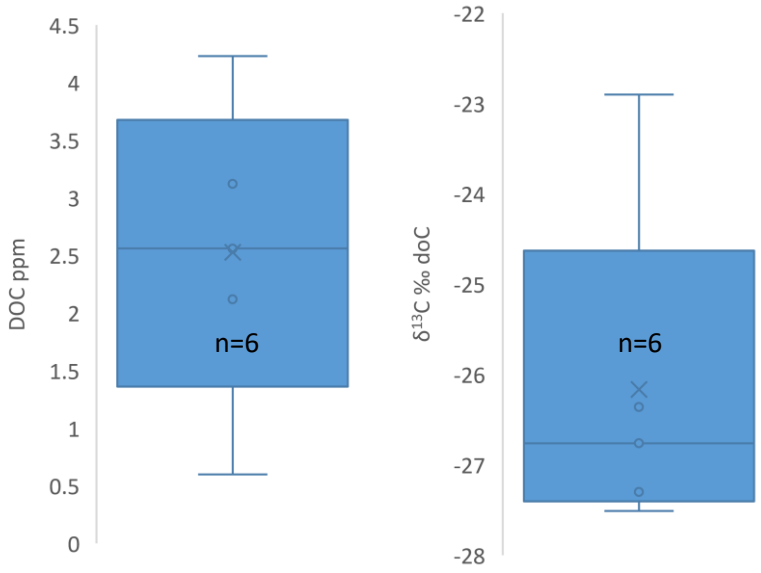

Four samples were taken below the water table in holes WR-314 and WR-439. No measurement was taken from at the water table for WR-314. DOC concentration remains nearly constant at depth in WR-314, and initially decreases from surface in WR-439 over the first 20 m interval and then increases over the final 20 m interval. Given the change, it's difficult to say how concentration behaves deeper. Isotopic composition was also measured, and δ13C appears to decrease with depth in WR-439, and remains nearly constant in WR-314.

Figure 52: Depth profiles of DOC concentration and composition

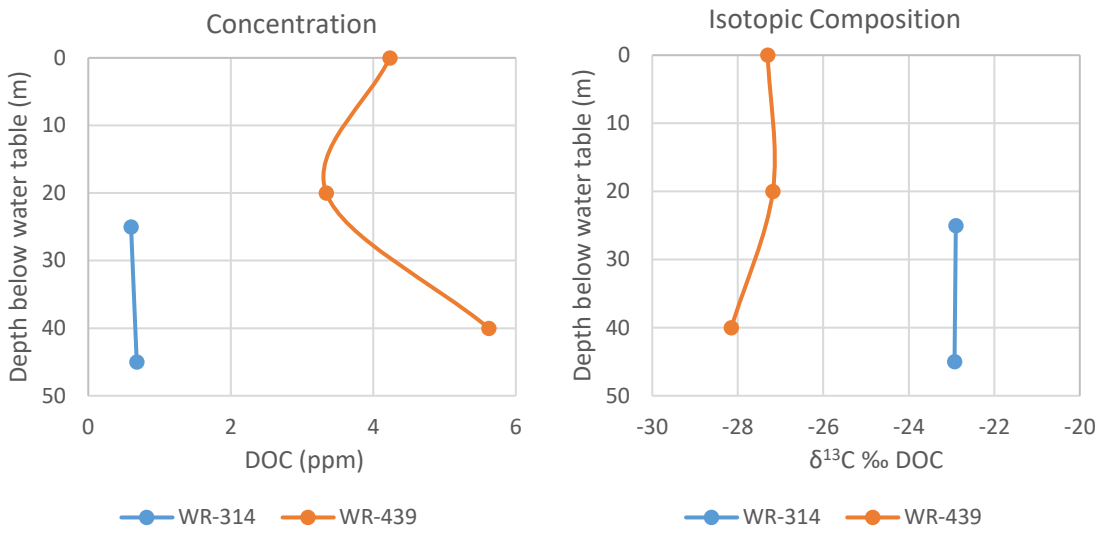

DOC values from hole WR-314 (blue) do not vary with depth. WR-314 is 1.1 k*m to the south-west from the surface projection of the Phoenix deposit. WR-439 DOC content appears to decrease with depth, and its isotopic composition proceeds to more negative values.*

Inorganic Carbon

Similar to DOC, dissolved inorganic carbon (DIC) concentrations and $\delta^{13}C$ were also measured from 8 samples in 5 holes; four samples from the water table, and four below. Average and median DIC concentrations were ~4 ppm, and median $\delta^{13}C$ was -11‰. $\delta^{13}C$ ranged between -6.3‰ and -20.7‰ typical of subsurface waters, and likely from HCO_3 produced by C4 plant respiration or decay (Kendall & McDonnel, 1998).

Table : DIC concentrations and compositions by drill hole

Sample	ppm C DIC	$\delta^{13}C$ ‰ DIC
WR-292	3.59	-10.8
WR-314-25*	3.06	-6.6
WR-314-45*	3.09	-6.3
WR-403	4.48	-12.8
WR-439	4.91	-12.7
WR-439-20*	4.41	-11.7
WR-439-40*	9.95	-20.7
WR-287	3.97	-12.0
Average	**4.00**	**-11.0**
Median	**3.97**	**-12.0**

*Average and median are calculated from samples taken near the water table only. Sample names marked with * are those taken below the water table.*

Figure 53: DIC concentrations and compositions

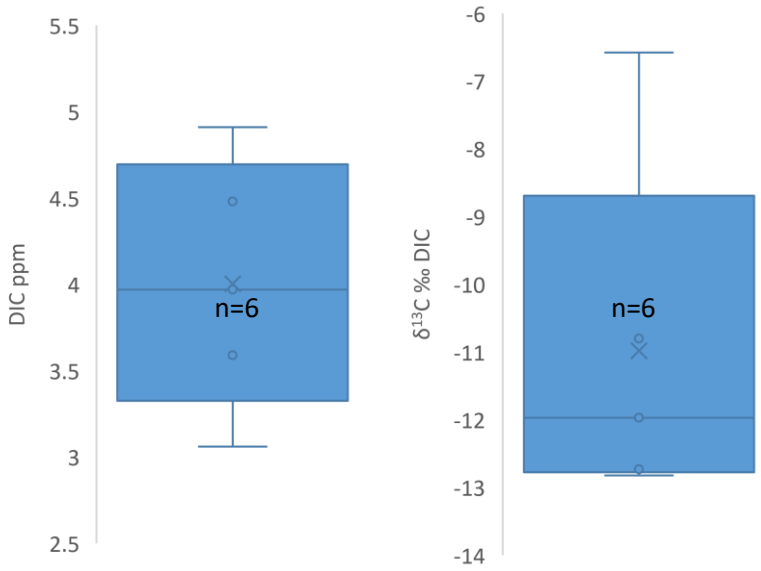

X marks the average value.

Four samples were taken from below the water table in holes WR-314 and WR-439. No sample was taken from at the water table for WR-314. Both concentration and composition of DIC remain approximately constant with depth in WR-314. Concentration of DIC increases for WR-439 over the 40m sample interval and ^{13}C compositions become more depleted with depth after the 20m mark.

Figure 54: Depth profiles of DIC concentration and $\delta^{13}C$

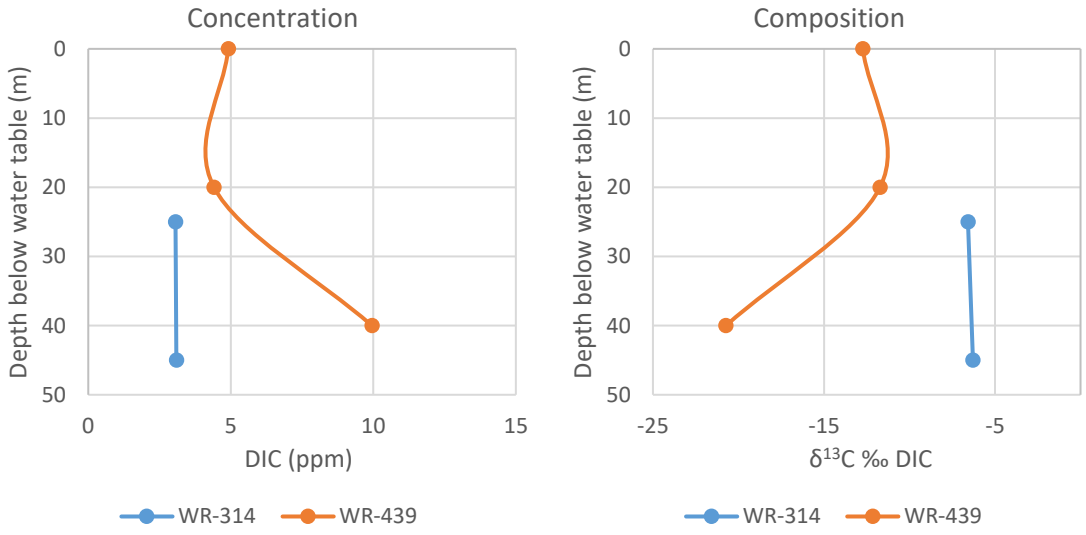

WR-314 is 1.4 km to the south-west of the Phoenix Deposit's surface projection. WR-439 is directly above the Phoenix Deposit's north-east end.

Any further implications of both DIC and DOC concentration and composition are not discussed.

Dissolved and Particulate Groundwater Chemistry

Results of groundwater chemistry analysis are presented below and are subdivided into two sections; cations and anions. Groundwater cation concentrations are total including both dissolved and particulate content of groundwater. Groundwater anion concentrations are total including both dissolved and particulate content of groundwater, and no samples taken from depth were analyzed.

Groundwater from drill hole WR-345 had consistently high major cation content (Ca, K, Na, Mg) as well as the second highest U content (as the total of dissolved and particulates). Drill hole WR-287 had the highest U content of any hole with nearly 500 ppb.

Drill hole WR-314, located approximately 1.4 km to the south-west of the Phoenix Deposit surface projection (refer to Figure 6 for map) also had notably high major cation content (compared to the following two drill holes to the south-west of the deposit surface projection), the highest major anion concentrations, and high U and Pb content. These characteristics may be related to WR-314's location; a few meters from a stream, and the water table was at surface. WR-314 was also the only hole having artesian flow momentarily.

Depth profiles were constructed from three samples each; one within 1-2 meters of the water table, and two subsequent samples at 20 meter intervals.

Total Cations – Combined Particulate and Dissolved

Calcium

Total Ca content of groundwater varies between approximately 2 and 4 ppm in holes measured with one outlying high concentration of approximately 8 ppm from WR-345. WR-314 also has a high Ca concentration, at the water table, compared to other holes distal to the surface projection of the Phoenix Deposit. Ca concentrations in WR-314 increase with depth, whereas WR-439 decrease over the first 20-meter interval, and then increase in the following interval. Use of cement in drill holes, with groundwater influx, likely exerts some control over Ca concentrations.

Figure 55: Groundwater total Ca concentration by hole and depth profile

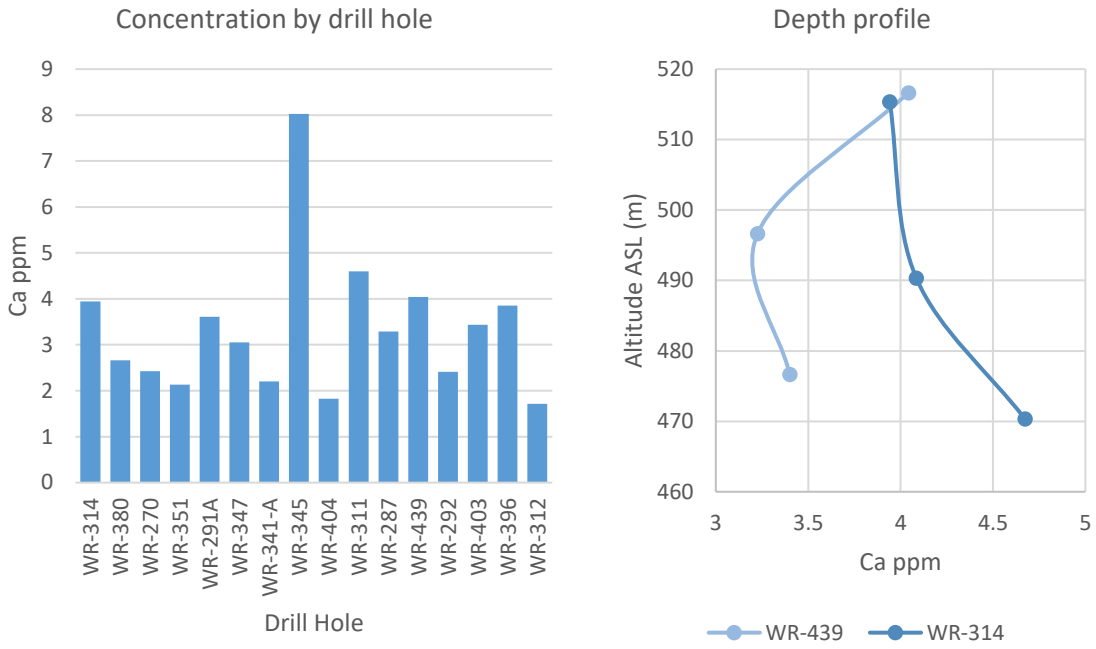

Drill holes are ordered from south-west to north-east along trend of the Phoenix Deposit. Drill holes WR-351 to WR-396 are directly above the deposit.

Potassium

Total K content in groundwater varies between approximately 0.3 and 0.8 ppm, with three high concentration outliers; WR-314, WR-345, and WR-292 with 1.5-2.2 ppm. In both depth profiles, K content initially decreases over the first 20 meters and then remain constant for the next 20 meters.

Figure 56: Groundwater total K concentrations by hole and depth profile

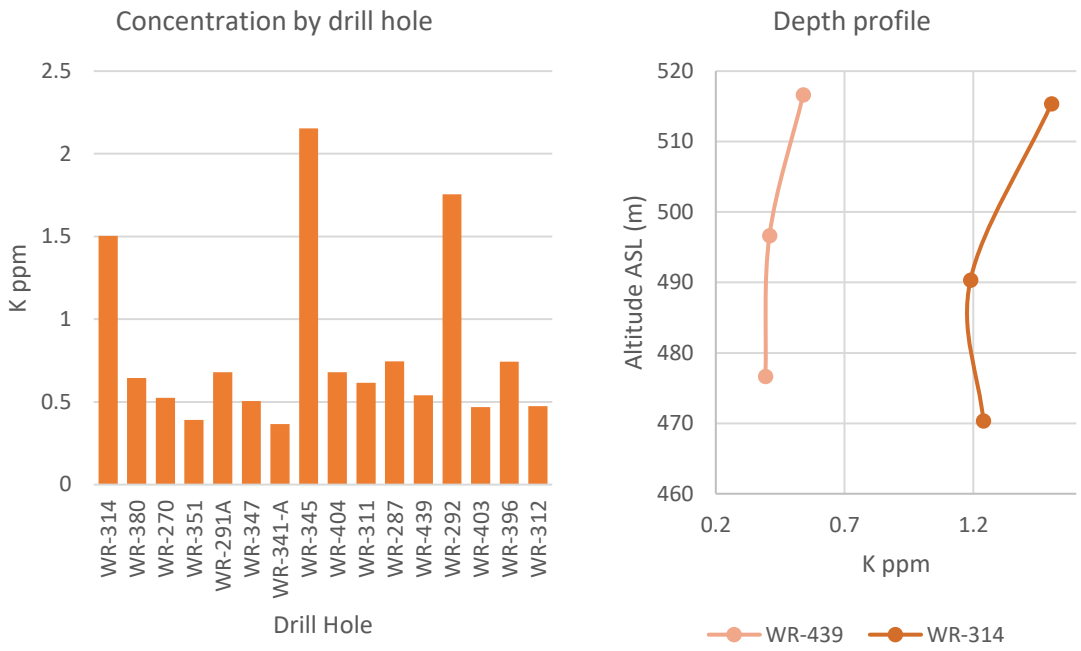

Drill holes are ordered from south-west to north-east along trend of the Phoenix Deposit. Drill holes WR-351 to WR-396 are above the Phoenix Deposit.

Magnesium

Total Mg content varies between 0.5 and 1.5 ppm, with two notable outliers; WR-345 with 2.5 ppm and WR-314 with 0.35 ppm. Groundwater from WR-314 also contains more Mg than other holes distal to the surface projection of the Phoenix Deposit. With depth, Mg content continues to increase in WR-314, and in WR-439 initially decreases with the first 20 meters and then increases over the following 20 meters.

Figure 57: Groundwater total Mg concentrations by hole and depth profile

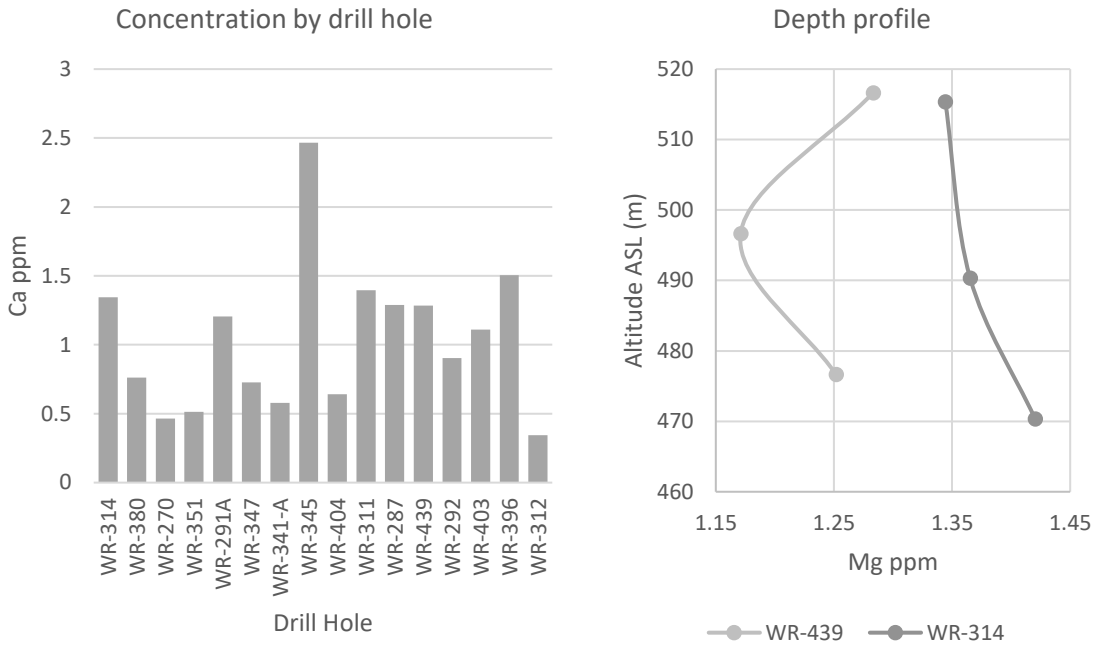

Drill holes are ordered from south-west to north-east along trend of the Phoenix Deposit. Drill holes WR-351 to WR-396 are directly above the Phoenix Deposit.

Sodium

Total Na groundwater content varies uniformly between approximately 1 and 5 ppm. Notable high values include WR-314, the highest value of the drill holes distal to the surface projection of the deposit (>100 m), and WR-345 with the highest total Na content measured (2.5 ppm). Both depth profiles show an initial decrease in Na content over the first 20 meters followed by an increase in the final 20 meters.

Figure 58: Groundwater total Na concentrations by hole and depth profile

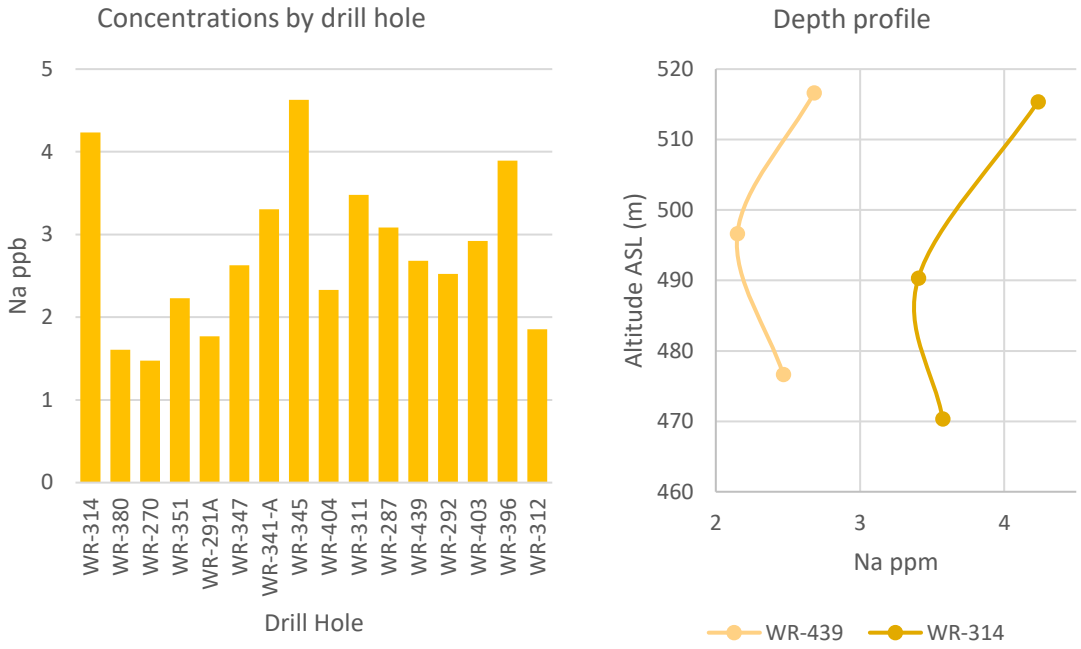

Drill holes are ordered from south-west to north-east along trend of the Phoenix Deposit. Drill holes WR-351 to WR-396 are directly above the Phoenix Deposit.

Pb

Total Pb content in samples (dissolved and particulates) varies lognormally between approximately 0.01 ppb and 21 ppb (detection limit is 0.003 ppb). Lowest value was measured in the groundwater from WR-311 (0.01 ppb), and the highest value from WR-287 (20.7 ppb). Groundwater in WR-314 has the highest total Pb content (1.5 ppb) of the drill holes distal to the surface projection though with WR-270 at a close second (1.2 ppb). In both depth profiles, groundwater total Pb content initially increases in the first 20 meters, then decreases over the following 20 meters.

Figure 59: Groundwater total Pb concentrations by hole and depth profile

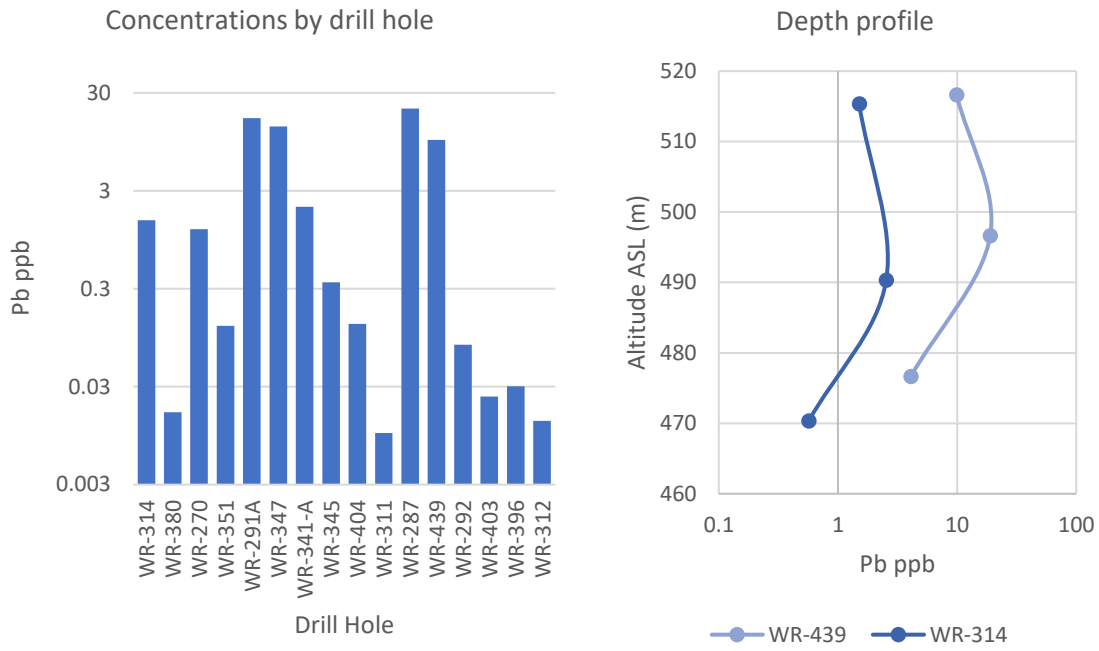

Drill holes are ordered from south-west to north-east along trend of the Phoenix Deposit. Drill holes WR-351 to WR-396 are directly above the Phoenix Deposit. Note that the y axis of the bar graph is logarithmic.

Thorium

Groundwater total Th content varies lognormally and ranged from below the detection limit (0.003 ppb) to 1 ppb. Highest Th contents were measured from groundwater in WR-291A and WR-287 (0.65 and 1 ppb respectively). Groundwater total Th content decreases with depth in WR-439 and in WR-314, though with an initial increase over the first 20 meters in the latter hole.

Figure 60: Groundwater total Th concentrations by hole and depth profile

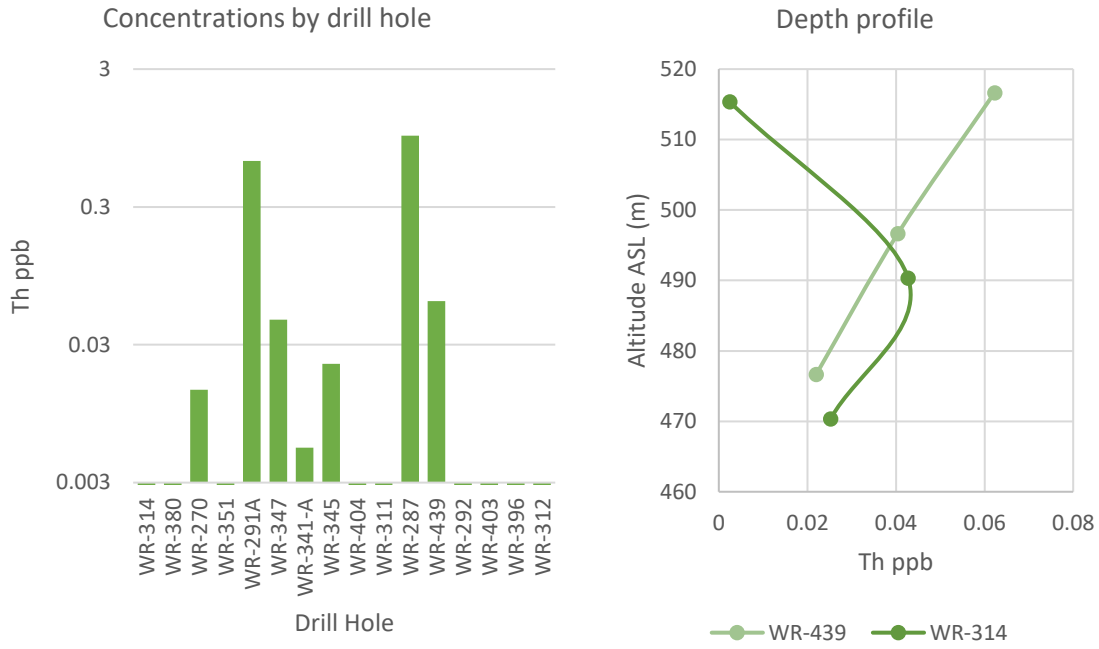

Drill holes are ordered from south-west to north-east along trend of the Phoenix Deposit. The Phoenix deposit is underneath WR-351 to WR-396. Note that hole WR-287 has a Th content (particulates) of 0.98 ppb. Holes without bars are below the detection limit of 0.003 ppb. The highest altitude point in the WR-314 depth profile is below the detection limit. Y axis of the bar graph is logarithmic.

Uranium

Total U content in water and particulates varies lognormally between 0.007 and 500 ppb (detection limit is 0.001 ppb). Notably, the highest total U content measured was in WR-287. In both depth profiles, total U increases over the first 20 meters, and then decreases. By similar calculations to those presented on page 36 (comparisons between U, Ra, Rn, and Pb), none of the groundwater sampled contains enough particulate and dissolved U to produce the measured Rn.

Figure 61: Groundwater total U concentrations by hole and depth profile

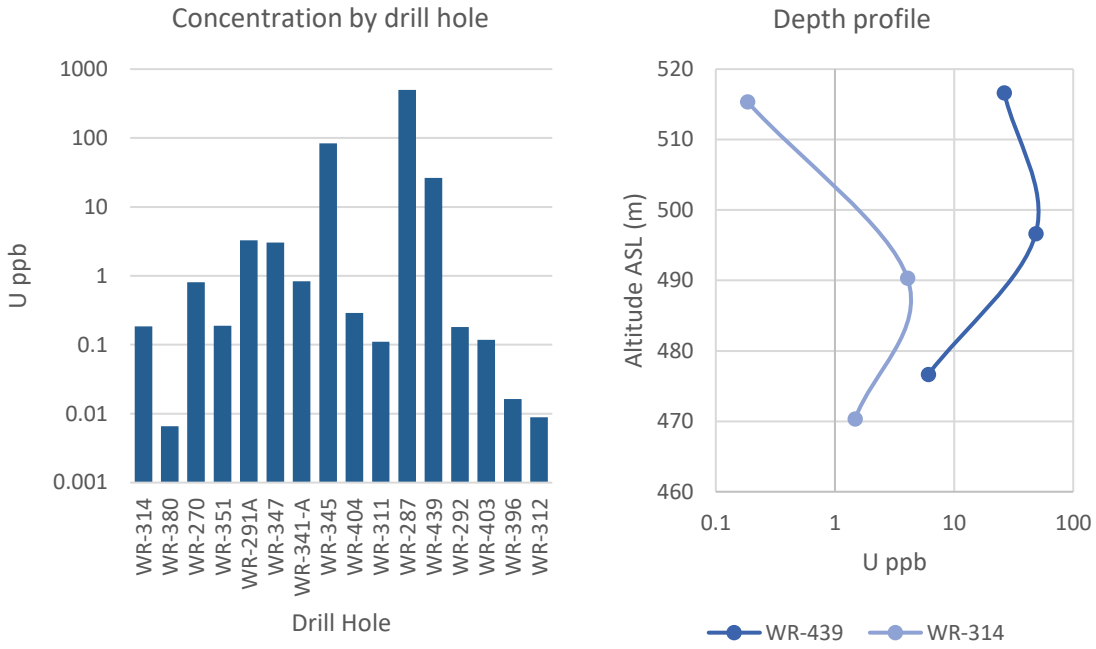

Drill holes are ordered from south-west to north-east along trend of the Phoenix Deposit. Drill holes WR-351 to WR-396 are directly above the Phoenix Deposit. Note that the y axis of the bar graph is logarithmic.

Anions – Dissolved

Fluorine

Total F concentrations in water and particulates vary between approximately 0.003 ppm and 0.1 ppm. Highest total F concentration was measured in WR-287, and a notable high concentration was also measured from WR-314. Detection limit is 0.002 ppm.

Figure 62: Groundwater total F concentrations by hole

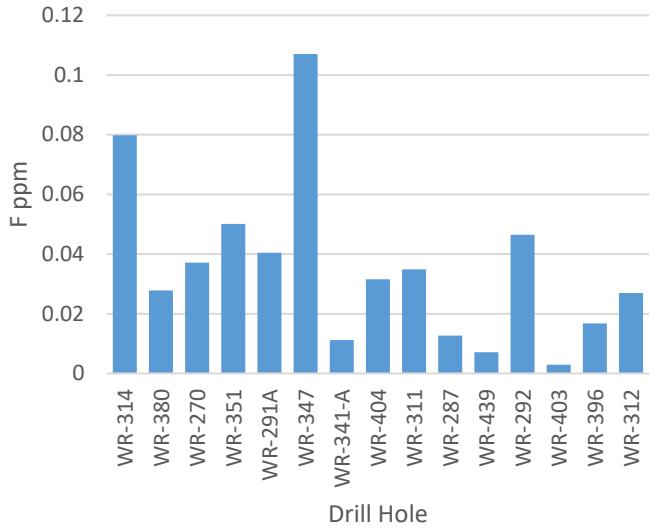

Drill holes are ordered from south-west to north-east along trend of the Phoenix Deposit. Drill holes WR-351 to WR-396 are directly above the Phoenix Deposit.

Chlorine

Groundwater total Cl concentrations are lognormally distributed, with a median value of approximately 0.4 ppm. Highest total value measured is in WR-314 with 5.4 ppm and lowest value in WR-404 with 0.08 ppm. Detection limit is 0.007 ppm.

Figure 63: Groundwater Cl concentrations by hole

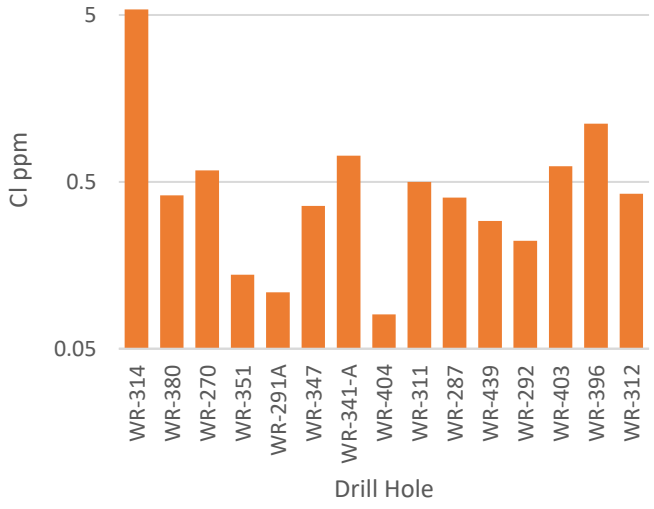

Drill holes are ordered from south-west to north-east along trend of the Phoenix Deposit. Drill holes WR-351 to WR-396 are directly above the Phoenix Deposit. Note y axis is logarithmic.

Bromine

Total Br concentrations are lognormally distributed, and vary between 0.001 and 0.005 ppm. One outlying high concentration of 0.04 ppm was measured in WR-314. Detection limit is 0.002 ppm.

Figure 64: Groundwater total Br concentrations by hole

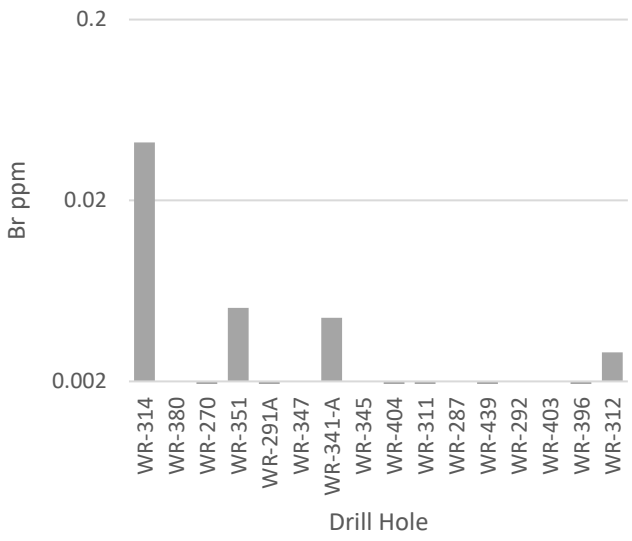

Drill holes are ordered from south-west to north-east along trend of the Phoenix Deposit. Drill holes WR-351 to WR-396 are directly above the Phoenix Deposit. Drill holes without associated bars are those either below the detection limit (0.002 ppm).

Discussion

Source of Rn

Diffusion

In determining the source of Rn, consideration must be made to how Rn can travel and how quickly. Diffusion in water is an extremely slow process considering the great distances, over 400 meters, between the Phoenix Deposit and the sampling sites.

By comparing approximate diffusion distance for given lengths of time with the half life of Rn (Figure 65), diffusion would be unable to transport Rn from deposit to the static water level. Within 40 days, 10 half lives of Rn have elapsed and any remaining Rn has only moved 15 cm.

Figure 65: Diffusion Distance and Half Lives

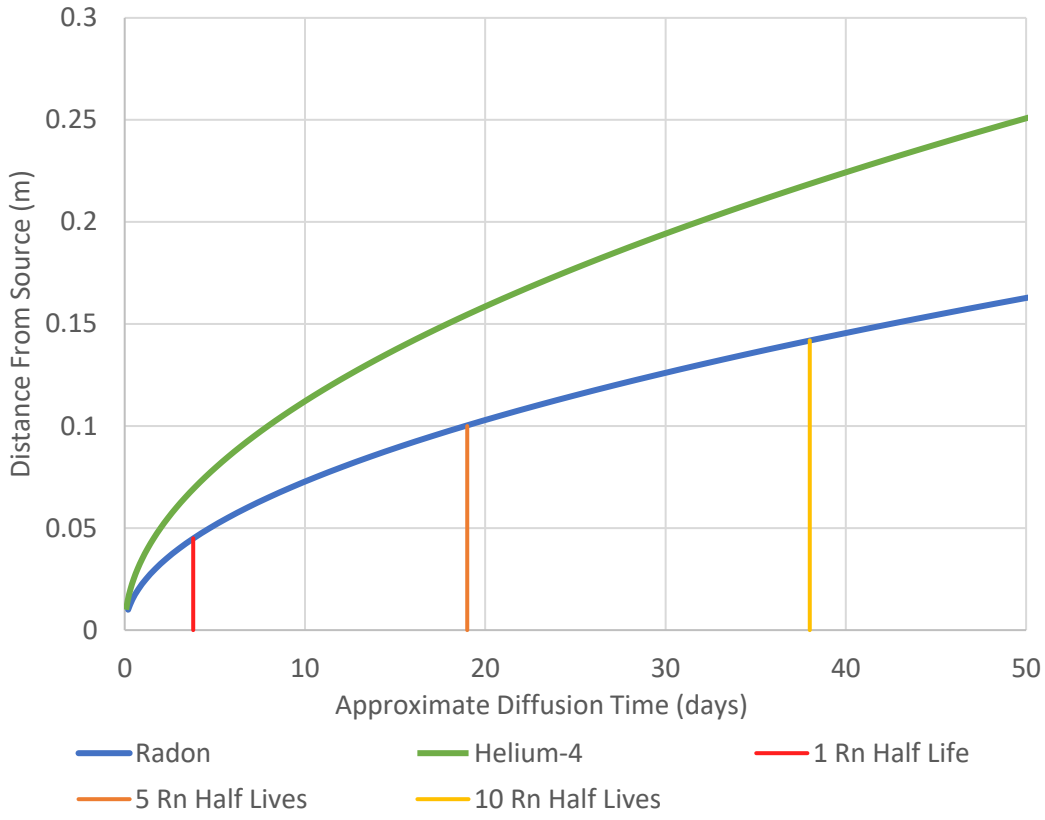

Figure showing the relation between elapsed time and diffusion distance for Rn and He. Three points in time are highlighted corresponding to the number of half lives past.

He-4 nuclei would also take upwards of thousands of years to travel from deposit to surface, but He-4 does not decay so this diffusion is theoretically possible.

Several nuclei, such as ^{238}U and ^{226}Ra, have longer half lives and so may be able to diffuse the larger distance as to produce an Rn anomaly. However, with longer half lives (4.5 Gy and 1602 years respectively) these nuclei exist for longer periods than Rn and so have potential to diffuse further.

Even in a situation where groundwater flow makes a significant contribution to the mobility of Rn, Rn nuclei would not be able to travel more than a few meters before decaying. In this study, Rn is most likely being produced from Ra decay in the MFd member.

Rn and drilling

Figure 66: Comparison of groundwater Rn from mineralized and non-mineralized holes

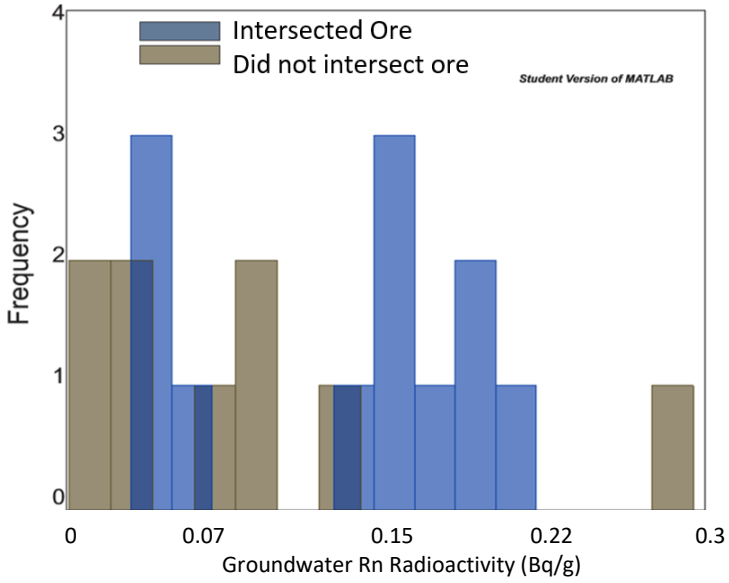

Double histogram of groundwater Rn concentrations taken from drill holes that intersected ore (blue) and from drill holes that did not intersect ore (grey).

Many drill holes had intersected mineralization. To rule out the possibility that groundwater Rn concentrations are from U or Ra rich materials left on the inner walls of the drill holes, drill holes were divided into two groups; those that had intersected mineralization and those that did not. A student T-test was then performed to determine if the division into two populations was statistically meaningful. Mineralization intercepts were provided by Denison Mines'.

The result was an insignificant difference between populations with an 80% certainty, indicating that mineralized material lining the inner walls of the drill holes, or spilled into surrounding sandstones and tills, is not a major contributor to measured groundwater Rn concentrations.

Groundwater Rn and sandstone U content

There are three possible sources of Rn; the deposit, sandstones, and overlying soil and till. By a process of elimination, the only remaining source of Rn parent nuclei to be assessed are the sandstone. Because of the potential of local scale mixing (1-2 m) caused by groundwater, and the unknown distance that U or Ra could travel, Rn contents were plotted against average U contents per bed, for each drill hole (Figure 21 - Figure 24).

Figure 67 shows a positive correlation between U contents per drill and the concentration of Rn measured from the respective drill holes for both 2AMS and 3AMS digestion. U concentrations in MFc and MFb also correlated with Rn radioactivity of groundwater, but it is unlikely to be due to Rn contributions from depths lower than MFd given the distance and slow diffusion of Rn.

Figure 67: MFd U concentration against groundwater Rn

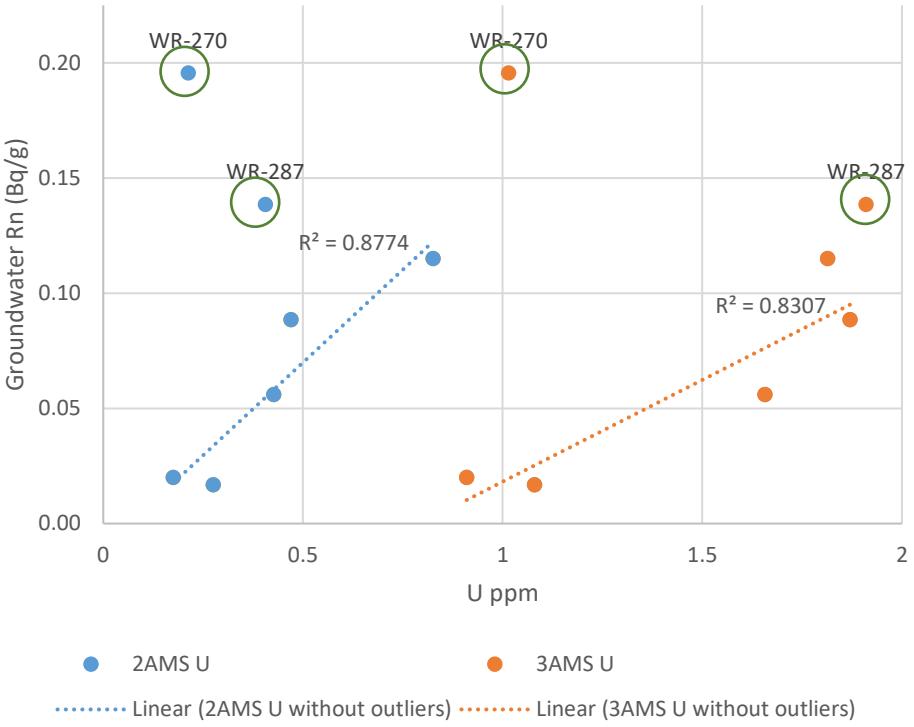

Positive correlation exists for both trends, when outliers (circled in blue) are sorted out.

In addition to correlating on an individual drill hole basis, the range in measured Rn radioactivities is high, but overlap with the ranges of expected Rn radioactivities, as calculated from all MFd U concentrations (Figure 68). It is important to note than measured Rn is not the same as total produced Rn, as emanation rates from Ra-containing crystals and rocks is unaccountable, and Rn can also be added from surrounding substrate (example: soil). However, both cases could be inferred to explain the outliers (WR-270 and WR-287), and the seemingly high range.

Figure 68: Rn measured vs expected MFd

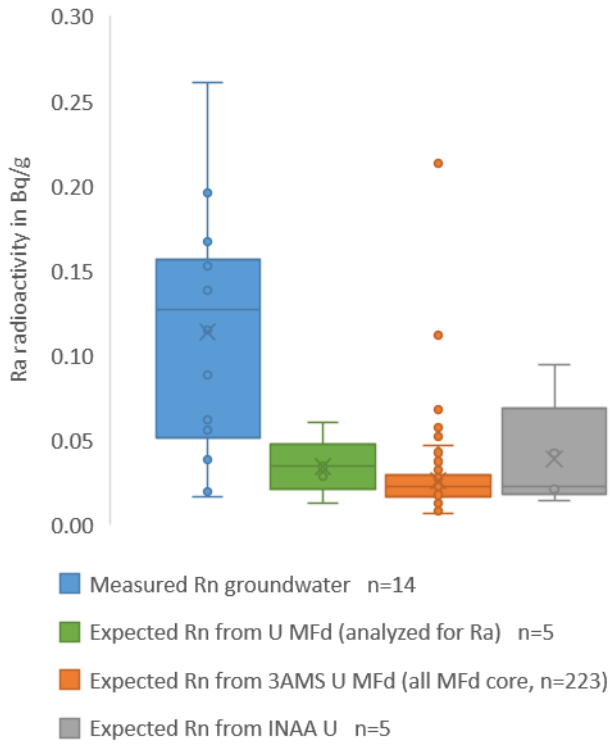

X marks the average for the individual data sets.

For the following discussion, emanation is the term used to describe the fraction of Rn nuclei (or other decay products) that escape the U-hosting (or Ra) crystal or solid and enter a surrounding fluid (air, interstitial fluids, groundwater, etc.) as to be later sampled. Rn that escapes a solid phase only to embed in a neighboring insoluble phase is not considered to have "successfully" emanated. Escape mechanisms would include alpha-recoil, fission track etching, or chemical weathering. (Fleischer, 1983)

Rn emanation rates have been calculated and experimentally measured and modelled (Semkow, 1990) given a wide range of differing substrates, grain size, water content and porosities, temperatures, internal radioactivity (from U, Ra, Th, etc.), and other controlling variables. Garver and Baskaran (2004) showed the effects temperature has on Rn emanation for varying materials. Experimental results from Barillon et al., (2005) attempted to measure Rn emanation from U mine tailings into surrounding air or water and found emanation coefficients between 10% and 35% (more water resulted in higher emanation rates), depending both on water mass fraction and grain size (from unsieved to <0.45 µm). Experiments have been conducted on soils by Greeman and Rose (1996) that found emanation coefficients for Rn ranged between 15% and 22%, with higher values associated with silt or clay. Organic coatings on soil had the highest emanation coefficients of 46% (Greeman & Rose, 1996). Pipe scale from petroleum production sites have also been measured for Rn emanation coefficients, and ranged between <5% to as high as 30%, with significant variation between locations measured (White & Rood, 2001). These values are all high in comparison to the wet (fluid in pore space) emanation coefficients measured by Garver and Baskaran (2004); for monazite (4%), zircon (0.6%), uraninite (without water in pore space; 0.5%), thorite (15%), and cerite (17%). However, the issue with comparing these values directly is that the radioactivities of the

substrates (from U or Ra content) vary significantly between studies and directly affect Rn released by water-etching (Fleischer, 1982).

Given the low Rn emanation rates determined by modelling and measurement (all lower than 35%), measured Rn in the groundwater above the Phoenix deposit is unlikely to represent the majority of Rn produced in the MFd member, or overlying soil. Thus, the offset between measured Rn and expected Rn in MFd (Figure 68) is unexpected, suggesting either significant additional sources of Rn to near-surface groundwater, or an issue with sampling or measurement.

Unlike Rn, He is stable and thus can travel great distances through air or water and despite dilution, the detection of radiogenic He surrounding and above U deposits is well documented (Brady & Rice, 1977) (Clarke et al., 1977) (Power, 2013). In the process of one atom of ^{238}U decaying to ^{206}Pb, 12 He nuclei are produced as alpha emissions. The lack of high He in the groundwater above the Phoenix deposit is unexpected, especially with drilling activities being common since 2005. However, the Phoenix deposit is not the only deposit without high He at surface; He diffusion samplers collected by Devine (2015) above MacArthur River Mine's deposit also resulted in low radiogenic He.

Two possible scenarios exist to explain the lack of geogenic He; a passive barrier or an active barrier. Both options are discussed on page 80.

Source of Ra and overabundance

Mobility of Ra in Wheeler River

Overabundance of dissolved Ra in groundwater is well documented in Cecil et al., 1987, Gilkeson and Cowart 1987, and Szabo et al., 2012. The amount of mobile Ra in groundwater is controlled by acidity or high concentrations of dissolved solute. H^+ ions outcompete Ra for absorption sites in any given substrate and force Ra into solution (Cecil et al., 1987) (Gilkeson & Cowart, 1987) (Szabo et al., 2012). Distinction is made between (true) solubility, and mobility of Ra atoms. Mobility is a broad term including solubility, mechanisms of transportation and relocation, and effects relating to absorption or desorption from surfaces (such as competition with other cations).

The Ra measured was in the soil and sandstone, not in groundwater. The groundwater (measured from within MFd) does not contain high solute concentrations (average conductivity = 47.3 µS/cm and median conductivity = 36.5 µS/cm) and is not very acidic (average pH = 7.13). This suggests that Ra is relatively immobile when below the water table within the MF and RD sandstones. Refer to Figure 69 for a comparison between pH and Ra radioactivity in groundwater from Szabo et al., (2012).

Figure 69: Effect of pH on groundwater Ra radioactivity

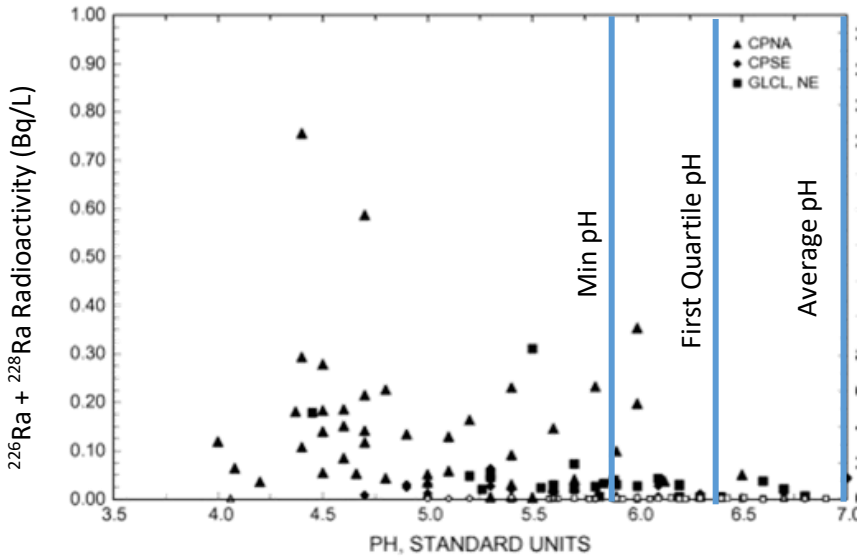

Modified from Szabo et al., (2012). Overlaying the figure are the minimum pH (first quartile pH, and average pH (median and third quartile are outside the figure) of sampled Wheeler River groundwater (n=16). Samples in Szabo et al., (2012) were taken from three aquifer systems in the U.S.; the Coastal Plain, North Atlantic (CPNA), the Coastal Plain, South-Eastern (CPSE), and the glacial sand and gravel from new England (GLCL NE). As has been noted, the ExStick tool used to measure pH was only calibrated prior to field work, and thus pH values may be in question.

Sources of Ra

Comparisons between Ra and U concentrations, taken from 3AMS and INAA, and the expected Ra radioactivities calculated from those concentrations, reveal that INAA is a far more accurate predictor of Ra radioactivities than 3AMS. INAA U and Ra correlate, and expected Ra produced by INAA U are similar in magnitudes. This can be explained by the differences in how Ra, 3AMS U, and INAA U are measured. 3AMS determines the concentration of U within phases soluble in HF, $HClO_3$, and HNO_3 or leachable from the surfaces of tougher phases exposed during the grinding and milling procedure. Although Ra was primarily sampled from exposed grain fragment surfaces or crystal sites near specified surfaces, Ra radioactivity trapped within crystal phases was corrected for by measuring samples unprocessed by the $BaSO_4$ precipitation method. Importantly to note, the INAA U data set is small, and in the case of the RD formation, the correlation is reliant on only three points.

MFd was the only unit that contained overabundant Ra, with between 10-50% too much Ra compared to Ra expected from INAA U. Of the lower three sandstone units (MFc, MFb, and RD) only two samples contained unsupported Ra, the majority had between 20-30% less Ra than expected. The two samples with unsupported Ra, DPX 199 from MFb, and DPX 240 from RD had 4.2x and 2.6x more Ra than expected respectively. Unsupported Ra may also be due to the loss of U, and similarly, missing Ra could also be from the gain of U.

If Ra has been added to MFd, it could be from soil and till. Both soil and till contain significant concentrations of soluble materials and the soil is acidic. Additionally, mid continent surface water can have a pH as low as 3.8-4.8 (Willey et al., 1987). As acidic surface water percolates through acidic soils (Schreiner, 1983), easily leached Ra dissolves and is transported downwards to the water table and MFd. Groundwater above the Phoenix deposit is neutral regarding pH and has a low concentration of dissolved

solutes, so as surface water mixes with groundwater, it is expected that Ra would drop from solution and be absorbed onto the silica and quartz surfaces. B horizon soil was also noted as having less Ra radioactivity than expected given its INAA U concentration, also supporting this interpretation. Excess Ra from soil and till may also explain the measured range of Rn radioactivity compared to expected from U. Further confirmation of this theory comes from Pb isotopes and can be found on page 79.

In the case of the two high Ra samples in MFb and RD, both are from drill holes above the north-east end of the Phoenix deposit (DPX 240 from WR-321 and DPX 199 from WR-286) (refer to Figure 70). Physical characteristics of both samples were noted. DPX 240 (from RD) was noted for having two distinct generations of jointing, with the first series having been partially infilled with "glassy" quartz. DPX 199 (from MFb) was composed entirely of poorly sorted sub-angular to rounded sand and was slightly hematized. The fractures in DPX 240 and the unsolidified nature of DPX 199 suggest that they represent zones of high permeability for groundwater, and potentially the conduit for Ra release from deposit (though limited by mobility) or the loss of U.

Figure 70: Location of WR-321 and WR-286

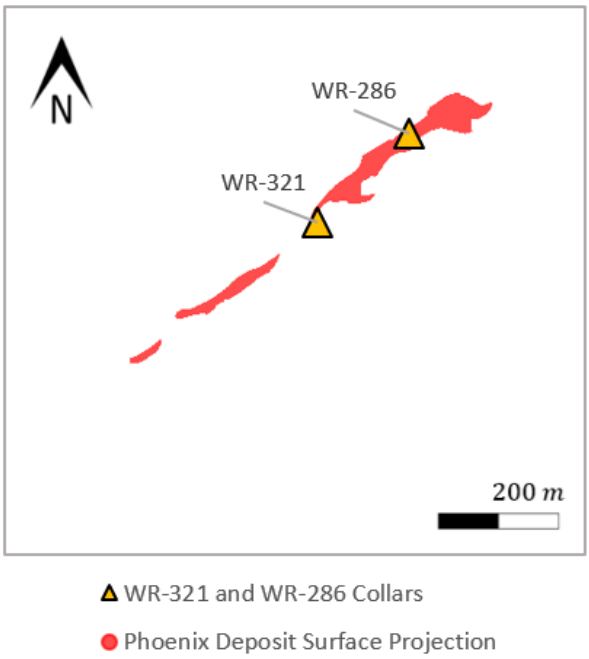

Sandstone samples DPX 240 and DPX 199 were taken from WR-321 and WR-286 respectively. Both samples contained unsupported Ra.

How long has there been unsupported Ra in MFd?

The overabundance of Ra within the MFd could be the result of Ra produced in soil, till, and MFd itself accumulating at the water table. Although the soil only formed after deglaciation (deglaciation occurred 8500 years ago) (Dyke, 2004). Unsupported Ra in MFd, if from soil, cannot be older than 8500 years.

If unsupported Ra is also from till, then the duration that unsupported Ra has been present in MFd can be significantly longer. The last glacial maximum was the Wisconsin glaciation and growth of the

Laurentide Ice sheet started ~115 thousand years ago (Andrews & Mahaffy, 1976). Glacial melt could leach till suspended in ice or lodgement till and so dump Ra into MFd sometime after 115 thousand years.

However, both cases (8500 years or 115 thousand years) are very long time periods for groundwater, it is very possible that the water table has moved significantly across that time. Current glacial rebound in the region is on the order of 5 mm/year (Sella et al., 2007), which could represent a cumulative 40-meter upward displacement, a very large difference for groundwater.

The effect of Ra mobility on Rn as an exploration tool

In Wheeler River, groundwater Rn concentrations were correlated with U concentrations of MFd, which is correlated within drill hole to U concentrations in deeper sandstone beds. This may only be possible because Ra is relatively immobile; regardless of supported or unsupported interpretation.

If the groundwater contained high concentrations of dissolved ions or was acidic, Ra would be mobile and more could escape from the metamorphic basement, deposit, or from the sandstones. It takes days for Ra and Rn to reach secular equilibrium, and thus sampling Rn produced by Ra originating distal to the sample site could overwhelm the Rn radioactivity produced by the high U zone above the deposit. If no deposit is present in this hypothetical scenario, then higher Rn concentrations could be very misleading. Thus, a condition on Rn's practicality as an exploration tool can be made. An understanding of basic groundwater chemistry in an exploration area is required. Measuring salinity or conductivity and pH of groundwater is critical for the application of Rn sampling and its usage for exploration. In the case of Wheeler River, this may be problematic as the water table is only accessible by drill hole when above the deposit.

Pb isotopic compositions, the missing He, and groundwater flow

Interpretation of sandstone Pb isotopic compositions

Overall, MFd Pb isotopic compositions are similar to the compositions obtained from B horizon soil (refer to Figure 71), regardless of leach. DPX 177, identified as having a Pb isotopic composition more like MFc compositions, MFb, and RD than MFd (page 53) is also the only MFd sample that has matching measured and expected Ra radioactivity. This suggests that DPX 177 has remained closed to interactions with surface waters and soil. DPX 177 is also shown in Figure 71.

Figure 71: Comparison of Pb isotopic compositions for MFd to B horizon soil and DPX 177 to MFc

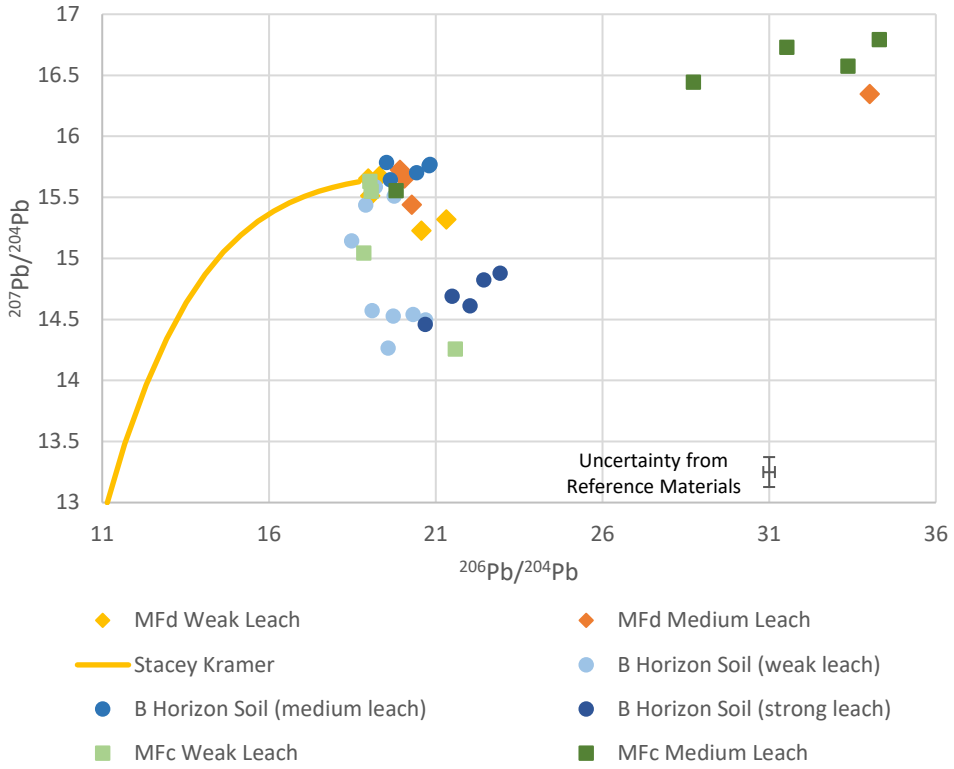

The uncertainty derived by measuring reference materials and comparing to recommended values is shown in the lower right and would apply to all points. Stacey-Kramer curve modified from Stacey & Kramer (1975).

Holk et al., 2003 showed that Pb isotopic compositions or sandstones above the Cigar Lake U deposit indicative of receiving input from the Cigar Lake U deposit ranged from 56.52 – 194.80 for $^{206}Pb/^{204}Pb$. Using Holk et al., (2003) threshold for U deposit input, only DPX 145 from RD showed indication of interaction with U ore ($^{206}Pb/^{204}Pb$ = 93.78 and $^{207}Pb/^{204}Pb$ =19.20). Notably, this does not have overabundant Ra.

Groundwater flow and the missing He

Diffusion gas samplers were deployed on two separate occasions in this study (2014, 2015) and data is also used from Power (2013) and Krahenbil (2013). Analysis of samples also occurred at two different labs (Université du Québec à Montréal, and University of Ottawa). In all cases, ^{4}He concentrations were indicative of equilibration between groundwater and atmosphere.

Figure 72: Diffusion sampler deployment sites

Figure 73: Distribution of He measurements above the Phoenix Deposit

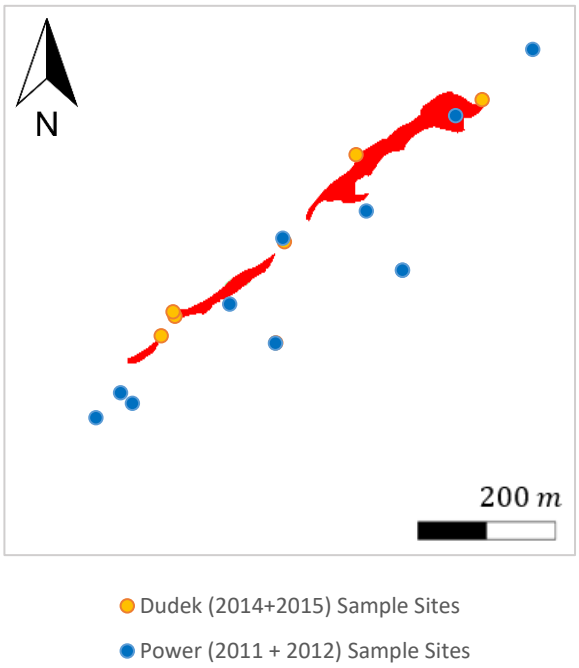

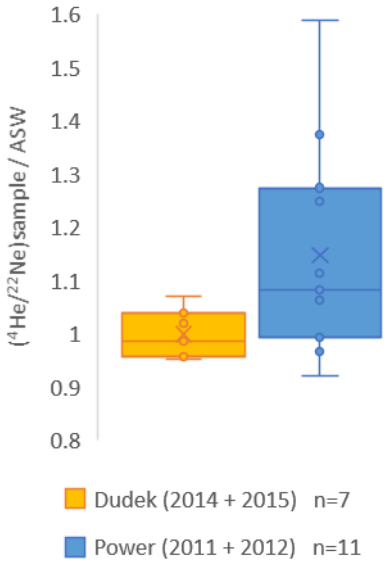

Figure 73: X marks the average value.

Unlike Rn, He is stable and thus can travel great distances through air or water and still be detected. Of course, dilution would be a concern, but the detection of radiogenic He surrounding and above U deposits is well documented (Brady & Rice, 1997), (Clarke et al., 1977), and Power, 2013). In the process of one atom of ^{238}U decaying to ^{206}Pb, 12 He nuclei are produced as alpha emissions. The lack of abnormal He isotopic compositions detected in the groundwater above the Phoenix deposit thus is surprising. Power (2013) using similar diffusion samplers, found $^{4}He/^{22}Ne*ASW^{-1}$ values as high as 786 above the Millennium U deposit. However, the Phoenix deposit is not the only deposit missing near surface expression of He, He diffusion samplers collected by Devine (2015) above MacArthur River Mine's deposit also resulted in missing radiogenic He.

Broadly speaking, two possible scenarios exist to explain the absense of He above the Phoenix Deposit; a passive barrier or an active barrier. All the sandstones beds above the Phoenix deposit are very porous as observed in the sandstone samples (refer to descriptions on page 90) and confirmed by Jefferson et al., (2007a), arguing against a passive barrier. The sandstones also contain minimal clay content (Ramaekers et al., 2007), further ruling out passive barriers. However, an active barrier, such as groundwater flow within the sandstones, could be whisking away He and transporting it away from where samples were taken. He being entrained and transported by water is a well known phenomenon (Andrews, 1985), (Torgerson, 1985), (Torgerson & Ivey, 1985), (Torgerson & Clarke, 1987), (Solomon et al., 1996). Given the current non-arid environment of the Wheeler River property, surface topography may have direct effects on shallow groundwater flow, so from Figure 6 looking to the south-east may find the lost He, and also Pb if it is being lost. Notably, deep groundwater may have different flow directions.

As has been discussed, such a scenario would have mixed implications for the use of Ra and Rn in exploration. The half life of Ra, approximately 1600 years, is a significant amount of time when compared with typical groundwater flow velocities. Hydraulic conductivity for sandstones can range from 10^{-2} to 10 m/year and range from 10 to 10^{5} m/year for sand (Freeze and Cherry, 1979). For highly mobile Ra, U

deposits could produce haloes of Ra and Rn that point down-flow with a possible Pb isotopic signature. Such a halo could be detected and used to vector towards a deposit. However, this assumes flow is fast enough and confined enough as to negate the impact of decay of Ra and dilution on concentration as is suggested by Jefferson et al., (2007a), though disagreed by Leybourne and Cameron (2007).

Residence time of groundwater

Because no significant spread exists in the $\delta^{2}H$-$\delta^{18}O$ sample set, the values can be approximated as having a uniform offset from the Meteoric Water Line. The angle of this offset is similar to the forecasted effects of evaporation, or interaction with a carbonate which can also offset values to higher ^{18}O (Figure 74). However, the offset of Wheeler River groundwater samples from the global meteoric water line most likely results from efficient evaporation, possibly assisted by the high porosity of the sandstones.

Figure 74: Meteoric water line and causes for deviation

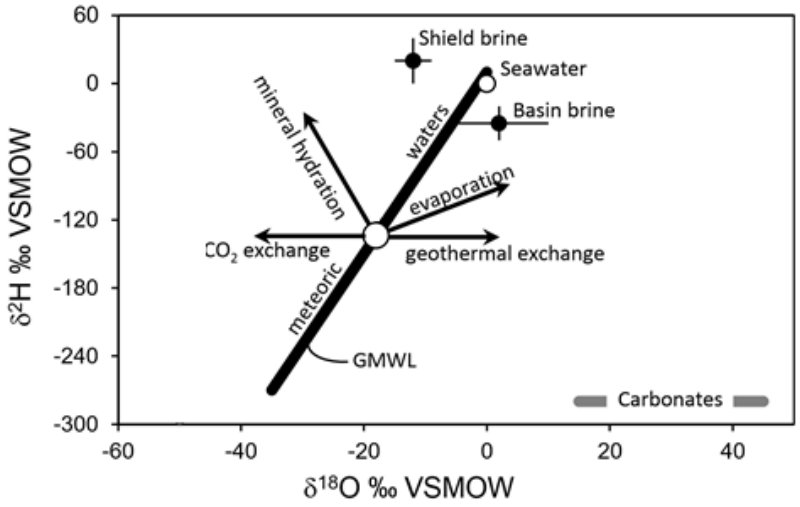

Directions and causes of deviation from the global meteoric water line. The offset shown by the Wheeler River samples rest below the meteoric water line. Figure modified after Clark (2015).

^{4}He concentrations are also generally higher in groundwater with a high residence time (Butt & Gole, 1986), also suggesting a short residence time. Groundwater was also sampled for its tritium and compared to regional tritium radioactivities, but unfortunately the results are ambiguously placed at the intersection between hypothetical 30 year reservoirs and modern precipitation (Figure 50).

Conclusions

Rn radioactivities were found to be highest, up to 0.261 Bq/g, in groundwater within 100 m of the Phoenix deposit surface projection, but were not causally associated with drilling of the deposit itself. High ^{4}He concentrations in groundwater were never detected above the Phoenix Deposit. Simple diffusion modeling indicates that Rn's ability to travel is significantly restricted by its short half life, thus Rn is likely detected in proximity to where it decayed. He, has limitless time for diffusion. Dissolved and particulate concentrations of U in groundwater were not high enough to account for the measured Rn concentrations. Groundwater Rn was sampled directly from within MFd (unless otherwise noted), and Rn radioactivities correlate well with sandstone-bed averaged 3AMS and 2AMS U contents per drill hole. Lower sandstone units are too far to be supporting Rn radioactivity in upper groundwater. Most measured Rn is thus produced by U and Ra decay within MFd, however measured Rn radioactivities are higher than expected Rn radioactivity as calculated from the U content of MFd.

Ra radioactivities measured in sandstone are positively correlated with INAA U, and Ra radioactivities are similar to expected from INAA U. No such correlation was found with B horizon soils, and Ra radioactivity expected from INAA U was slightly higher than measured. A 10-50% overabundance of Ra was identified in MFd and the overlying soil and till was suggested to be the source of Ra. Soil Ra entering MFd explains some of the discrepancy between measured and expected Rn radioactivities in near-surface groundwater. Two samples, one from MFb and one from RD were also noted for having unsupported Ra and the Phoenix Deposit was inferred to be the source.

Pb isotopic compositions as well as unsupported Rn in shallow groundwater within the MFd member suggest input from soil, and these interactions were attributed to percolation of acidic surface water towards the water table in MFd. The ^{4}He produced by the Phoenix Deposit is likely being entrained in groundwater, as a physical barrier is unlikely in porous sandstones. Depending on speed of groundwater flow and limits of detection, sampling to the south-west of the deposit could uncover missing He.

Limited Rn travel time means the effect of Ra's mobility is an important consideration. Because Ra's mobility is limited by the neutral-alkaline pH of groundwater above the Phoenix Deposit, and Rn decays so quickly, sampled Rn likely was produced by decay of U in MFd. In a hypothetical environment with very mobile Ra, sampling groundwater Rn or sandstone Ra could produce very different results. More mobile Ra could allow for slightly radioactive units to produce false anomalies of Ra and subsequently Rn. Alternatively, in an environment supporting very mobile Ra, deeply buried U deposits could produce a plume of elevated radionuclide concentration/radioactivities. As such, usage of Rn as an exploration tool is limited by understanding how groundwater chemistry affects the mobility of Ra.

References

Alexandre, P., Kyser, K., Jiricka, D., & Witt, G. (2011). Formation and evolution of the Centennial Unconformity-Related uranium deposit in the South-Central Athabasca Basin, Canada. Economic Geology, 107(3), 385-400.

Andrews, J. (1985). The isotopic composition of radiogenic helium and its use to study groundwater movement in confined aquifers. Chemical Geology, 49(1-3), 339-351.

Andrews, J., & Mahaffy, M. (1976). Growth rate of the Laurentide Ice Sheet and sea level lowering (with Emphasis on the 115,000 BP Sea Level Low). Quaternary Research, 6(2), 167-183.

Barillon, R., Ozgumus, A., & Chambaudet, A. (2005). Direct recoil radio emanation from crystalline phases. Influence of moisture content. Geochimica et Cosmochimica Acta, 69(11), 2735-2744.

Bonham-Carter, G., & Hall, G. (2010a). Multi-media Techniques for Direct detection of covered unconformity uranium deposits in the Athabasca Basin: Results of soil geochemistry using Selective Leaches, Final Report on Results of Soil Geochemistry Using Selective Leaches. Canadian Mining Industry Research Organization Exploration Division, Project 08E01. 280.

Bonham-Carter, G., & Hall, G. (2010b). Multi-media techniques for direct detection of covered unconformity uranium deposits in the Athabasca Basin: Final report on results of soil geochemistry using selective leaches. Addendum. Canadian Mining Industry Research Organization Exploration Division, Project 08E01. 19.

Bowie, S. (1958). Helium in natural gas in the Witwatersrand. Letters to Nature, 182, 1082-1083.

Brady, B., & Rice, R. (1977). Helium determinations as an exploration technique at the Ambrosia Lake uranium district, McKinley County, New Mexico. U.S. Geological Survey. Open-File Report 77-669.

Butt, C., & Gole, M. (1986). Groundwater helium surveys in minera exploration in Australia. Journal of Geochemical Exploration, 25(3), 309-344.

Cameron, E. (2013). From Chile to Nevada to the Athabasca Basin: earthquake-induced geochemical anomalies from near-field to far-field. Geochemistry: Exploration, Environment, Analysis, 13, 41-51.

Campbell, J. (2007). Quaternary geology of the Eastern Athabasca Basin, Saskatchewan. Geological Survey of Canada, Bulletin 588, 211-228.

Cecil, L., Smith, R., Reilly, M., & Rose, A. (1987). Radium-228 and radium-226 in ground water of the Chickies Formation, Southeastern Pennsylvania, in Graves, Barbara (Ed.), Radon in Ground Water – Hydrogeologic Impact and Indoor Air Contamination [Conference on radon, radium, and other radioactivity in groundwater – Hydrogeologic impact and application to indoor airborne contamination, Somerset, N.J., April 7-9, 1987]. Somerset, NJ: Lewis Publishers Inc., 437-447.

Clark, I. (2015). Groundwater Geochemistry and Isotopes. CRC Press. 456.

Clarke, W., Top, Z., Beavan, A., & Gandhi, S. (1977). Dissolved helium in lakes; uranium prospecting in the Precambrian terrain of central Labrador. Economic Geology, 72(2), 233-242.

Dann, J., Hattori, K., Potter, E., & Sorba, C. (2014). Discrimination of elemental assemblages in the alteration halo of the Phoenix Deposit, Saskatchewan, through applied GIS. Geological Survey of Canada, Open File 7463, 1-66.

Denison Mines. (2016). Denison Mines Corp. Uranium Development & Exploration in the Eastern Athabasca Basin; PDAC Investor Update. Presented in Toronto during the Prospectors & Developers Association of Canada, 2016 conference.

Devine, M. (2016). Sources and pathways of radiogenic elements in surface media above the Millennium and McArthur River uranium deposits in the Athabasca Basin, Saskatchewan, Canada. Unpublished MSc thesis at the University of Ottawa, Ottawa.

Doerner, H., & Hoskins, W. (1925). Co-precipitation of radium and barium sulfates. Journal of the American Chemical Society, 47(3), 662-675.

Dudek, N., & Hattori, K. (2015). Evaluating the use of radon for exploring deeply buried uranium deposits. Toronto: Prospectors & Developers Association of Canada, Mineral's Colloquium.

Dudek, N., & Hattori, K. (2015). Radon distribution and concentrations above buried uranium ore: The Phoenix deposits, Saskatchewan. Geological Survey of Canada, Scientific Presentation 33, 1 poster. Poster originally presented at the 2014 SK Geologic Open House.

Dyck, W. (1976). The use of helium in mineral exploration. Journal of Geochemical Exploration, 5(1-2), 3-20.

Dyck, W. (1980). Uranium, radon, helium and other trace elements and gases in well waters of parts of the St. Lawrence low-lands, (Ottawa region) Canada. Journal of Geochemical exploration, 13(1), 27-39.

Dyke, A. (2004). An outline of North American deglaciation with emphasis on central and Northern Canada. Quaternary Glaciations - Extent and Chronology - Part II: North America, 2 part B, 373-424.

Earle, S., & Drever, G. (1983). Hydrogeochemical exploration for uranium within the Athabasca Basin, Northern Saskatchewan. Journal of Geochemical Exploration, 19, 57-73.

Earle, S., McGill, B., & Murphy, J. (1989). Glacial boulder lithogeochemistry: An effective new uranium exploration technique in the Athabasca Basin, Saskatchewan. In L. S. Beck, & C. T. Harper (Ed.), Saskatchewan Geological Society Special Publication 10: Modern Exploration Techniques. 10, pp. 94-114. Regina: Saskatchewan Geological Society.

Earle, S., & Sopuck, V. (1987). Regional lithogeochemistry of the Eastern part of the Athabasca Basin uranium province, Saskatchewan, Canada. International Atomic Energy Agency (IAEA), 20(19), 1-529.

Fission Uranium Corp. (2013a) New Radon Survey Identified Strongest Anomaly to date. Retrieved May 17th, 2017, from fissionuranium.com

Fission Uranium Corp. (2013b) Fission Announced $6.95M 11,000m Drill Summer Program at PLS. Retrieved May 17th, 2017, from fissionuranium.com

Fission Uranium Corp. (2013c) Fission Hits 13.41m Total Composite "Off-Scale" Radioactivity in 48.5m of Mineralization at R780E Zone. Retrieved May 17th, 2017.

Fleischer, R. (1982). Alpha-recoil damage and solution effects in minerals: uranium isotopic disequilibrium and radon release. Geochemica et Cosmochemica Acta, 46(11), 2191-2201.

Fleischer, R. (1983). Theory of alpha recoil effects on radon release and isotopic disequilibrium. Geochimica et Cosmochimica Acta, 47, 779-784.

Fleischer, R. (1988). Alpha-recoil damage: Relation to isotopic disequilibrium and leaching of radionuclides. Geochimica et Cosmochimica Acta, 52, 1459-1466.

Freeze, A., & Cherry, J. (1979). Groundwater. Upper Saddle River, New Jersey: Prentice Hall, Inc.

Garver, E., & Baraskaran, M. (2004). Effects of heating on the emanation rates of radon-222 from a suite of natural minerals. Applied Radiation and Isotopes, 61(6), 1477-1485.

Giblin, A., & Snelling, A. (1983). Application of hydrogeochemistry to uranium exploration in the pine creek geosyncline, Northern territory, Australia. Journal of Geochemical Exploration, 19(1-3), 33-55.

Gilkeson, R., & Cowart, J. (1987). Radium, radon and uranium isotopes in groundwater from Cambrian-Ordovician sandstone aquifers in Illinois. In Graves, Barbara (Ed.), Radon in Ground Water – Hydrogeologic Impact and Indoor Air Contamination [Conference on radon, radium, and other radioactivity in groundwater – Hydrogeologic impact and application to indoor airborne contamination, Somerset, N.J., April 7-9, 1987]. Somerset, NJ: Lewis Publishers Inc., 403-422.

Greeman, D., & Rose, A. (1996). Factors controlling the emanation of radon and thoron in soils of the Eastern U.S.A. Chemical Geology, 129, 1-14.

Hamilton, S., Hattori, K., & Clark, I. (2005). Investigation into the source of forest-ring-related natural gas in Northern Ontario. Ontario Geological Survey Open File Report, 19-1 - 19-4.

Herczeg, A., Simpson, H., Anderson, R., Trier, R., Mathieu, G., & Deck, B. (1988). Uranium and radium mobility in groundwaters and brines within the Delaware Basin, Southeastern New Mexico, U.S.A. Chemical Geology, 72(2), 181-196.

Holk, G., Kyser, K., Chipley, D., Hiatt, E., & Marlatt, J. (2003). Mobile Pb-isotopes in Proterozoic sedimentary basins as guides for exploration of uranium deposits. Journal of Geochemical Exploration, 80(2-3), 297-320.

International Atomic Energy Agency/Water Isotope System for Data Analysis, Visualization, and Electronic Retrieval. (2016). Global Network of Isotopes in Precipitation. The GNIP Database. Retrieved from http://www.iaea.org/water

International Energy Agency. (2015). Technology Roadmap; Nuclear Energy. Paris: Nuclear Energy Agency. Retrieved 2016, from https://www.iea.org/publications/freepublications/publication/technology-roadmap-nuclear-energy-2015-.html

Isotope Geochemistry and Geochronology Research Centre. (2012). Sr-N-Pb-U-Th Isotope Procedures. Retrieved 2016, from http://iggrc.carleton.ca/info-clients/analytical-information

Jefferson, C., Thomas, D., Gandhi, S., Ramaekers, P., Delaney, G., Brisben, D. Cutts, C., Quirt, D., Portella, P., & Olson, R. (2007a). Unconformity-associated uranium deposits of the Athabasca Basin, Saskatchewan and Alberta. Mineral Deposits of Canada, 5, 273-305.

Jefferson, C., Thomas, D., Quirt, D., Mwenifumbo, C., & Brisbin, D. (2007b). Empirical models for Canadian unconformity-associated uranium deposits. Ore Deposits and Exploration Technology, 741-769.

Kendall, C., & McDonnel, J. (1998). Effects of organic and inorganic cycling on isotopic composition of carbon. In C. Kendall, & J. McDonnel, Isotope Tracers in Catchment Hydrology (611-646). Amsterdam: Elsevier Science B.V.

Krahenbil, A., Hattori, K., Power, M., & Kotzer, T. (2014). Surficial Geochemistry associated with the deeply buried Millennium and Phoenix Uranium Deposits, Athabasca Basin, Northern Saskatchewan. Geological Survey of Canada, Open File 7611, 1 poster. Poster originally presented at the 2014 SEG-PDAC Student Mineral Colloquium

Langmuir, D., & Chatham, J. (1980, November). Groundwater prospecting for sandstone-type uranium deposits: a preliminary comparison of the merits of mineral-solution equilibria, and single-element tracer methods. Journal of Geochemical Exploration, 13(2-3), 201-219.

Leaney, F., & Herczeg, A. (2006). A rapid field extraction method for determination of radon-222 in natural waters by liquid scintillation counting. Limnology and Oceanography: Methods, 4(7), 254-259.

Lefebvre, K., Barbecot, F., Ghaleb, B., Larocque, M., & Gagne, S. (2013). Full range determination of 222 Rn at the watershed scale by liquid scintillation counting. Applied Radiation and Isotopes, 75, 71-76.

Leyborne, M., & Cameron, E. (2007). Groundwaters in geochemical exploration: methods, applications, and future directions, Milkereit, B (Ed.), Proceedings of Exploration 07 [Fifth decennial international conference on mineral exploration, 2007]. 201-221.

Cecil, L., Smith, R., Reilly, M., & Rose, A. (1987). Radium-228 and radium-226 in ground water of the Chickies Formation, Southeastern Pennsylvania, in Graves, Barbara (Ed.), Radon in Ground Water – Hydrogeologic Impact and Indoor Air Contamination [Conference on radon, radium, and other radioactivity in groundwater – Hydrogeologic impact and application to indoor airborne contamination, Somerset, N.J., April 7-9, 1987]. Somerset, NJ: Lewis Publishers Inc., 437-447.

Leybourne, M., & Cameron, E. (2010). Groundwater in geochemical exploration. Geochemistry: Exploration, Environment, Analysis, 10, 99-118

Natural Resources Canada. (2009). Annual Mean Total Precipitation. The Atlas of Canada. Canada: Natural Resources Canada.

Natural Resources Canada. (2009). Distribution of Freshwater - Wetlands. The Atlas of Canada. Canada: Natural Resources Canada.

Natural Resources Canada. (2015). Energy Fact Book 2015-2016. Ottawa: Natural Resources Canada.

Pereira, E. (1980). Some problems concerning the migration and distribution of helium-4 and radon-222 in the upper sediments of the crust - A theoretical model; and the development of a quadrupole

ion filter for measuring helium at the soil-air interface. Unpublished PhD thesis at Rice University, Geology. Houston: University Microfilms International.

Power. (2013). Geochemical Surface Expression of the Phoenix and Millennium Uranium Deposits, Athabasca Basin, Saskatchewan. 186. Unpublished MSc thesis at the University of Ottawa.

Rainbird, R., Stern, R., Rayner, N., & Jefferson, C. (2007). Age, provenance, and regional correlation of the Athabasca Group, Saskatchewan and Alberta, constrained by igneous and detrital zircon geochronology. Bulletin-Geological Survey of Canada, 588(23), 1-17.

Ramaekers, P., Jefferson, C., Yeo, G., Collier, B., Long, D., Drever, G., McHardy, S., Jiricka, D., Cutts, C., Wheatley, K., Catuneanu, O., Bernier, S., Kupsch, B., & Post, R. (2007). Revised geological map and stratigraphy of the Athabasca Group, Saskatchewan and Alberta. Geological Survey of Canada, Bulletin 588, Special Publication No. 18, 155-191.

Ramaekers, P., Yeo, G., & Jefferson, C. (2001). Preliminary overview of regional stratigraphy in the Late Paleoproterozoic Athabasca Basin, Saskatchewan and Alberta. Summary of Investigations 2001, Saskatchewan Geological Survey, 2, 240-251.

Roscoe, W. (2012). Technical Report on a Mineral Resource Estimate Update for the Phoenix Uranium Deposits, Wheeler River Project, Eastern Athabasca Basin, Northern Saskatchewan, Canada. NI 43-101 Report. Toronto: Roscoe Postle Associates Inc.

Sanford, W., Shropshire, R., & Solomon, D. (1996). Dissolved gas tracers in groundwater: Simplified injection, sampling, and analysis. Water Resources Research, 32(6), 1635-1642.

Schreiner, B. T., 1983, Quaternary geology of the Precambrian shield, Saskatchewan. Saskatchewan Geological Survey. Report 221. 106.

Sella, G., Stein, S., Dixon, T., Craymer, M., James, T., Mazzotti, S., & Dokka, R. (2007). Observation of glacial isostatic adjustment in "stable" North America with GPS. Geophysical Research Letters, 34(2), 1-6.

Semkow, T. (1990). Recoil-emanation theory applied to radon release from mineral grains. Geochimica et Cosmochimica Acta, 54, 425-440.

Sheldon, A., Solomon, D., Poreda, R., & Hunt, A. (2003). Radiogenic helium in shallow groundwater within a clay till, Southwestern Ontario. Water Resources Research, 39, 1331.

Singh, R., Sinha, R., Bisht, B., & Banerjee, D. (2002). Hydrogeochemical exploration for unconformity-related uranium mineralization: Example from Palnadu sub-basin, Cuddapah Basin, Andhra Pradesh, India. Journal of Geochemical Exploration 76(2), 71-92.

Smith, C., & Steger, H. (1983). Radium-226 in certified uranium reference ores DL-1a, BL-4a, DH-1a and BL-5. CANMET; Canada Centre for Mineral and Energy Technology, 1-22.

Solomon, D., Hunt, A., & Poreda, R. (1996). Source of radiogenic helium 4 in shallow aquifers: Implications for dating young groundwater. Water Resources Research, 32(6), 1805-1813.

Stacey, J., & Kramer, J. (1975). Approximation of terrestrial lead isotope evolution by a two-stage model. Earth and Planetary Science Letters (26), 207-221.

Swedish Nuclear Fuel and Waste Management Co. (1994). Final report of the AECL/SKB Cigar Lake Analog Study. Technical Report, 1-404.

Szabo, Z., dePaul, V., Fischer, J., Kraemer, T., & Jacobsen, E. (2012, March). Occurrence and geochemistry of radium in water from principal drinking-water aquifer systems of the United States. Applied Geochemistry, 27(3), 729-752.

Tanimizu, M., & Ishikawa, T. (2006). Development of rapid and precise Pb isotope analytical techniques using MC-ICP-MS and new results for GSJ rock reference samples. Geochemical Journal, 40, 121-133.

Tatsumoto, M., Knight, R., & Delevaux, M. (1972). Uranium, thorium, and lead concentrations in three silicate standards and a method of lead isotope analysis. U. S., Geological Survey, Professional Paper No. 800D, 4(11), 111-115.

Torgerson, T. (1985). Helium accumulation in groundwater, I: An evaluation of sources and the continental flux of crustal 4He in the Great Artesian Basin, Australia. Geochemica et Cosmochimica Acta, 49(5), 1211-1218.

Torgerson, T., & Clarke, W. (1987). Helium accumulation in groundwater, III. Limits on helium transfer across the mantle-crust boundary beneath Australia and the magnitude of mantle degassing. Earth and Planetary Science Letters, 84(2-3), 345-355.

Torgerson, T., & Ivey, G. (1985). Helium accumulation in groundwater. II: A model for the accumulation of the crustal 4He degassing flux. Geochimica et Cosmochimica Acta, 49(11), 2445-2452.

Wheatley, K., Murphy, J., Leppin, M., Cutis, C., & Climie, J. (1996). Advances in the genetic model and exploration techniques for unconformity-type uranium deposits in the Athabasca Basin. Saskatchewan Geological Society Special Publication Number 14: Minexpo'96 Symposium-Advances in Saskatchewan Geology and Mineral Exploration. 14, pp. 126-136. Saskatoon: Saskatchewan Geological Society.

White, G., & Rood, A. (2001). Radon emanation from NORM-contaminated pipe scale and soil at petroleum industry sites. Journal of Environmental Radioactivity, 54(3), 401-413.

Willey, J., Bennet, R., Williams, J., Denne, R., Kornegay, C., Perlotto, M., & Moore, B. (1987). Effect of storm type on rainwater composition in Southeastern North Carolina. Environmental Science and Technology, 22(1), 41-46.

Wolfe, B., Karst-Riddoch, T., Hall, R., Edwards, T., English, M., Palmini, R., McGowan, S., Leavitt, P., & Vardy, S. (2007). Classification of hydrological regimes of Northern floodplain basins (Peace-Athabasca Delta, Canada) from analysis of stable isotopes (d18O, d2H) and water chemistry. Hydrological Processes, 21, 151-168.

Yaws, C. (2009). Diffusion Coefficients in Water - Inorganic Compounds. In C. L. Yaws, Transport of Chemicals and Hydrocarbons (pp. 594-596). Beaumont, Texas: Beaumont: Elsevier.

Appendices

Appendix I – Groundwater-Sampled Drill Collars, Chemistry, and Composition

- Table I-1: Drill hole collars and locations
- Table I-2: Groundwater Chemistry
- Table I-3: Groundwater Properties

Appendix II – Soil Sample Locations, Trace Element Abundances from INAA, Pb Isotopic Compositions, and Ra Radioactivity

- Table II-1: Soil Sample Locations
- Table II-2: Trace Element Abundances from INAA
- Table II-3: INAA Quality Control
- Table II-4: Pb Isotopic Compositions
- Table II-5: ^{226}Ra Radioactivity

Appendix III – Sandstone Sample Locations, Trace Element Abundances from INAA, Pb Isotopic Compositions, and Ra Radioactivity

- Table III-1: Sandstone Sample Locations
- Table III-2: Trace Element Abundances from INAA
- Table III-3: INAA Quality Control
- Table III-4: Pb Isotopic Compositions
- Table III-5: Ra Radioactivity

Appendix IV – Sandstone Sample Descriptions

Primary sedimentary textures are important in the discussion of aqueous transport, as porosity is partly controlled by primary sedimentary features. A description of sandstone textures is also important for the discussion of the source of radiogenic isotopes found within. Secondary textures, such as alterations were also noted when apparent. Sandstone sample lengths were not measured, but were generally between 10 and 30 cm.

Below, samples are listed by name, drill hole, and approximate depth. An arbitrary color chart and a sediment scale/texture card were used in the description of these samples to maintain consistency, and both can be found in Appendix V. Color terms and terms such as “very coarse-lower” come from here.

MFd Core Descriptions

DPX 182; Hole WR-286, Depth: 55.8 m

Sample is composed of 5 pieces that were split sub-vertically as well as pulverized material in the sample bag. It is unclear whether the debris is from drilling or originating from within the fracture. Sample is mostly white sandstone, with traces of driller mud. Grain size ranges from medium-lower sand (0.25-0.35 mm) to medium-upper (0.35-0.5 mm) with occasional lenses of coarse-lower sand (0.5-0.71 mm) spaced 0.5 – 1 cm vertically through the core. Grains are held together by a very fine (but poor) white silicate cement. It is possible that very fine sand is located within this cement. Medium layers are generally well sorted, and coarse lenses are poorly sorted with clasts that can be very-coarse in size (1.4 - 2 mm). Coarse layers transition gradationally to finer layers, though the direction of gradation is unknown (up or down). Lenses range from 0.5 cm to 2.7 cm thick, and are not completely horizontal with apparent dips

ranging from 10 degrees both rightwards and leftwards. There are no apparent alterations or secondary structures besides the mentioned fracture. The pulverized color is an oyster/sandstone pale beige.

DPX 257; Hole WR-291, Depth: 29 m

Sample is composed of 1 solid core piece. Sample is a mostly white sandstone with light beige blotches that can be up to 1 cm wide, with very little driller mud. Grain sizes range from fine-upper sand (0.177 – 0.25 mm) to very coarse (1-1.4 mm). Grains are held together by a very fine and good silica cement. Very fine sand is potentially a component of the cement. The sandstone piece is very smooth; generally, of 'counter top' quality, with sand grains very difficult to pluck from the cement. Majority of the sample is composed of 1 poorly sorted bed, with sub-rounded to rounded grains. One end of the sample contains an abrupt transition to a lens of sub-angular / sub-rounded very coarse material. The coarser bed contains traces (<1%) of lithic fragments. The sample has one prominent sub-vertical fracture with non-connected dextral jogs spaced between fracture planes of 0.5 mm to 0.2 mm. Upon wetting the sample, the jogs appear to not immediately end but will continue as a very fine iron oxide/rusted vein. Wetting the sample also reveals dark (blackish grey) alteration splotches alongside the fractures. No such dark patches are apparent near the rusted veins. Blue smudges are present in a light abundance, but it is likely marking wax. The pulverized color of the sample is a pale clay/oyster beige color.

DPX 177; Hole WR-286, Depth: 28.7 m

Sample is composed of 7 core fragments, split generally sub-vertically, and a fine-grained powder. Sample is a mostly white sandstone, though with very thin (~ 1mm) lenses of darker material, possibly clays. Wide rusty alteration is present on both the drill surface and the fracture surfaces, indicating that alteration extends between. Along the fracture planes several radial iron oxidation fronts are easily visible, appearing to progress from somewhere outside the core (1 – 2 cm outside). Radius of the fronts range from 2-3 cm (inner front) to 25 cm (outer front). The core is cross-stratified, with fine erosive surfaces associated with dune/ripple formation, and these surfaces are commonly marked with the darker material. The erosive surface also allows orientation of the core in space (up vs down). Short (< 1cm) fining upward sequences are common. Grain size ranged from medium-lower (0.25 mm – 0.35 mm) to very coarse-lower (1 – 1.4 mm). Grains are generally rounded, with the entire sample being well sorted. Sample is held together by moderately-good silica cement. Drill side is generally smooth, but grains can be relatively easily dislodged from the fracture surface. The pulverized color is a perfect ivory beige.

DPX 167; Hole WR-277, Depth: 45 m

Sample is composed of numerous small rocks, and a large amount of sand. The sample was either poorly cemented, or was pulverized after/during drilling. The former option is likely correct, as the silica cement is poor, and feeling grainy to the touch. Pebbles and sand are white silica, with splotches and possibly veins of iron/oxidation. Several interlayered well sorted laminations are visible, with specific clast size sorting limiting individual beds to fine-upper, medium-lower, and coarse-upper. Lenses composed of medium-sized clasts are greater than 1 cm wide, and those composed of coarse-sized clasts are below a cm. No fining/coarsening direction could be determined. Lithic fragments are present in the coarser laminations.

DPX 282; Hole WR-353, Depth: 43.5 m

Sample is composed of one solid piece of core and several smaller pieces that likely fractured from the larger main piece. Sample is a white sandstone. The sample is composed of three cross-stratified beds with dune travel directions/orientations that vary between beds by as much as 20 degrees. Between dune

beds are erosive surfaces, allowing for easy orientation in space. Lenses within the cross-stratification range from fine-upper to coarse-lower and vary significantly on short scales (1-2 mm) as well as larger scales (7-10 mm). Rusted filament-shapes can be found on the core, but does not appear to be a secondary structure/alteration, and likely originates from drilling. Sample is moderately well cemented, with only a slight grainy feel. The pulverized color is a green-tinged ivory/beige.

MFc Core Descriptions

DPX 162; Hole WR-277, Depth: 113.8 m

Sample is composed of 6 smaller rocks, and 1 large vertically cut section of core. There is a large fracture running approximately 20 degrees off core orientation and is coated in a brownish mud. Driller mud in MFd samples was typically white, so it is unclear if this is a natural or artificial material. Sample is a beige sandstone (with small lenses of white sandstone), with large (very coarse, >2 mm) grains scattered throughout. All grains are sub-rounded to rounded. These coarser grains are darker in color, though could be transparent, and are metamorphic in origin with clear sub grains contained within. Fanning cross stratification is abundant, with very clear dune lenses. Thin laminations of dark material are visible on the cut surfaces and follow the fine-grained contacts between dune forms within layer, and between layers. One complete layer of an unusual dune form (hummocky or swaley?) is visible, and is approximately 2 cm wide, and is bracketed by much larger dunes. The silica cement is of moderate quality, and differing color (the mentioned beige and white). The pulverized color is a very light clay/caramel beige.

DPX 147; Hole WR-284, Depth: 92.8 m

Sample is fragmented into three large pieces and several smaller ones. Sample is a heavily altered sandstone, and appears to be at the contact between two differing alteration fronts; an iron oxide/hematization front and some darker unidentified alteration. Sandstone that is rusted/hematized also contains dark orange vertical veins. Sandstone that has dark alternation also contains very dark purple/black diagonal veins and are near parallel (0.7 – 1 cm apart). These veins appear to extend somewhat into the hematized regions of the sandstone, but quickly change to dark orange and fade with distance. Sample is poorly sorted, with grains ranging in size from very coarse-upper to medium-lower. Smaller grains are difficult to distinguish due to pervasive alterations. This sample has the lowest $^{206}Pb/^{208}Pb$ ratio of the five MFc samples chosen for this project. The pulverized color is a brick/papaya reddish orange with black and grey specks.

DPX 187; Hole WR-286, Depth: 87 m

Sample is composed of one solid piece of core. A dark mud initially coated the sample. Sample is a beige sandstone but with thin (2-4 mm wide) lenses of white sandstone. There is no obvious overall structure to the core, besides a hair line fracture infilled with darker material at one end of the core. Individual beds/laminations can be made out due to changes from medium-upper coarse grains and very coarse-upper grains. These beds are at a slight angle from horizontal and dip directions varies slightly between beds. There is a possible erosive surface associated with two examples of cross stratification that would allow orientation, but it could be a secondary structure. Two sets of rust-like marks are visible on the core, though only the fainter appear to be natural, and these associate, and often outline, the cross-stratification. There is no obvious fining or coarsening direction. One of the larger quartz grains has a notable red “inclusion”. The pulverized color is a French-vanilla/oyster color.

DPX 143; Hole WR-380, Depth: 31.5 m

Sample is composed of four vertically fractured core pieces and several smaller core-pucks. The sample also appears to be made from two distinct sandstones; a reddish/pink sandstone, and a white/grey sandstone. The white/grey sandstone is fine grained (upper and lower intervals). It is unclear whether the sample is cemented with silica or a fine-grained matrix, regardless it is held together well with only a mild gritty feel. Very small cross-stratification (resembling swaley?) is present. The pink sandstone is lightly hematized/rusted, with several concentrated splotches of hematite-coated grains. Dune cross stratification is present, and is about 3 cm tall. This section of the sample is very poorly sorted, with grains ranging from very coarse-upper to medium-lower, but there is some correlation between bed and coarseness. One location in the core, the grains have a fining direction, possibly allowing for orientation of the core. Several hematization alteration fronts are visible on this core. The pulverized color is a clay/oyster beige.

DPX 269; Hole WR-291, Depth: 131.9 m

Sample is composed of four large vertically fragmented core, and several smaller pucks and core fragments. Sample is a white (with hints of grey) sandstone, with overall poor sorting, but locally very good sorting. Cross stratification is visible near one of the largest core piece and on the side of one of the smaller pieces. Although the texture is quite low, it appears to be part of a 3d dune or ripple. Sample has experienced clear silicification, producing gem-quality reflective faces visible within the sample's pseudo vertical fractures. Additionally, the cement is very competent and of good quality being smooth to the touch. Vertical fractures occasionally have a sinistral offset. The pulverized color is oyster with a hint of mint-green.

MFb Core Descriptions

DPX 148; Hole WR-277, Depth: 276 m

Sample is composed of some very roughly surfaced core pieces, and a large amount of sand and small pebbles. Core pieces are extremely poorly cemented and can be deformed by lightly pressing with a finger. These softer pieces are also extremely porous, with a visible sponge-like texture. A fine-mud/sand matrix is likely a more accurate description than a cement. Grains within the matrix are very poorly sorted, with some pieces being larger than very coarse. The entire sample is heavily hematized/iron oxidized, with a pink/red overall color. The solid pieces have blacker sections that are likely stronger hematization. These solid core fragments have abundant lithic fragments, and are overall composed of sub-rounded grains with very poor sorting. Medium sized cross-stratification textures are visible in these solid pieces. Alteration has removed most primary textures. The pulverized color is a sort of brick red/orange.

DPX 199; Hole WR-286, Depth; 255.9 m

Sample is composed completely of very poorly sorted sand. Lithic fragments make up 1-2 % of the sand. Grains range from sub-angular to rounded. The sand has undergone slight hematization, and now has a dull pink color. The pulverization color is a pale-brick red color.

DPX 229; Hole WR-321, Depth; 280.4 m

Sample is composed of three large vertically split core fragments (potentially 2 of which are from the opposite sides of the split) and a very fine powdery sand. Sandstone is a pale orange with thin 2-3 mm thick beds with a hematitic or iron oxide cement. Sample has very clean and clear horizontal bedding with no evidence of wave action or controlling flow. Sample is moderately sorted at both small and large scales with grain size ranging from medium-upper to very coarse-upper. Some of the smallest grains are tiny

dark lithic fragments. Quartz fragments vary significantly in color, with at least one piece of rose quartz, and several dark quartz pieces of varied size and shape. The overall color of the sample is derived from the cement, as most grains are glassy clear. Outer surfaces of the core have experienced additional rusting. The pulverized color is a pale sandstone/clay beige.

DPX 289; Hole WR-353, Depth: 202.1 m

Sample is composed of two core pieces, and some pulverized material. The core pieces are made of interlayered conglomerate (clast supported) and medium-upper coarse sandstone. Different matrix exists within the sample, with a generic white/grey silica matrix for the sandstone, but two distinct matrices for the conglomerate; a yellow matrix and an iron-oxide rich matrix. Conglomerate grains are mostly quartz, though some are also lithic, and a rare selection are feldspathic. Majority of grains are sub-angular, though angular and sub-rounded grains are also present. There is faint cross-stratification within the sandstone and conglomerate layers. There are no clear individual beds, as there are (short) gradations between large conglomerate and medium-coarse sandstone. Sample has visible and tactile porosity in the conglomerate, but considerably less in the sandstone. A quick dye using an HF scour and cobalt nitrate resulted in no visible changes, and thus no potassic minerals. The pulverized color is a clay/salmon beige.

DPX 131; Hole WR-380, Depth: 215.4 m

Sample is composed of 1 large core section and 1 smaller one. The sample is a hybrid conglomerate-sandstone with conglomerate at one end and sandstone at the other. The conglomerate clasts range between 0.2 to 1 cm wide; very poorly sorted. The conglomerate has a yellow matrix, with up to 10% iron oxide occurring in limited patches. The middle of the core is a medium-upper coarse sand, with a yellow cement and occasional very coarse-upper grains. Generally, well sorted. The opposite end to the conglomerate is a poorly sorted medium-upper coarse sand with three distinct forms of hematization / iron oxide alteration (listed here as H1, H2, and H3). H1 occurs as small 1-2 mm wide hematite halos coating grains. H2 occurs as diffuse bands that lie horizontally in the core and are about 1 cm wide when approximately 90% diffuse. H3 occurs as blood-colored string-like veins at the end of the core (opposite to the conglomerate) and typically become fractures with distance. H1 and H2 appear to be spatially correlated, and H3 is distinct by a half cm gap from the other two alteration forms. There are no discernable macroscopic primary textures. This sample stands out from other MFb core described as it is still well cemented, though still rough to the touch. Sample has visible porosity. A quick dye using HF as a scour and cobalt as dye reveals a mild yellowing, and under microscope the yellowing occurs around quartz lined cavities revealing potassic minerals. The pulverized color is a pale red-tinged clay beige.

RD Core Descriptions

DPX 069; Hole WR-329, Depth: 406.5 m

Sample is composed of half a piece of core (that was vertically cut). The sample is a highly iron-oxide altered sandstone with no discernable primary textures. Grains are mostly quartz, but with up to 5% lithic fragments. Grains range from sub-angular to sub-rounded are poorly sorted, ranging in size from medium-upper to very coarse-upper. Despite pervasive replacement of silica cement with iron-oxides, the sample is still very well cemented and has a polished feel to the touch. However, there are still notable cavities. The pulverized color is a pale coral / brick red.

DPX 240; Hole WR-321, Depth: 363.9 m

Sample is composed of two large pieces of core and one core fragment. Sample is a bedded sandstone with medium-upper coarse beds and very coarse-upper beds. The very coarse beds have a

white silica matrix, and the medium coarse beds have a yellow matrix. Grains are all sub-rounded and gem-like. Sample has two generations of jointing (listed here as J1 and J2). J1 is composed of diagonal crisscrossing fractures that have undergone separation of 1-2 mm, and then infilling with coarsely grown white, glassy quartz crystals. Quartz crystal infilling is not complete, and vugs are present. J2 is composed of newer crisscrossing fractures (pseudo parallel to J1) though without infilling with quartz, allowing for relative dating. The sample is very well cemented and is smooth to the touch. A quick dye using HF as a scour and cobalt nitrate as the dye resulted in no new coloration and thus no potassium bearing minerals are present. The pulverized color is a pale white/oyster.

DPX 077; Hole WR-301, Depth; 342.1 m

Sample is composed of 1 large and 1 small core fragment. The sample is a conglomerate sandstone hybrid with beds grading into one another. Grains ranger from very coarse-upper, if not conglomerate sized, to medium-upper and appears to be poorly sorted on a local and global scale. Cement is a strange lime-green color and of good quality. Besides the rare occasion of sponge-like porosity, the sample is smooth and solid. Along an open diagonal fracture, there is a mass of green material, which appears to be some sort of clay cement/matrix and contains well rounded quartz grains different from the more angular grains of the rest of the sample. This localized roundness suggests some sort of grinding took place along the fracture. A quick dying, using HF for scouring and cobalt nitrate as dye resulted in bleaching of the lime green color; indicating magnesium/aluminum clays and no potassic minerals. Possibly illite. The pulverized color is an oyster/stone beige.

DPX 145; Hole WR-380, Depth: 324.8 m

Sample is composed of 1 large solid core piece. The sample is a sandstone conglomerate hybrid with poorly defined boundaries between the beds; gradational transitions. Sample has a lime-green silica cement, but also a hematitic cement specifically around the larger conglomerate grains. All the grains are made of quartz, and range from being sub rounded to angular. The sample is well cemented, though with abundant sponge-like porosity. Very similar to DPX 077, though without the dark green plaque as no fractures are present in the sample. The pulverized color is a clay/French vanilla beige.

DPX 256; Hole WR-373, Depth: 394.5 m

Sample is composed of three small core fragments and pulverized rubble. The sample is composed of sand grains loosely held together by white clay, though with hints of yellow and green matrix as well (1-2%). Washing the sample is a bad idea, as pieces washed dissolve/break apart. There are no discernable primary textures. The sample is very different from other RD core, as it is not solid and is heavily altered. Staining using an HF scour and cobalt nitrate as dye results in a significant color bleaching, indicating magnesium/aluminum clays. The pulverized color is a pale mint-green.

Appendix V – Presentations

- Appendix I-1.1: 2015 PDAC-SEG Abstract
- Appendix I-1.2: 2015 PDAC-SEG Poster
- Appendix I-2: 2015 GSC Scientific Presentation
- Appendix I-3.1: 2016 AESRC Abstract
- Appendix I-3.2: 2016 AESRC Poster